

Doctoral Dissertation

Study on Performance Improvement of Resonator-Coupled Type Wireless Power Transfer System Using Spiral Resonators Towards Practical Use

スパイラル共振器を用いた共振器結合型無線電力伝送システムの実用化に向けた性能改善に関する研究

March 2022

Nur Syafiera Azreen Binti Norodin

Graduate School of Sciences and Technology for Innovation

Yamaguchi University

Table of Contents

CHAPTER 1: INTRODUCTION	1
1.1 Historical Background	1
1.2 Classification of Wireless Power Transfer (WPT) Systems	4
1.3 Motivation	8
1.4 Configuration of the Thesis	10
CHAPTER 2: PRINCIPLE OF THE RESONATOR-COUPLED TYPE WIRELESS POWER TRANSFER SYSTEM	12
2.1 Foreword	12
2.2 Configuration Setup of RC-WPT System	12
2.3 Structural Parameters of Elements Composing the RC-WPT System	14
2.4 Q -factors for the Resonant System	19
2.4.1 Measurement Setup of Q -factors	19
2.4.2 Results of Q -factors for Spiral-Resonators	26
2.5 Coupling Coefficient between Resonators	30
2.5.1 Measurement Setup of Coupling Coefficients	30
2.5.2 Results of Coupling Coefficients for Spiral-Resonators	38
2.6 Power Transmission Efficiency of RC-WPT System	39
2.6.1 Measurement Setup of Power Transmission Efficiency of RC-WPT System	39
2.6.2 Results of Power Transmission Efficiency of RC-WPT Systems	48
2.7 Summary	51
CHAPTER 3: EFFECT OF LOSSY MEDIUMS ON THE RC-WPT SYSTEM	52
3.1 Foreword	52
3.2 Measurement Setup for the RC-WPT System with Lossy Mediums	53
3.2.1 Q -factors with Lossy Mediums	56
3.2.2 Coupling Coefficients with Lossy Mediums	59
3.2.3 Power Transmission Efficiency with Lossy Mediums	62
3.3 Modified Structure of Spiral Resonators	68

3.4 RC-WPT System using Modified Spiral Resonators with Lossy Mediums	72
3.4.1 Q -factors of Dual-Spiral Resonator	72
3.4.2 Q -factors with Lossy Mediums	74
3.4.3 Coupling Coefficients with Lossy Mediums	76
3.4.4 Power Transmission Efficiency with Lossy Mediums	79
3.5 Summary	84

**CHAPTER 4: EFFECTS OF SOME MISALIGNMENTS BETWEEN TX/RX
UNITS OF RC-WPT SYSTEM**

	85
4.1 Foreword	85
4.2 Configuration Setup for RC-WPT System with Angular Misalignment	85
4.3 Measurement of Power Transmission Efficiency with Angular Misalignment	87
4.4 Improvement of Power Transmission Efficiency with Some Misalignments	90
4.5 Measurement of Improvement of Power Transmission Efficiency with Some Misalignments	92
4.6 Summary	108

CHAPTER 5: CONCLUSIONS

ACKNOWLEDGEMENTS

REFERENCES

Chapter 1: Introduction

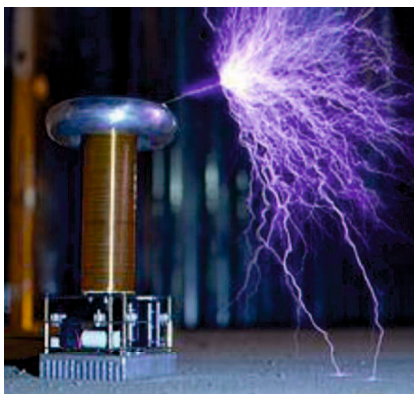
Recently, various utilizations of the Wireless Power Transfer (WPT) system have been extensively studied. A WPT system is defined as the transmission of electrical energy from a power source to consumers' electronic appliances without power lines. In some electronic applications, the WPT system has particular advantages over traditional wired power transmission technology, such as its safe handling, reliability, and layout-free placement against electric outlets. Therefore, more active research is required to advance Wireless Power Transfer technology.

1.1 Historical Background

The origin of the WPT system, which uses the electromagnetic (EM) field energy transfer, began in the 19th century with the discovery of the EM induction law by M. Faraday, who established the fundamental theory of electromagnetic fields. The law of EM induction, one of his contributions, states that a change in magnetic flux density in space produces a potential difference. The application of this phenomenon later became the basis of non-contact wireless power transmission over short-range distances, *i.e.*, a type of WPT system. Following M. Faraday, J. C. Maxwell established traditional electromagnetics through the derivation of Maxwell's equations and predicted the existence of electromagnetic waves in 1861. Afterward, H. R. Hertz experimentally proved the

existence of EM waves in 1881 [1]. After this discovery, new WPT systems that could transmit electric power over long-range distances using electromagnetic waves also began to be studied.

After the experimental discovery of H. R. Hertz, Nikola Tesla proposed the WPT system at the end of the 19th century. In 1890, he experimentally presented the “Tesla coils” [2], which generated high AC voltage, and in 1901, he made an experimental attempt to transmit power wirelessly around the world [3] using the Wardenclyffe Tower, now known as the Tesla Tower (see Figure 1.1). Unfortunately, since he had not considered the spreading characteristics of electromagnetic waves, the EM energy density delivered could not reach the value desired by customers, so the practical application and promotion of this technology were unsuccessful [4]. However, Tesla’s inventions



(a) Tesla Coil



(b) Wardenclyffe Tower, now called the Tesla Tower

Figure 1.1 Nicola Tesla’s Inventions.

contributed to the evolution of long-distance energy transfer through radio communications.

More than a hundred years later, in 2006, the WPT system reached a turning point when the research team of Dr. Marin Soljačić at the Massachusetts Institute of Technology (MIT) proposed a resonant wireless power transmission system based on the strong coupling of solenoidal coil type resonators, as shown in Figure 1.2. This system was capable of turning on a 60W light bulb at a distance of 2 meters from the transmitting coil with a transmission power efficiency of around 40% [5]-[7]. The presentation of this method had a major impact on researchers and engineers in various fields and considerable attention was attracted to the possibility of new and even unexpected expansions of this concept in practical applications of non-contact power transmission technology.

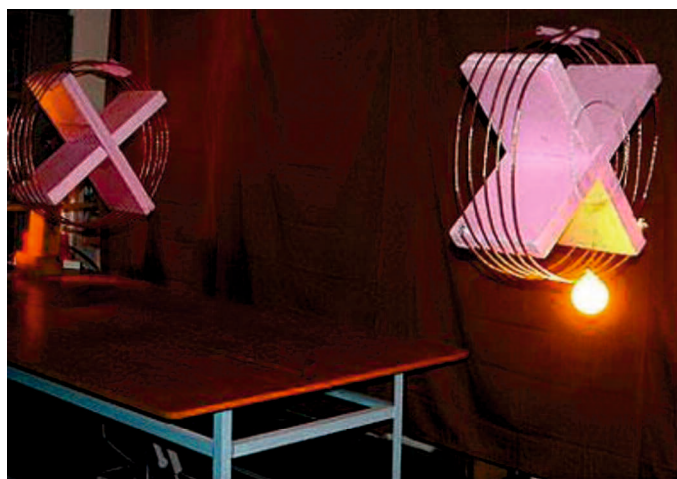


Figure 1.2 Magnetic Field Resonance System Proposed by MIT Group.

Since the MIT group proposed the WPT system using coupling between resonators, many researchers worldwide have tried to confirm and improve the power transmission characteristics of similar systems. In general, the performance of Resonator-Coupled types of WPT (RC-WPT) systems is highly dependent on the characteristics of the resonators. Therefore, many studies have been published on WPT systems that employ various improved resonators. Among them, the solenoidal coil and planar coil types are currently being used and investigated by numerous research groups. According to Ref. [8], a system using a planar-type spiral resonator can easily reduce the power transmission loss and also realize a much compact system due to its in-plane structure. The author's laboratory has conducted a number of fundamental studies using this type of resonator.

1.2 Classification of Wireless Power Transfer (WPT) Systems

WPT systems can be classified into two categories based on the relative distance between the power source and the load, which are the far-field type and the near-field type. The general classification of WPT systems is presented in Figure 1.3.

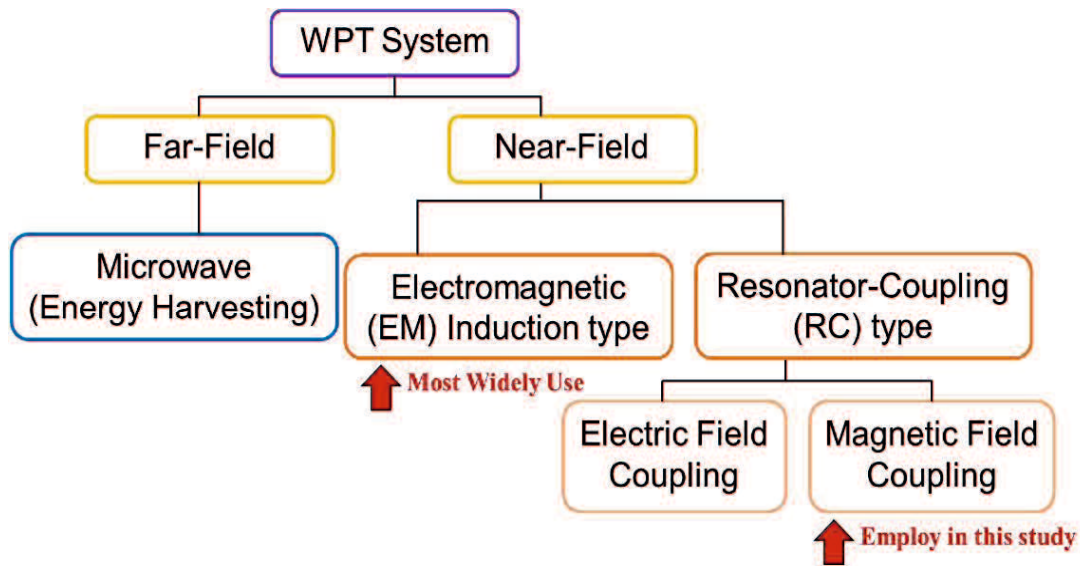


Figure 1.3 Classification of WPT Systems.

In a far-field or radiative technique type of WPT system, electric power is transmitted by beams of EM radiation, like microwaves or laser beams. With advanced beamforming and energy harvesting methods [9], this kind of field involves a greater separation between the power source and the load, whereby the energy transmit distance is greater than that of the signal wavelength. Proposed applications of this kind of WPT system are solar power satellites [10], wireless drone aircraft [11], and others. Based on Figure 1.4, the transmission distance of this far-field type of WPT system is long but the transmission power is very low. In terms of consumer applications, this kind of far-field type of WPT system is unsuitable due to human safety issues [12].

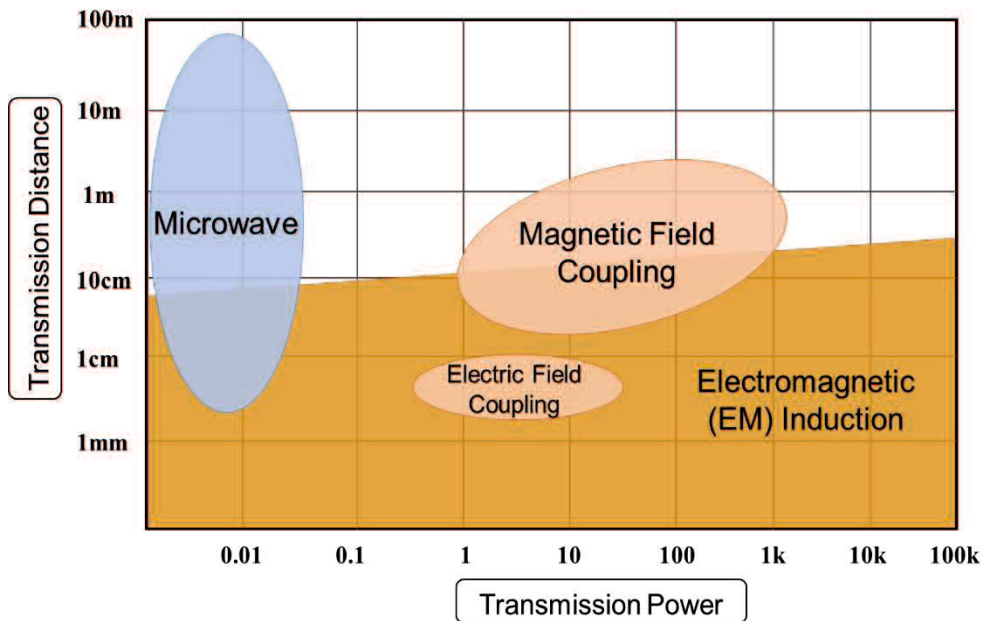


Figure 1.4 Transmission Power and Transmission Distance for Each Types of WPT System [13].

On the contrary, in a near-field or non-radiative type of WPT system, high power transmission efficiency can be achieved although the power transmission distance is limited. Near-field types of WPT systems can be divided into two: the electromagnetic (EM) induction type and the resonator-coupled type of WPT (RC-WPT) system. In the above WPT systems, the EM induction type of WPT system is the most widely used for non-contact power transfer systems. The applications that have accelerated the development of this kind of power supply include chargeable shavers, toothbrushes, mobile phones [14], [15], and power implemented sensors and devices [16], all of which are currently on the commercial equipment market. However, the commercialized systems that already use the EM induction type of WPT system still have some minor

issues. The EM induction type of WPT system transmits electric energy from a transmitting (Tx) coil to a receiving (Rx) coil through an AC magnetic field. The strength of magnetic coupling in this system is determined by the mutual inductance between the two coils. The two coils should have good mutual inductance so that the magnetic field generated in the Tx coil can pass efficiently through the Rx coil. For this reason, as shown in Figure 1.5, the power transmission distance in the EM induction type of WPT system is extremely short, only a few centimeters, and the Tx and Rx coils are almost in contact with each other. If the Tx and Rx coils are misaligned, the strong electromagnetic coupling cannot be maintained. In other words, EM induction type of WPT systems are sensitive to misalignment [17], and the Rx coil must be placed strictly within the magnetic path of the Tx coil to maintain good power transmission efficiency [18]. In addition, due to the low induced power, which is limited by the standard regulation [19], [20] of the

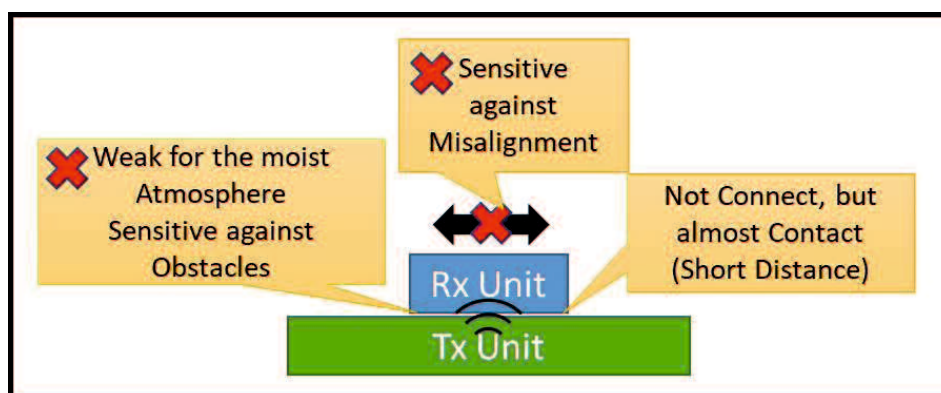


Figure 1.5 The EM Induction-based WPT System.

inductive system, the transmitted power of the inductive system drops drastically when lossy obstacles enter the power transmission path.

Meanwhile, in RC-WPT systems, there are two kinds of near-field-based WPT systems, as shown in Figure 1.3. The first is the electric field coupling type and the other is the magnetic field coupling type of RC-WPT system. Based on Figure 1.4, the electric field coupling type of WPT system has a short transmission distance and low transmitted power. On the contrary, the magnetic field coupling type of RC-WPT system has a longer transmission distance, and the power transmission efficiency is far higher than that of the electric field coupling type. Therefore, in this study, the magnetic field coupling type of RC-WPT system was employed.

1.3 Motivation

The fundamental mechanism of the magnetic RC-WPT system used in this study was the same as that proposed by the MIT group, but the type of resonator was different. In addition, most research to date has mainly focused on the improvement of the power transmission efficiency and operability of the WPT system itself, and only a few studies have focused on improving the practicality of the system, which is essential for its widespread adoption. In this paper, the RC-WPT system using a planar spiral coil type of resonator is discussed and its performance was improved from a practical perspective.

The RC-WPT system, as shown in Figure 1.6, uses the coupling between the EM fields formed by the resonators, so it is far more robust to obstacles along the power transmission path [21] and more resistant to any misalignment of the Tx and Rx units than the EM induction type and can extend the power transmission distance from tens of centimeters to several meters (see Figure 1.4) [13]. However, as the length of the power transmission path increases, the possibility of obstacles appearing in the transmission path and the positioning tolerance between internal units of the system increase. In addition, when the obstacles or lossy mediums exist around the power transmission path, depending on the type of resonator used in the system, there are concerns about adverse effects such as reduced power transmission efficiency due to conductive and dielectric losses acting on the electric field [22]-[25]. Moreover, considering that the power supply to IoT devices [26], [27] as shown in Figure 1.7, has recently become popular, it is

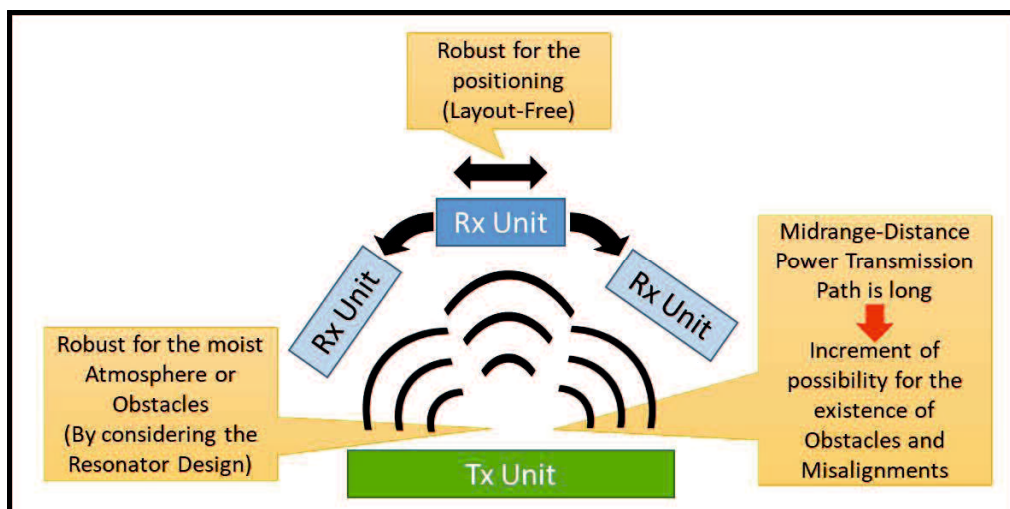


Figure 1.6 The RC-WPT System (Magnetic Field Coupling Type).

desirable to maintain high power transmission efficiency even if the misalignment between the Tx and Rx units is considerable. According to Refs. [28] and [29], when the Rx unit is rotated or tilted, the amount of magnetic flux that passes through the Rx units decreases and causes the power transmission efficiency of the RC-WPT system to decrease. Solving these problems formed the motivation for the research undertaken in this paper.



Figure 1.7 Sensors Used in the Internet of Things (IoT) Applications.

1.4 Configuration of the Thesis

The historical background of WPT systems in general, the types of RC-WPT systems, and the objectives and significance of studying them have been described above. Chapter 2 describes the principle of the RC-WPT system. It also describes the configuration settings of the RC-WPT system, the design procedures and characteristics of the elements of which the system is composed, the Q -factors of the RC-WPT system, the coupling

coefficient between the resonators, and the performance of the system' power transmission efficiency. Next, Chapter 3 discusses the effect of lossy mediums on RC-WPT systems. When a lossy medium is adjacent to the system, the leakage electric field around the resonator acts as a loss and reduces the transmission efficiency of the system. Next, this chapter discusses a method to ensure that the RC-WPT system is unaffected by lossy mediums so that the influence of lossy mediums can be reduced. Furthermore, Chapter 4 discusses the changes in power transmission efficiency due to misalignments between the Tx and Rx units of the RC-WPT system. In this chapter, the measured power transmission efficiency of the RC-WPT system with angular misalignment is studied and presented. Then, the chapter outlines the attenuation of the power transmission efficiency of the RC-WPT system with angular misalignment. The next section discusses a method to recover the degraded performance by appropriately selecting the location of the Rx units in the system. Finally, Chapter 5 is the conclusions that have presented summary of this study and also future perspectives.

Chapter 2: Principle of the Resonator-Coupled type Wireless Power Transfer System

2.1 Foreword

In this chapter, the basic principle and design procedure of the Resonator-Coupled type of Wireless Power Transfer (RC-WPT) system are described in detail using the equivalent circuit model of the system. In addition, the measurement methods and results of the properties of the key elements of the RC-WPT system are presented. Furthermore, using these results, the ways to obtain the optimum conditions necessary to construct a high-performance RC-WPT system will be demonstrated.

2.2 Configuration Setup of RC-WPT System

Figure 2.1 shows the basic structure of the RC-WPT system. This system consists of transmitting (Tx) and receiving (Rx) units. Each unit has a set of spiral resonators and

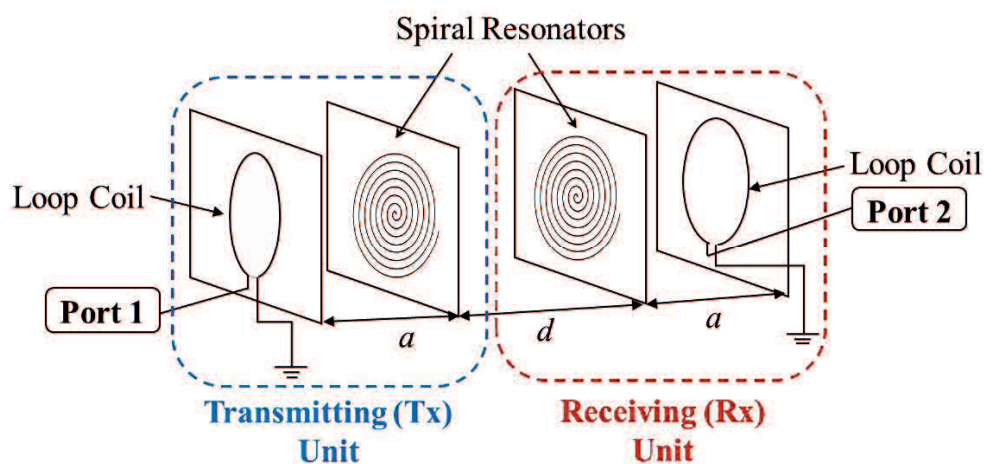


Figure 2.1 Configuration Setup of RC-WPT System.

loop coils. Here, a [cm] is the distance between the spiral resonator and the loop coil, while d [cm] is the distance between the spiral resonators. In our RC-WPT system, port 1 supplies electric power to the loop coil, and port 2 provides electric power to connected loads, such as an electric appliance. The electric power supplied from the power source is converted into electromagnetic energy by the loop coil in the Tx unit and stored as an eigenmode electromagnetic field with a resonator-specific frequency. Here, the resonator in the Tx unit forms an electromagnetic field and excites it to the resonator in the Rx unit, which has the same resonant frequency as the Tx unit. The energy of the electromagnetic field formed by the resonator in the Rx unit is then transformed into electric power via the output loop coil and fed to port 2 [30]-[33]. This is the principal mechanism of wireless power transmission in our RC-WPT system

Meanwhile, according to Refs. [34]-[36], the RC-WPT system in Figure 2.1 can be converted to an equivalent circuit, as shown in Figure 2.2. The configuration of the

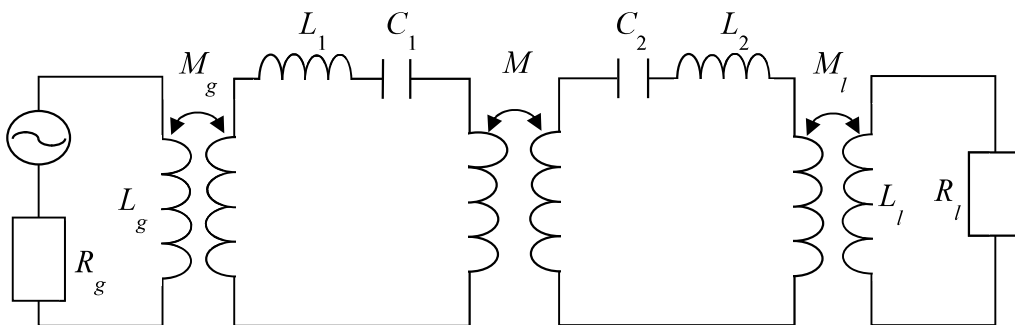


Figure 2.2 Equivalent Circuit of RC-WPT System.

equivalent circuit is identical to the two-stage Band Pass Filter (BPF) circuit. In Figure 2.2, L_g and L_l denote the self-inductance of the loop coil while M_g and M_l are the mutual inductance between the loop coil and the adjacent spiral resonator in the Tx and Rx units, respectively. Meanwhile, L_1 and L_2 represent the self-inductance of the spiral resonator, and C_1 and C_2 represent the proximity capacitance between the wires composing the spiral resonator.

In the RC-WPT system, the resonant frequency of each resonator is made equal [34]. Since the equivalent circuit of the RC-WPT system can be expressed by 2-stage BPF circuit, it was assumed that the inductance $L = L_1 = L_2$, the capacitance $C = C_1 = C_2$ and the operating frequency, ω could be presented as follows:

$$\omega = 2\pi f = \frac{1}{\sqrt{LC}} \quad (2.1)$$

Under these situations, the theory of BPF can be applied to the design of this RC-WPT system by obtaining the fundamental properties of resonators, such as the Q -factors and the coupling coefficient between resonators [35].

2.3 Structural Parameters of Elements Composing the RC-WPT System

As explained, the RC-WPT system consists of a pair of loop coils and spiral resonators in the Tx and Rx units. These loop coils and spiral resonators are the fundamental

elements of which the system is composed. The loop coils are used as an intermediate element between the power source or load and the resonators in the Tx and Rx units of our RC-WPT system are connected through a 50Ω SMA connector to a Vector Network Analyzer (VNA; Keysight Technology, E5071C). Here, the VNA serves as the power supply and induces the electric power contained with the several frequency waves, as well as the receiver in which the dispersive characteristics of the transmitted power can be obtained. The shape and structural parameters of the loop coils used in our RC-WPT system are shown in Figure 2.3. Two identical loop coils were designed and fabricated on a Polystyrene (PS) board using Cu wire with a $1.0\text{ mm}\phi$ and a diameter of 17.5 cm.

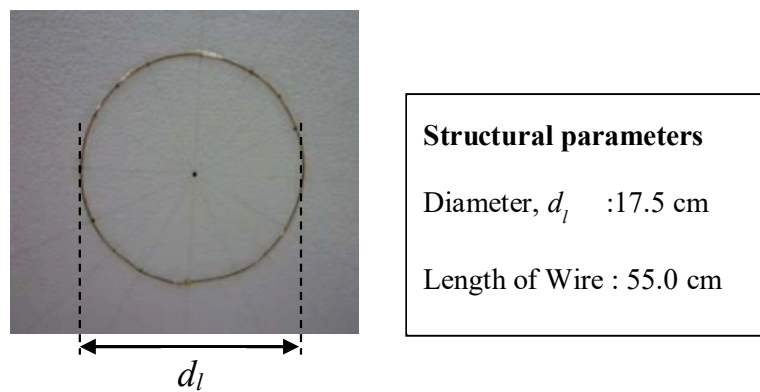


Figure 2.3 Fabricated Loop Coil.

The resonator plays the most important role in the RC-WPT system as it determines the outreach of power transfer and the power transmission efficiency of the system [34]. In terms of the spiral resonators, single-spiral resonators were used for our RC-WPT system at first. The single-spiral resonator is a kind of spiral coil resonator so

it shows strong magnetic coupling. Since the structure of the single-spiral resonator is a planar type, it can be made compact the system toward the power transmission direction and it is low transmission loss nature [8]. In addition, the spiral resonator is a kind of coil type, so the coupling between them by dominantly magnetic fields.

To construct a uniform spiral resonator, the "spiral guide" with spiral grooves 1.2 mm in width and 1.0 mm in depth was created on a 2.0 mm thick polyethylene (PE) substrate, as shown in Figure 2.4. Then, the Cu wire with a diameter of 1.0 mm of the designed length was embedded in the groove of the spiral guide to form a spiral resonator with a spiral guide.

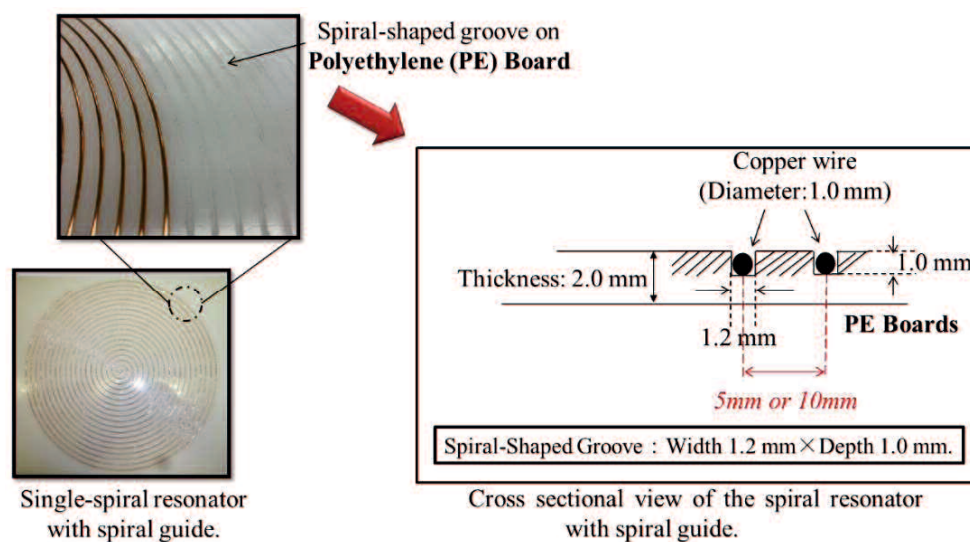
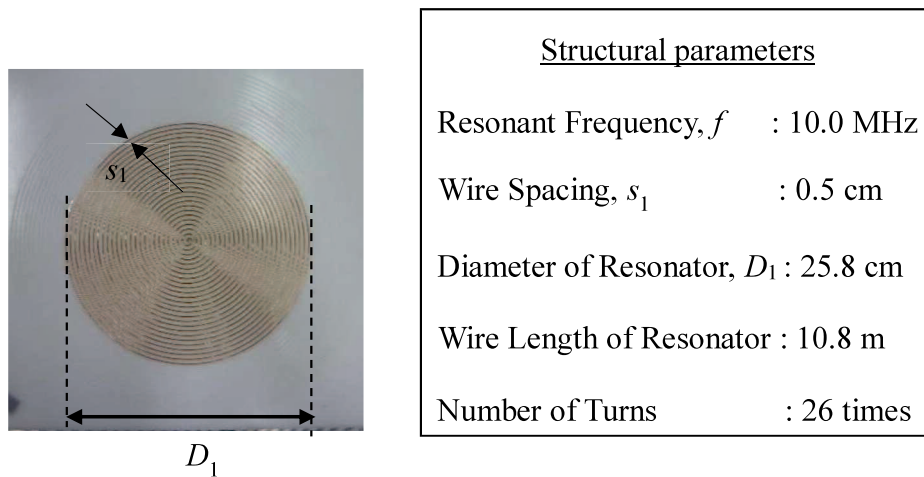
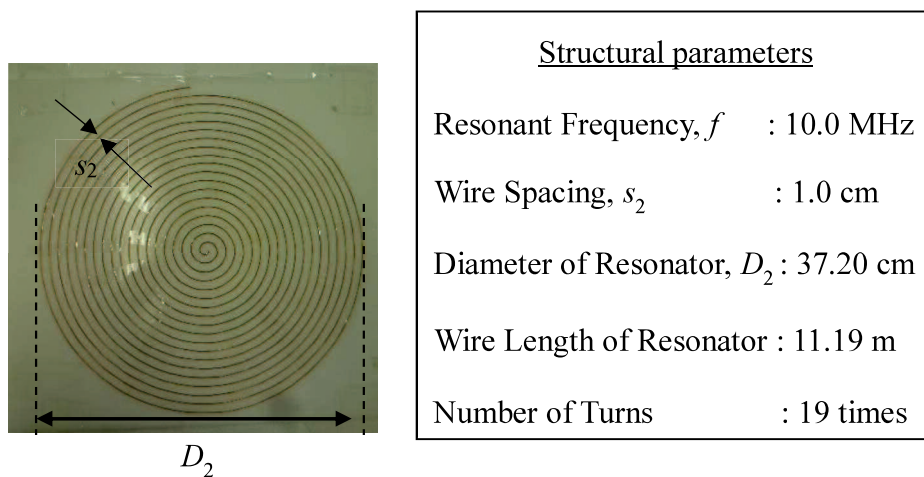


Figure 2.4 Single-Spiral Resonator with Spiral Guide.

In this study, the resonant frequency of the spiral resonators was set as $f=10.0$ MHz which is close to the ISM band. In this study, two kinds of single-spiral resonators were treated, Single-Spiral #1 and Single-Spiral #2, as shown in Figures 2.5 (a) and (b), respectively. For Single-Spiral #1, the wire spacing, $s_1 = 0.5$ cm and the diameter of the resonator is 25.8 cm. On the contrary, for Single-Spiral #2, the wire spacing, $s_2 = 1.0$ cm and its diameter is 37.2 cm. This difference in diameter is due to not only the length of the Cu



(a) Single-Spiral #1



(b) Single-Spiral #2

Figure 2.5 Fabricated Single-Spiral Resonators.

wire used for the spiral resonator but also the distributed proximity capacitance caused by the difference in wire spacing.

In general, the capacitance C between two parallel wires in a resonator can be estimated by the following equation:

$$C = \frac{\pi\epsilon}{\log_e \frac{D}{r}} \quad (2.2)$$

where ϵ is the permittivity between the electrodes, D is the electric flux density and r is the radius of the electrode. In the case of Figure 2.6, the electrodes are assumed to be a part of the Cu wire within the resonator.

The equivalent circuit of the RC-WPT system is identical to the two-stage BPF circuit, so the relationship between the LC circuit and the spiral resonator is shown in Figure 2.6, where L represents the self-inductance of the spiral resonator, and C represents

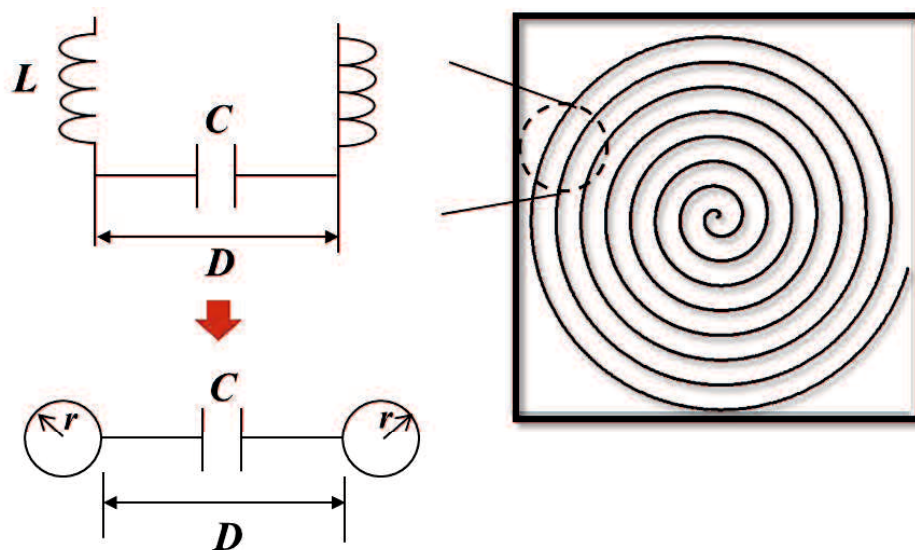


Figure 2.6 Relationship between LC Circuit and Spiral Resonators.

the proximity capacitance between the wires of the spiral resonator. In the system, the resonant frequency, f [Hz] had been decided by using the following relationship:

$$f = \frac{1}{2\pi\sqrt{LC}} \quad (2.3)$$

Based on the above equations, when the electric flux density D decreased, the capacitance C between the two parallel wires in the resonator increased, resulting in a smaller resonant frequency f . Therefore, even if the resonant frequency between Single-Spiral #1 and Single-Spiral #2 is the same (10.0 MHz), Single-Spiral #1 has a smaller radial size because the capacitance C is smaller than that of Single-Spiral #2.

2.4 Q -factors for the Resonant System

After the structural parameters of the resonators and the resonant frequency had been determined, the performance of the single-spiral resonators was investigated by examining the quality factors or Q -factors of the resonant system, including the Unloaded Q : Q_u , External Q : Q_e , and External k : k_e .

2.4.1 Measurement Setup of Q -factors

The measurement setup of the Q -factors for the resonant system is shown in Figure 2.7. A Q -factor, also known as a Quality Factor, has been defined as a parameter that describes the condition of the resonator. Q -factors measure the performance of a resonator in terms of its losses and can be used to measure the center frequency of the passband.

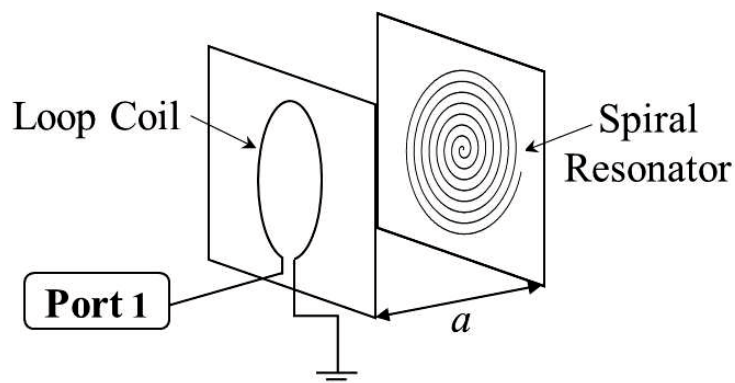


Figure 2.7 Measurement Setup of Q -factors.

The Q -factors denote the energy loss relative to the amount of energy stored inside the system. In this research, since the resonant circuit is the focus, the Q -factors are defined in terms of the ratio of the amount of energy stored within the resonant circuit to the energy supplied per unit time. Q -factors show the energy loss due to the quantity of energy contained in the RC-WPT system. Thus, the larger the Q -factors, the lower the rate of energy loss.

In this study, the Q -factors of the entire resonator system, including the loop coil, are called loaded Q : Q_L . Meanwhile, the Q -factors due to the loss of the surrounding because of the resonator are known as unloaded Q : Q_u , and the factors other than those of the resonators are known as external Q : Q_e . These Q -factors can be determined by measuring the frequency characteristics of the S -parameter and the changing distance between the loop coil and the spiral resonator, a .

The system design shown in Figure 2.7 can be simplified to an equivalent circuit, as shown in Figure 2.8 (a). This type of resonant circuit also can be deformed as an RLC series circuit, as shown in Figure 2.8 (b), if the Detuned Open-Circuit (DOC) surface is considered. The DOC plane refers to the position of the input voltage standing wave when

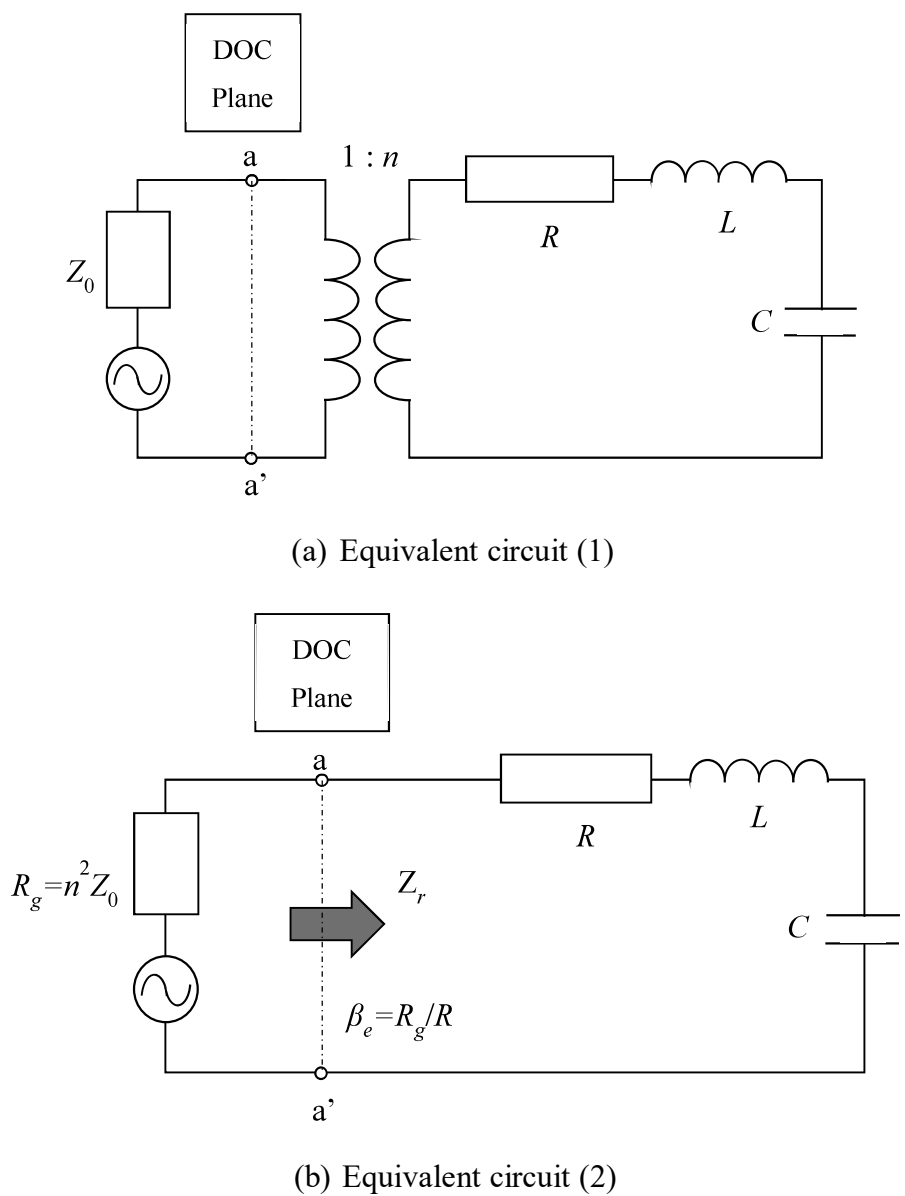


Figure 2.8 Equivalent Circuit of Q Factor Measurement System

the frequency of the transmitter, f [Hz] is adjusted to the resonant frequency, f_0 [Hz] and then the resonator is perturbed and detuned to a frequency sufficiently far from the frequency band where f_0 is used to the state in which a perturbation is applied to the resonator after adjusting the transmitter frequency f to the resonant frequency f_0 [37]. To achieve maximum power transmission efficiency, the resonance frequency must be fixed within the MHz band.

As shown in Figure 2.8 (b), the impedance of the RLC series circuit on the right from a–a' terminal is Z_r , while the coupling coefficient between the loop coil and the resonator β_e is given by the following equation:

$$\beta_e = n^2 \frac{Z_0}{R} = \frac{R_g}{R} \quad (2.4)$$

$$Z_r = R + j \left(\omega L - \frac{1}{\omega C} \right) \quad (2.5)$$

Based on the Ref. [38], Q_u and Q_L were defined as follows:

$$Q_u = \frac{\omega_0 L}{R} = \frac{1}{\omega_0 C R} \quad (2.6)$$

$$Q_L = \frac{Q_u}{1 + \beta_e} \quad (2.7)$$

Then, using equation (2.6), equation (2.5) can be transformed into the following equation:

$$Z_r = R \left[1 + j Q_u \left(\frac{\omega_r}{\omega_0} - \frac{\omega_0}{\omega_r} \right) \right] \quad (2.8)$$

In the same figure, the following equation obtained the amplitude reflection coefficient

$|S_{11}(\omega_r)|$ at a-a' terminal and can be expressed as follows:

$$\begin{aligned}
 |S_{11}(\omega_r)|^2 &= \frac{|Z_r - R_g|^2}{|Z_r + R_g|^2} = \frac{\left| R - R_g + j\left(\omega_r L - \frac{1}{\omega_r C}\right) \right|^2}{\left| R + R_g + j\left(\omega_r L - \frac{1}{\omega_r C}\right) \right|^2} \\
 &= \frac{\left(\frac{1 - \beta_e}{1 + \beta_e}\right)^2 + \frac{Q_u^2}{(1 + \beta_e)^2} \left(\frac{\omega_r}{\omega_0} - \frac{\omega_0}{\omega_r}\right)^2}{1 + \frac{Q_u^2}{(1 + \beta_e)^2} \left(\frac{\omega_r}{\omega_0} - \frac{\omega_0}{\omega_r}\right)^2} \\
 &= \frac{\left(\frac{1 - \beta_e}{1 + \beta_e}\right)^2 + Q_L^2 \left(\frac{\omega_r}{\omega_0} - \frac{\omega_0}{\omega_r}\right)^2}{1 + Q_L^2 \left(\frac{\omega_r}{\omega_0} - \frac{\omega_0}{\omega_r}\right)^2} \quad (2.9)
 \end{aligned}$$

From the definitions of Q_L , Q_e , and Q_u , $1/Q_L$ is defined by the loss of the entire resonator system, $1/Q_u$ is defined by the loss of only the resonator, and $1/Q_e$ is defined by the loss due to the coupling between the resonator and the external circuit, so the following relationship between each Q factor can be established as follows [38], [39]:

$$\frac{1}{Q_L} = \frac{1}{Q_u} + \frac{1}{Q_e} \quad (2.10)$$

As shown in Figure 2.7, to measure the Q -factors of the RC-WPT system, the spiral resonators are set at the loop coil. Then, the end of the loop coil is connected to Port 1 of the VNA and S -parameter.

Figure 2.9 shows the schematic diagram of the frequency characteristic of the amplitude reflection coefficient, S_{11} of the VNA. Here, the minimum value due to resonance can be observed and the minimum value of S_{11} is set to $-L_0$ [dB]. The frequency at that point is the resonant frequency f_0 [Hz], and the frequency when the value $|S_{11}|$ is set to $-L_1$ are f_1 and f_2 ($f_1 < f_0 < f_2$). Since this system works in a resonant state, the driving angular frequency ω equals the angular resonant frequency $\omega_0 = 2\pi f_0$ [rad/s].

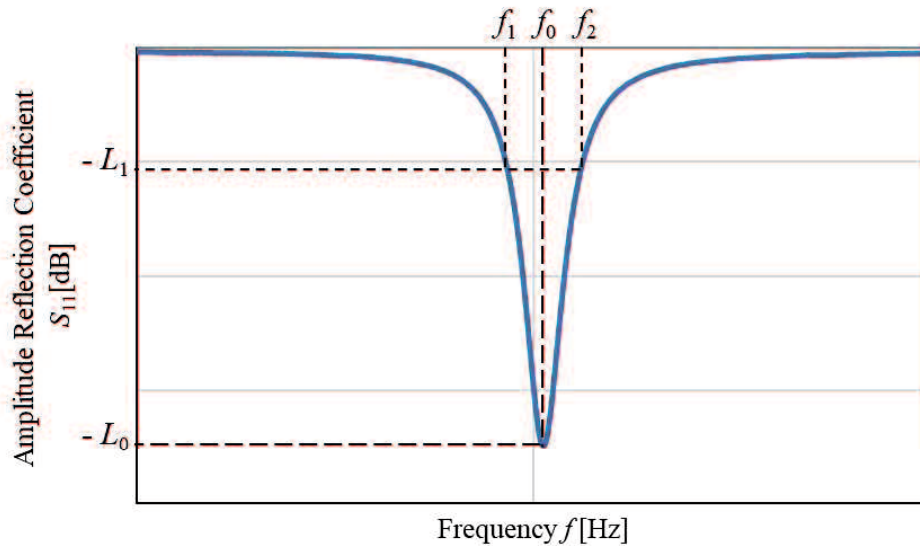


Figure 2.9 Frequency Response of Amplitude Reflection Coefficient S_{11} .

Hence, the reflection loss, L_0 [dB] can be expressed by the following equation:

$$L_0 = -10 \log |S_{11}(\omega_0)|^2 = -10 \log \left(\frac{1 - \beta_e}{1 + \beta_e} \right)^2 \quad [\text{dB}] \quad (2.11)$$

For this equation to be satisfied, it is necessary that $\left(\frac{1+\beta_e}{1-\beta_e}\right)^2 > 0$, so the β_e in equation

(2.11) should be calculated using the following equation for each range of β_e :

$$\beta_e = \begin{cases} \frac{1 + 10^{-\frac{L_0}{20}}}{1 - 10^{-\frac{L_0}{20}}} & (0 < \beta_e < 1) \\ \frac{1 - 10^{-\frac{L_0}{20}}}{1 + 10^{-\frac{L_0}{20}}} & (\beta_e \geq 1) \end{cases} \quad (2.12)$$

$$\beta_e = \begin{cases} \frac{1 - 10^{-\frac{L_0}{20}}}{1 + 10^{-\frac{L_0}{20}}} & (0 < \beta_e < 1) \\ \frac{1 + 10^{-\frac{L_0}{20}}}{1 - 10^{-\frac{L_0}{20}}} & (\beta_e \geq 1) \end{cases} \quad (2.13)$$

Meanwhile, from the power half-width theorem [37],

$$Q_L \left(\frac{\omega_1}{\omega_0} - \frac{\omega_0}{\omega_1} \right) = -1 \quad \text{and} \quad Q_L \left(\frac{\omega_2}{\omega_0} - \frac{\omega_0}{\omega_2} \right) = 1 \quad (2.14)$$

Considering $\omega_1 = 2\pi f_1$ and $\omega_2 = 2\pi f_2$ ($f_1 < f_0 < f_2$) from equation (2.14), the

following relational expression can be obtained:

$$\omega_0 = \sqrt{\omega_1 \omega_2} \quad (2.15)$$

Thus, from equations (2.14) and (2.15), the loaded Q : Q_L can be written as follows:

$$Q_L = \frac{f_0}{f_2 - f_1} \quad (2.16)$$

Then, by substituting equations (2.11) and (2.14) into equation (2.9), the reflection loss

L_1 [dB] at the frequencies f_1 and f_2 can be found and expressed as follows:

$$L_1 = -10 \log \left(\frac{10^{-\frac{L_0}{20}} + 1}{2} \right) \quad [\text{dB}] \quad (2.17)$$

Furthermore, from equations (2.6), (2.7), and (2.10), the relation equation is concluded as follows:

$$Q_u = Q_L(1 + \beta_e) \quad (2.18)$$

$$Q_e = Q_L \left(1 + \frac{1}{\beta_e}\right) \quad (2.19)$$

where the unloaded Q : Q_u indicates the inverse of loss for the resonator itself, which is isolated from the rest of the circuit. Meanwhile, the external Q : Q_e is defined by the Q -factors due to the loss of surrounding because of the coupling between the loop coil and the spiral resonator. Then, since k : k_e indicates the strength of the coupling between the surrounding substances (the loop coil) and the spiral resonator, the external k : k_e is defined by the inverse of the external Q : Q_e as follows:

$$k_e = \frac{1}{Q_e} \quad (2.20)$$

2.4.2 Results of Q -factors for Spiral-Resonators

To examine the Q -factors of the resonant system, the measurement setup of the Q -factors is used, as shown in Figure 2.7. At this stage, the loop coil and the single spiral resonator were attached to Styrofoam boards that had a thickness of 1.0 cm so that they could stand independently. The distance between the loop coil and the spiral resonator is a [cm]. Then, by changing the distance a and following the procedure in Section 2.4.1, the Q -factors,

which are the unloaded Q : Q_u , the external Q : Q_e , and the external k : k_e for the single-spiral resonators, can be examined.

Figure 2.10 below shows the results of the unloaded Q : Q_u for Single-Spiral #1 and Single-Spiral #2 as a function of the distance between the loop coil and the spiral resonator, a .

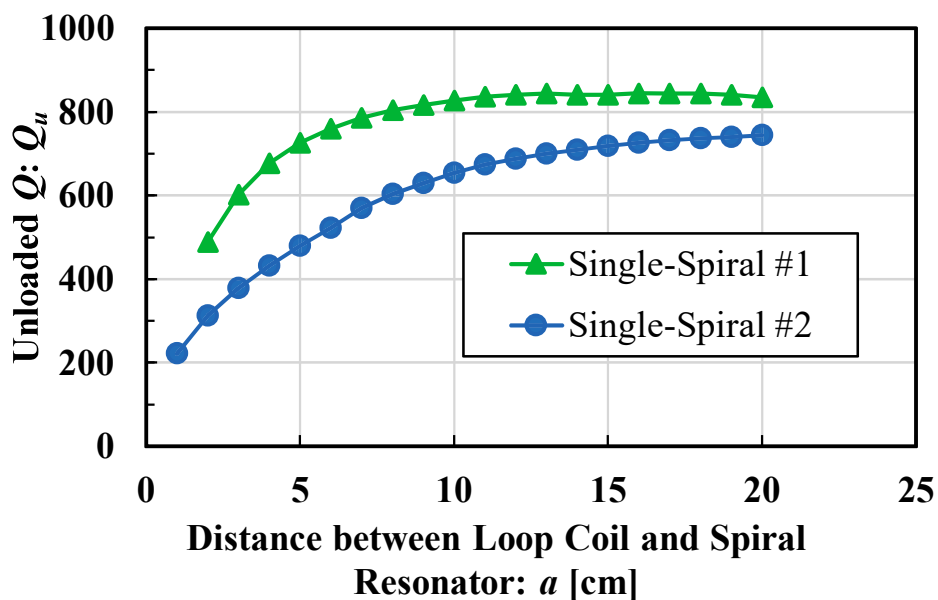


Figure 2.10 Measured Unloaded Q : Q_u for the Single-Spiral Resonators.

As the results shown in Figure 2.10 indicate, as the distance a is short, the value of the unloaded Q : Q_u in each resonator becomes small. Here, the unloaded Q : Q_u indicates the inverse of loss for the resonator itself, which is isolated from the rest of the circuit. It might be affected by the effects of interference from the loop coil when the spiral resonator is too close to the loop coil. In the same figure, the unloaded Q : Q_u for the

Single-Spiral #1 is converged to 840. Meanwhile, the unloaded Q : Q_u of Single-Spiral #2 asymptotes at 740 and is lower than that of Single-Spiral #1.

The measured results of the external Q : Q_e as a function of distance a for Single-Spiral #1 and Single-Spiral #2 are presented in Figure 2.11.

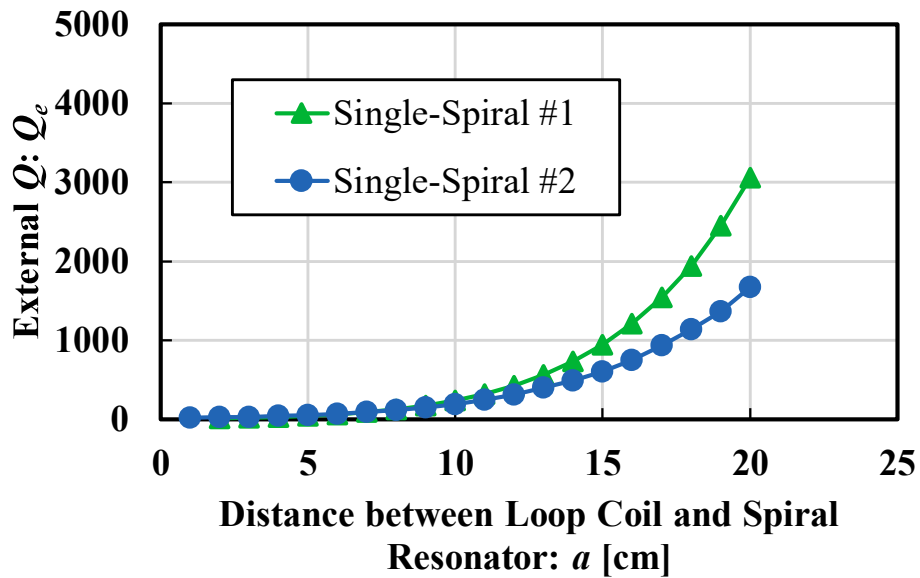


Figure 2.11 Measured External Q : Q_e for the Single-Spiral Resonators.

As the results shown in Figure 2.11 indicate, when the distance a increased, the external Q : Q_e for each spiral resonator increased. In the same figure, when the distance a is short, the external Q : Q_e for Single-Spiral #2 is higher than it is for Single-Spiral #1. However, when the distance a is long, the external Q : Q_e for Single-Spiral #1 is higher than it is for Single-Spiral #2.

Next, Figure 2.12 shows the measured external $k: k_e$ for each single-spiral resonator as a function of the distance a .

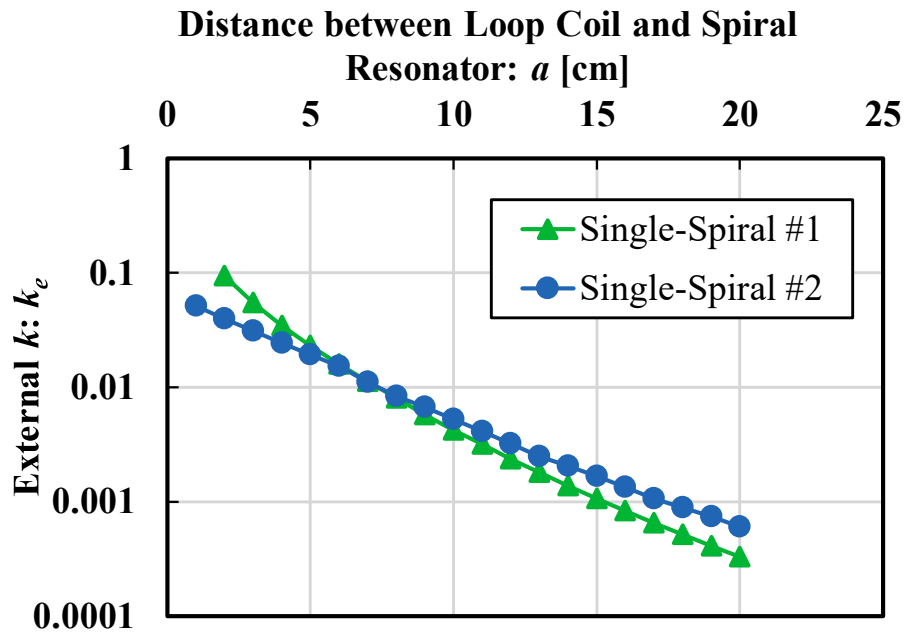


Figure 2.12 Measured External $k: k_e$ for the Single-Spiral Resonators.

As the results in Figure 2.12 indicate, in each spiral resonator, the external $k: k_e$ decreased as the distance a increased. Here, when the loop coil is further away from the spiral resonator, the mutual coupling between the spiral resonator and the loop coil becomes weak, resulting in large external quality factors. In the same figure, when the loop coil is close to the spiral resonator, the external $k: k_e$ for Single-Spiral #1 is higher than that of Single-Spiral #2. However, when the loop coil is further away from the spiral resonator, the external $k: k_e$ for Single-Spiral #2 is higher than that of Single-Spiral #1.

2.5 Coupling Coefficient between Resonators

The RC-WPT system consists of two loop coils and two spiral resonators, and it can transmit electric power through the couplings between each loop coil and spiral resonator, and the coupling between two spiral resonators. In the previous section, the external $k: k_e$, which is the coupling between the loop coil and the spiral resonator was examined. Next, the coupling coefficient between the resonators, k , defined as the degree of coupling between two spiral resonators, will be examined.

2.5.1 Measurement Setup of Coupling Coefficients

The measurement setup of the coupling coefficient k is shown in Figure 2.13. The distance between the loop coil and the spiral resonator, d [cm], is fixed at 15.0 cm by inserting 15 polystyrene boards, each with a thickness of 1.0 cm, into the Tx and Rx units because the unloaded $Q: Q_u$ for single-spiral resonators are asymptote to a constant at which the

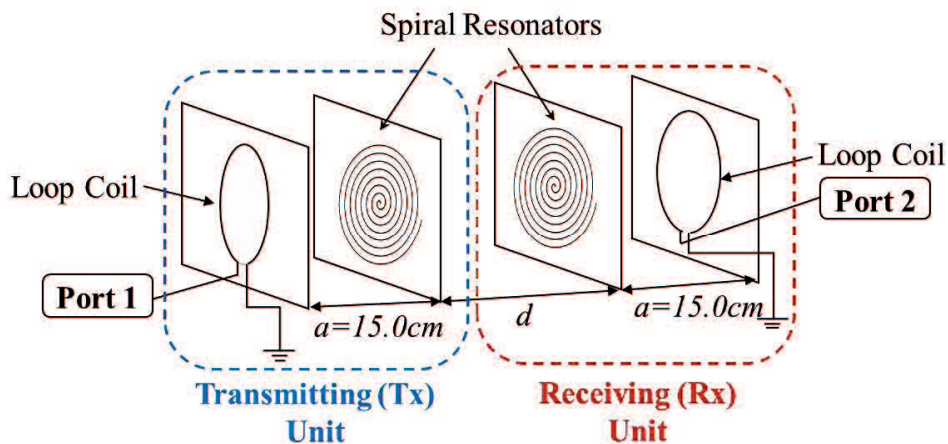
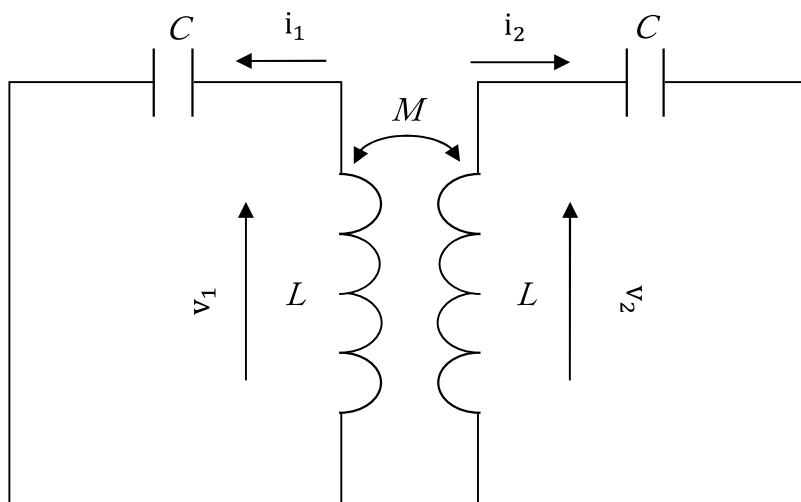
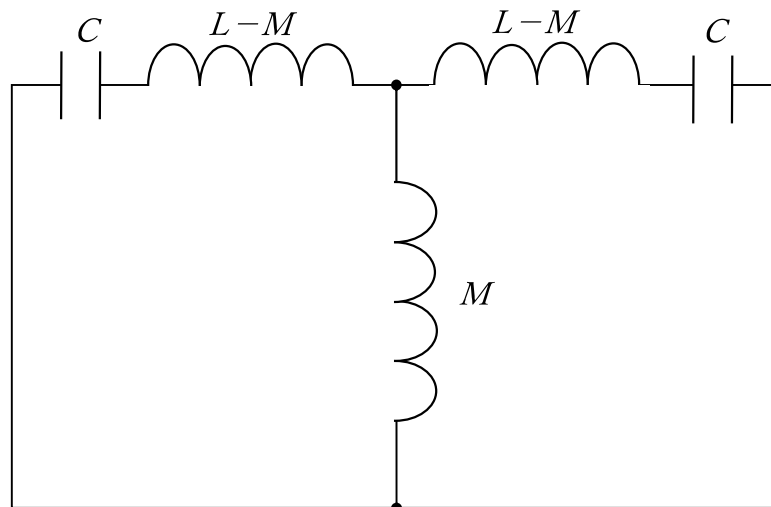


Figure 2.13 Measurement Setup of Coupling Coefficient k .

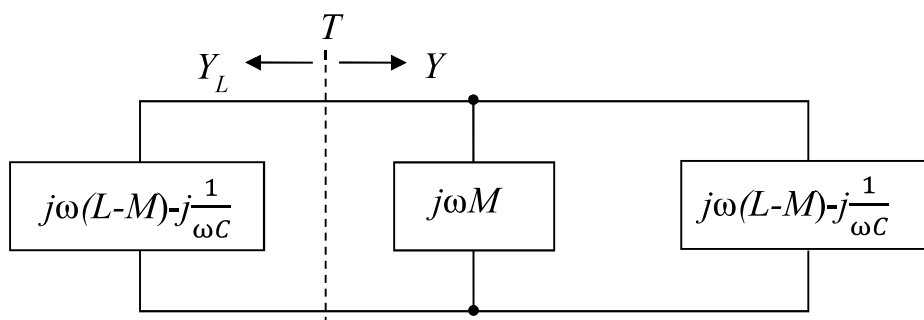
distance a is greater than 15.0 cm. This prevents the loop coil from being affected because of the electromagnetic distribution from the spiral resonators [34]-[35], [40]-[41]. In other words, the influence of the external parts is prevented so that the pure coupling coefficients between the spiral resonators can be examined. The measurement system in Figure 2.13 can be converted into an equivalent circuit, as shown in Figure 2.14. In this study, two identical spiral resonators tuned at the same resonant frequency were constructed. Since the parameter of the resonant circuit is the same, it was considered coupled in mutual inductance, as shown in Figure 2.14 (a).



(a) Equivalent Circuit



(b) Mutual Inductance in Coupled Resonant Circuit



(c) Impedance Values for Each Branch

Figure 2.14 Coupling between Resonators.

The resonance frequency, ω_0 for each resonant circuit is given by the following equation:

$$\omega_0 = \frac{1}{\sqrt{LC}} \quad (2.21)$$

The coupling coefficient between the spiral resonators can be obtained from the relationship between the self-induction and mutual inductive when the current is flowing

in each of the circuits. Figure 2.14 (a) shows the inductance L_1 and L_2 in the primary side and the secondary side, respectively.

Firstly, when there are current flows on the primary side, the v_1 and v_2 are given by the following equation:

$$\begin{cases} v_1 = L_1 \frac{di_1}{dt} \\ v_2 = -M \frac{di_1}{dt} \end{cases} \quad (2.22)$$

where L_1 and M are the self-induction and the mutual inductive, respectively.

Thus, it is possible to derive the following equation from the previous equation:

$$\frac{v_1}{v_2} = -\frac{M}{L_1} \quad (2.23)$$

Firstly, the voltage ratio between the primary circuit and the secondary circuit can be expressed in terms of the number of coil windings N and the coupling coefficient k , as shown below:

$$\frac{v_1}{v_2} = -k \frac{N_2}{N_1} \quad (2.24)$$

By substituting equation (2.23) into equation (2.24), the following equation can be obtained:

$$k \frac{N_2}{N_1} = \frac{M}{L_1} \quad (2.25)$$

Next, when current is flowing in the secondary side, the v_1 and v_2 are given by the following equation:

$$\begin{cases} v_2 = L_2 \frac{di_2}{dt} \\ v_1 = -M \frac{di_2}{dt} \end{cases} \quad (2.26)$$

where L_2 and M are the self-induction and the mutual inductive, respectively.

The following equation can be derived from equation (2.26):

$$\frac{v_2}{v_1} = -\frac{M}{L_2} \quad (2.27)$$

The inverse relationship between the coupling coefficients for the primary side and the secondary side is expressed in the equation below:

$$\frac{v_2}{v_1} = -k \frac{N_2}{N_1} \quad (2.28)$$

By substituting equation (2.27) into equation (2.28), the following equation is obtained:

$$k \frac{N_1}{N_2} = \frac{M}{L_2} \quad (2.29)$$

Then, equations (2.25) and (2.29) are multiplied by each other on both sides of the equation, resulting in the following equation [42] :

$$k^2 = \frac{M^2}{L_1 L_2} \quad (2.30)$$

Equation (2.30) shows a general expression for the coupling coefficient when two resonant circuits are coupled by mutual inductance. Since the parameters of the two resonant circuits are the same, the inductance of each resonant circuit [40] is defined as follows:

$$L = L_1 = L_2 \quad (2.31)$$

Then, by applying equation (2.31) to equation (2.30), the following equation is obtained.

$$k = \frac{M}{L} \quad (2.32)$$

As shown in Figure 2.14 (a), when two resonators are in close proximity, they become magnetically coupled and exhibit mutual inductance, which can be modified into an equivalent circuit, as shown in Figure 2.14 (b). As Figure 2.14 (c) shows, Y_L and Y_R are used to define the admittance of the left and right sides, respectively. Since it is considered a resonance state, the resonance frequency of the coupled resonant circuit, ω_0 is defined as follows:

$$Y_L + Y_R = 0 \quad (2.33)$$

Therefore,

$$\frac{1}{\omega_r(L - M) - \frac{1}{\omega_r C}} + \frac{1}{\omega_r M} + \frac{1}{\omega_r(L - M) - \frac{1}{\omega_r C}} = 0$$

$$\omega_r^4 \left(1 - \frac{M^2}{L^2}\right) + \frac{1}{L^2 C^2} - \frac{2\omega_r^2}{LC} = 0 \quad (2.34)$$

By substituting equations (2.34) into equation (2.32) and inserting $\omega_0 = 1/\sqrt{LC}$, the following equation can be obtained:

$$\omega_r^4(1 - k^2) - 2\omega_0^2\omega_r^2 + \omega_0^4 = 0 \quad (2.35)$$

Equation (2.35) can be written in quadratic form as follows:

$$\omega_r^2 = \frac{2\omega_0^2 \pm \sqrt{4\omega_0^4 - 4(1 - k^2)\omega_0^4}}{2(1 - k^2)} \quad (2.36)$$

From equation (2.36), ω_r can be expressed as follows:

$$\omega_{r1} = \frac{\omega_0}{\sqrt{1 + k}} > 0 \quad \text{and} \quad \omega_{r2} = \frac{\omega_0}{\sqrt{1 - k}} > 0 \quad (2.37)$$

Therefore, when the resonators are coupled, the resonant frequency can be separated into two different frequencies. If ω_0 from equation (2.37) is eliminated, the following relation is established:

$$k = \frac{\omega_{r2}^2 - \omega_{r1}^2}{\omega_{r2}^2 + \omega_{r1}^2} \quad (2.38)$$

In particular, when $k \ll 1$, the following equation can be derived:

$$k \approx 2 \frac{\omega_{r2} - \omega_{r1}}{\omega_{r2} + \omega_{r1}} \quad (2.39)$$

As $\omega_0 = 2\pi f$, where ω is the resonance angular frequency and f is the resonance frequency at resonant states. Thus, for equations (2.38) and (2.39), even if the resonant angular frequency is replaced by the resonant frequency, the relationship remains the same, as follows:

$$k = \frac{f_2^2 - f_1^2}{f_2^2 + f_1^2} \quad (2.40)$$

$$k \approx 2 \frac{f_2 - f_1}{f_2 + f_1} \quad (2.41)$$

From the equation above, the coupling coefficient between the spiral resonators can be determined by observing the two peaks of resonant frequency, f_1 and f_2 . These were observed from the frequency characteristic of amplitude transmission coefficient, S_{21} shown in Figure 2.15 and applied to equations (2.40) and (2.41).

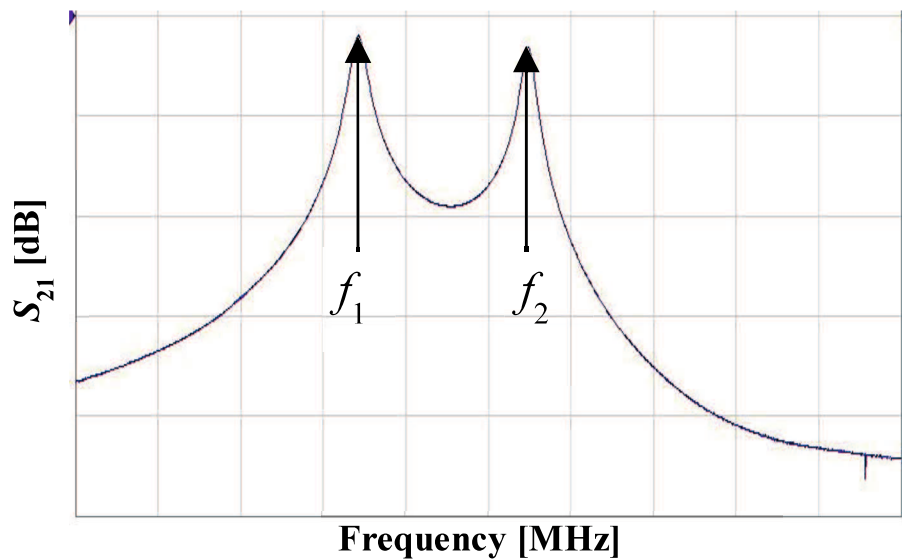


Figure 2.15 Frequency Characteristic of Amplitude Transmission Coefficient S_{21}

2.5.2 Results of Coupling Coefficients for Spiral-Resonators

Figure 2.16 shows the coupling coefficient k results as a function of the distance between the spiral resonators, d for the single-spiral resonators.

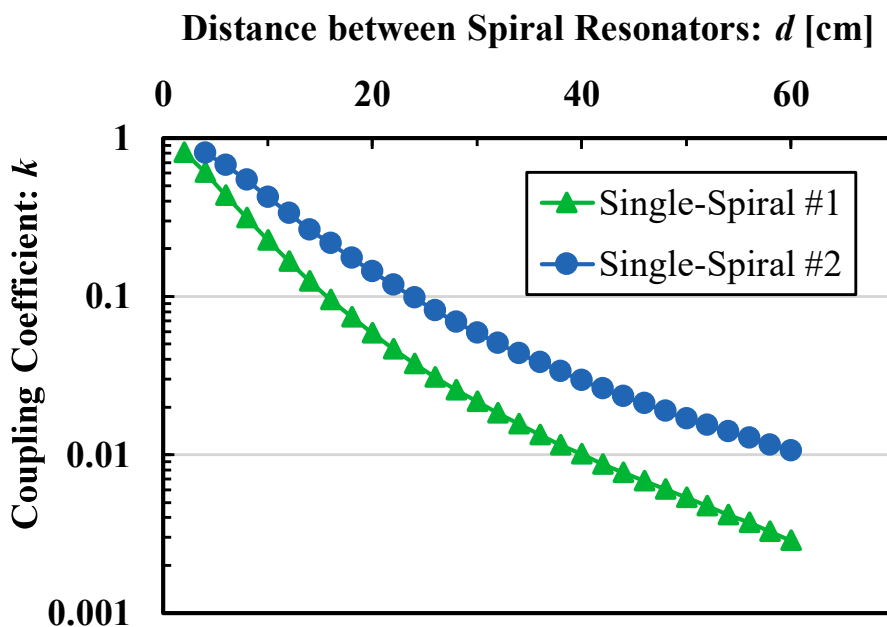


Figure 2.16 Measured Coupling Coefficient k for the Single-Spiral Resonators.

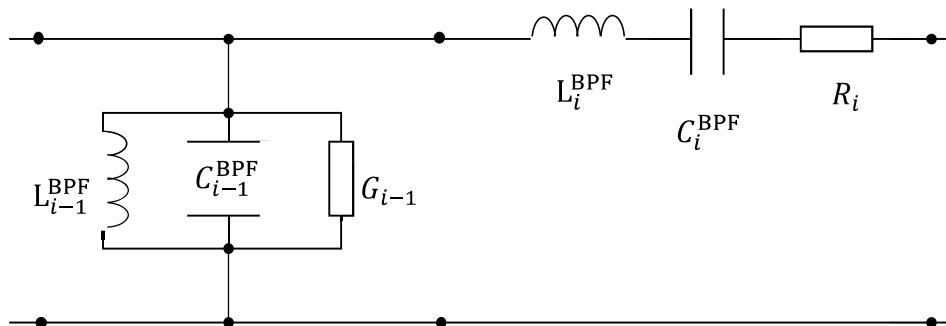
As shown in Figure 2.16, when the spiral resonators are further away from each other, the coupling coefficient between the spiral resonators decreases. Since the coupling coefficient k is determined by the shape and size of the spiral coil, it becomes larger as the surface area of the resonator increases. Here, the diameter of Single-Spiral #2 is larger than that of Single-Spiral #1. Therefore, the coupling coefficient of Single-Spiral #2 is larger than that of Single-Spiral #1.

2.6 Power Transmission Efficiency of RC-WPT System

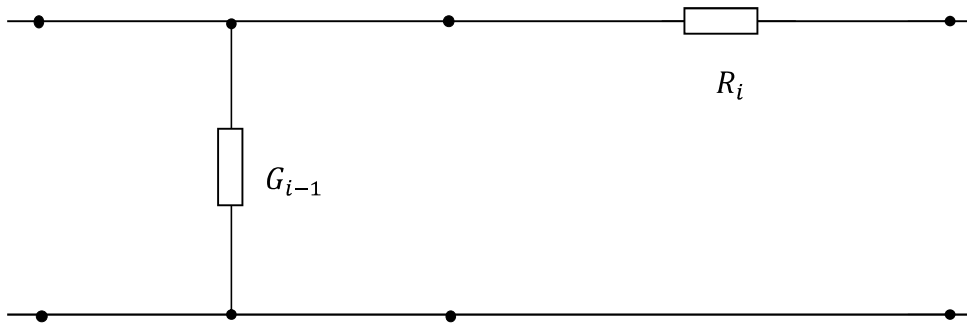
The next parameter is the power transmission efficiency of the RC-WPT system, which can be evaluated after the Q -factors and coupling coefficients have been examined.

2.6.1 Measurement Setup of Power Transmission Efficiency of RC-WPT System

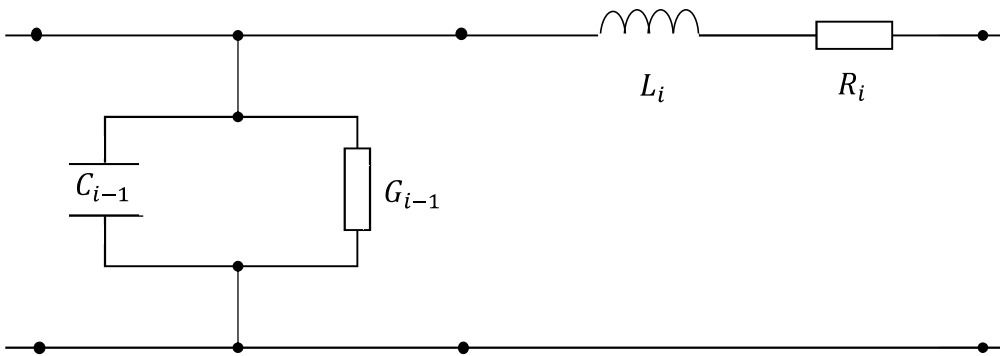
The measurement setup of the power transmission efficiency of the RC-WPT system is the same as that shown in Figure 2.1. Since the design of the RC-WPT system used in this paper is based on the BPF theory, the power transmission efficiency of the system can be determined by the same theory. When considering the power loss generated in the BPF circuit, the equivalent circuit can be expressed as shown in Figure 2.17 (a). Here, G_{i-1} represents the conductance of the $(i-1)$ th prototype element values in the parallel resonant circuit, while R_i represents the resistance of the i th prototype element values in the series resonant circuit.



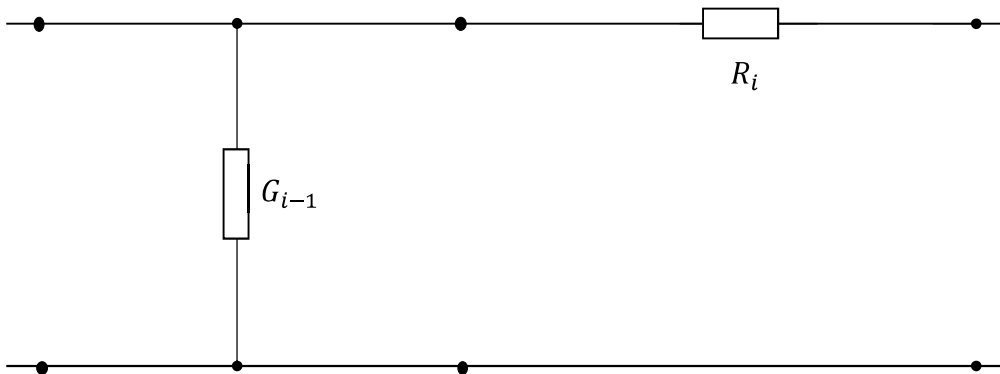
(a) The i th and $(i-1)$ th prototype element values in the resonant circuit



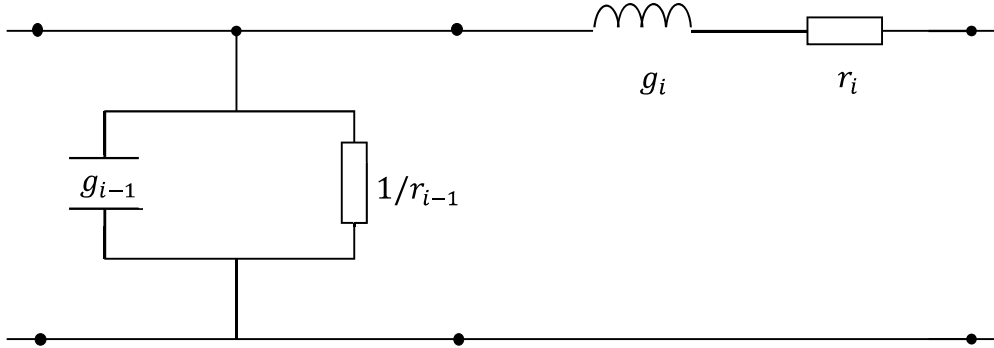
(b) Equivalent circuit of BPF circuit in resonance state



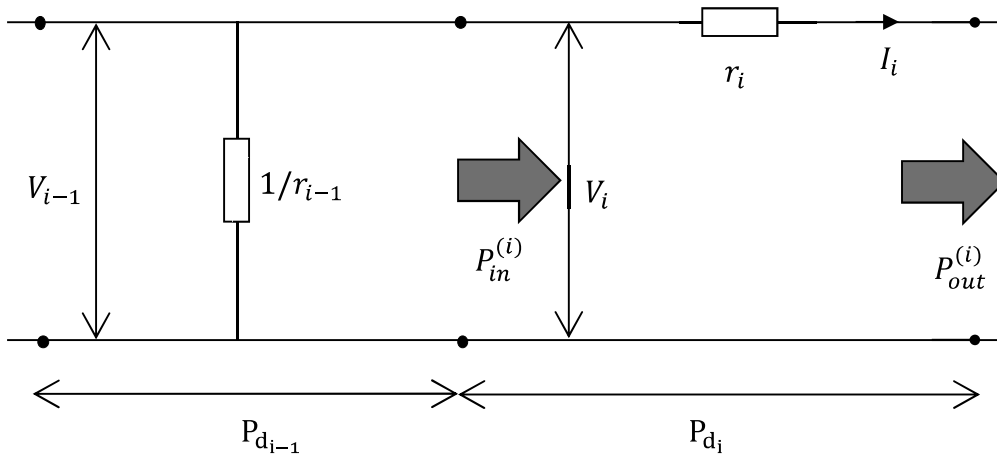
(c) LPF circuit based on BPF circuit



(d) Equivalent circuit of LPF circuit in direct current (DC)



(e) Fundamental element values of LPF circuit



(f) Fundamental element values of LPF circuit in direct current (DC)

Figure 2.17 Equivalent Circuit of n -stage BPF Resonant Circuit.

In Figure 2.17 (a), the unloaded Q : Q_u of the i_{th} prototype element value and the $(i-1)_{th}$ prototype element value in the resonant circuit are given by the following equations:

$$Q_{u_{i-1}} = \frac{\omega_0^{BPF} C_{i-1}^{BPF}}{G_{i-1}} \quad (2.42)$$

$$Q_{u_i} = \frac{\omega_0^{BPF} L_i^{BPF}}{R_i} \quad (2.43)$$

In this case, the resonance frequencies of both resonant circuits are set as equal, as follows:

$$\omega_0^{BPF} = \frac{1}{\sqrt{L_{i-1}^{BPF} C_{i-1}^{BPF}}} = \frac{1}{\sqrt{L_i^{BPF} C_i^{BPF}}} \quad (2.44)$$

Next, Figure 2.17 (a) is converted into an RLC ladder-type low-pass filter (LPF) circuit, as shown in Figure 2.17 (c). However, because of the conversion from the LPF to BPF relationship, the equation can be expressed using C_{i-1}^{BPF} , C_{i-1} , L_i^{BPF} and L_i as follows:

$$C_{i-1}^{BPF} = \frac{\omega_c}{\omega_{c2}^{BPF} - \omega_{c1}^{BPF}} C_{i-1} \quad (2.45)$$

$$L_i^{BPF} = \frac{\omega_c}{\omega_{c2}^{BPF} - \omega_{c1}^{BPF}} L_i \quad (2.46)$$

Figure 2.17 (c) can be modified to Fig 2.17 (d) when $\omega = 0$. Then, by substituting equations (2.45) and (2.46) into equations (2.42) and (2.43), respectively, the following equations are obtained:

$$Q_{u_{i-1}} = \frac{\omega_0^{BPF}}{G_{i-1}} \left(\frac{\omega_c}{\omega_{c2}^{BPF} - \omega_{c1}^{BPF}} \right) C_{i-1} \quad (2.47)$$

$$Q_{u_i} = \frac{\omega_0^{BPF}}{R_i} \left(\frac{\omega_c}{\omega_{c2}^{BPF} - \omega_{c1}^{BPF}} \right) L_i \quad (2.48)$$

By modifying equations (2.47) and (2.48), the following equations are established:

$$G_{i-1} = \frac{\omega_0^{BPF}}{Q_{u_{i-1}}} \left(\frac{\omega_c}{\omega_{c2}^{BPF} - \omega_{c1}^{BPF}} \right) C_{i-1} \quad (2.49)$$

$$R_i = \frac{\omega_0^{BPF}}{Q_{u_i}} \left(\frac{\omega_c}{\omega_{c2}^{BPF} - \omega_{c1}^{BPF}} \right) L_i \quad (2.50)$$

The normalized element values for C_{i-1} of equation (2.49) and L_i of equation (2.50) can be expressed as follows:

$$C_{i-1} = \frac{1}{\overline{\omega_c R_0}} g_{i-1} \quad (2.51)$$

$$L_i = \frac{\overline{R_0}}{\overline{\omega_c}} g_i \quad (2.52)$$

Similarly, the normalized element values for R_i in equation (2.50) and G_{i-1} in equation (2.49) can be expressed as follows:

$$R_i = \overline{R_0} r_i \quad (2.53)$$

$$G_{i-1} = \frac{1}{\overline{R_0} r_{i-1}} \quad (2.54)$$

where $\overline{R_0}$ and $\overline{\omega_c}$ are dimensionless quantities, $\overline{R_0}$ is a value corresponding to the internal impedance of the power supply side, and $\overline{\omega_c}$ is a quantity corresponding to the cutoff frequency. Then, equations (2.51) and (2.54) are substituted into equation (2.47), resulting in the following equation:

$$r_{i-1}^{-1} = \frac{1}{Q_{u_{i-1}}} \left(\frac{\omega_c}{\omega_{c2}^{BPF} - \omega_{c1}^{BPF}} \right) g_{i-1} \quad (2.55)$$

Again, equations (2.52) and (2.53) are substituted into equation (2.50) to obtain

$$r_i = \frac{1}{Q_{u_i}} \left(\frac{\omega_c}{\omega_{c2}^{BPF} - \omega_{c1}^{BPF}} \right) g_i \quad (2.56)$$

where

$$\frac{\omega_0}{\overline{\omega_0}} = 1 \quad [\text{rad/s}] \quad (2.57)$$

If normalized element values are applied to Figure 2.15 (c), the circuit can be expressed as shown in Figure 2.17 (e). Then, the equivalent circuit when $\omega = 0$ can be drawn as shown in Figure 2.17 (f). In this case, if each parameter for the voltage and current values

is defined as Figure 2.17 (f), the power loss for the both ($i-1$ th) and i th prototype element values is given as follows:

$$P_{d_{i-1}} = \frac{V_{i-1}^2}{r_{i-1}} = \frac{\omega_0^{BPF}}{\omega_{c2}^{BPF} - \omega_{c1}^{BPF}} \frac{g_{i-1}}{Q_{u_{i-1}}} V_{i-1}^2 \quad (2.58)$$

$$P_{d_i} = r_i I_i^2 = \frac{\omega_0^{BPF}}{\omega_{c2}^{BPF} - \omega_{c1}^{BPF}} \frac{g_i}{Q_{u_i}} I_i^2 \quad (2.59)$$

Here, if the power loss of the resonant circuit is too small, the following approximations can be used:

$$V_i \approx V \quad (i = 1, 2, 3, \dots) \quad (2.60)$$

$$I_i \approx I \quad (i = 1, 2, 3, \dots) \quad (2.61)$$

The element value for the termination resistance is

$$r_0 = \frac{R_0}{R_0} = 1 \quad [\Omega] \quad (2.62)$$

Hence, from the termination resistance above, the relationship equation between the voltage and the current can be derived as follows:

$$I = \frac{V}{r_0} = V \quad (2.63)$$

Next, equations (2.60), (2.61), and (2.63) are substituted into equation (2.58) and equation (2.59), respectively; hence, the following equation can be obtained:

$$P_{d_{i-1}} = \frac{\omega_0^{BPF}}{\omega_{c2}^{BPF} - \omega_{c1}^{BPF}} \frac{g_{i-1}}{Q_{u_{i-1}}} V^2 \quad (2.64)$$

$$P_{d_i} = \frac{\omega_0^{BPF}}{\omega_{c2}^{BPF} - \omega_{c1}^{BPF}} \frac{g_i}{Q_{u_i}} V^2 \quad (2.65)$$

Here, the i_{th} prototype of the element value for the resonator is applied to the input power source in the LPF circuit shown in Figure 2.17 (f), so the input power can be expressed as follows:

$$P_{in}^{(i)} (= P_{out}^{(i-1)}) = IV + \frac{1}{2}P_{d_i} = V^2 + \frac{1}{2}P_{d_i} \quad (2.66)$$

Therefore, the output power from this circuit is given as follows:

$$P_{out}^{(i)} (= P_{in}^{(i+1)}) = IV - \frac{1}{2}P_{d_i} = V^2 - \frac{1}{2}P_{d_i} \quad (2.67)$$

The insertion loss based on the i_{th} prototype element value of the resonator can be expressed as follows:

$$L_i = 10 \log_{10} \frac{P_{in}^{(i)}}{P_{out}^{(i)}} = 10 \log_{10} \frac{V^2 + \frac{1}{2}P_{d_i}}{V^2 - \frac{1}{2}P_{d_i}} = 10 \log_{10} \frac{1 + \frac{1}{2}\frac{P_{d_i}}{V^2}}{1 - \frac{1}{2}\frac{P_{d_i}}{V^2}} \quad (2.68)$$

Next, the above equation can be further approximated as follows:

$$\begin{aligned} L_i &\approx 10 \log_{10} \frac{\left(1 + \frac{1}{2}\frac{P_{d_i}}{V^2}\right)^{\frac{1}{2}}}{\left(1 - \frac{1}{2}\frac{P_{d_i}}{V^2}\right)^{-\frac{1}{2}}} = 10 \log_{10} \left(1 + \frac{P_{d_i}}{V^2}\right) \\ &\approx 4.343 \log_e \left(1 + \frac{P_{d_i}}{V^2}\right) \\ &\approx 4.343 \frac{P_{d_i}}{V^2} \end{aligned} \quad (2.69)$$

$$\because \frac{P_{d_i}}{V^2} \ll 1 \text{ and } \log_e(1+x) \approx x \text{ (} 0 < x \ll 1 \text{)} \quad (2.70)$$

Hence, equation (2.69) is substituted into equation (2.65), so the insertion loss for the i_{th} prototype element value of the resonator would be:

$$L_i \approx 4.343 \frac{\omega_0^{BPF}}{\omega_{c2}^{BPF} - \omega_{c1}^{BPF}} \frac{g_i}{Q_{u_i}} \quad [\text{dB}] \quad (2.71)$$

The overall insertion loss of the BPF circuit is given by the following equation:

$$L = \sum_{i=1}^n L_i = 4.343 \frac{\omega_0^{BPF}}{\omega_{c2}^{BPF} - \omega_{c1}^{BPF}} \sum_{i=1}^n \frac{g_i}{Q_{u_i}} \quad (2.72)$$

The fractional bandwidth w is defined as follows:

$$w = \frac{\omega_{c2}^{BPF} - \omega_{c1}^{BPF}}{\omega_0^{BPF}} \quad (2.73)$$

Based on equation (2.66), the insertion loss of the n -stage BPF can be transformed into a two-stage BPF circuit, so the transmission loss [40] of the circuit would be:

$$L = 4.343 \frac{1}{w} \sum_{i=1}^n \frac{g_i}{Q_{u_i}} \quad [\text{dB}] \quad (2.74)$$

where the value of g is determined by the type of the filter.

Since the design of the equivalent circuit of the RC-WPT system was based on the two-stage Wagner Butterworth filter model, $g_1 = g_2$ is inserted into equation (2.74) and the following relationship can be established between the specific bandwidth w and the coupling coefficient k :

$$w = \sqrt{2}k \quad (2.75)$$

Since the unloaded Q : Q_u of the two spiral resonators used are the same, equation (2.74) can be modified and expressed as follows:

$$L = \frac{8.686}{kQ_u} \quad [\text{dB}] \quad (2.76)$$

Hence, the theoretical value of the power transmission efficiency of the RC-WPT system, η_T [%] is obtained from the transmission loss, L using the following equation:

$$\eta_T = 10^{-\frac{L}{10}} \times 100 \quad [\%] \quad (2.77)$$

To measure the experimental power transmission efficiency of the RC-WPT system, the spiral resonators were placed in the measurement setup shown in Figure 2.1 and the VNA was connected to the loop coils for the Tx and Rx units. From the amplitude reflection coefficient $|S_{11}|$ and the amplitude transmission coefficient $|S_{21}|$ measured by the VNA, the experimental value of power transmission efficiency of the system, η [%] is as follows:

$$\eta_E = \frac{10^{\frac{|S_{21}|}{10}}}{1 - 10^{\frac{|S_{11}|}{10}}} \times 100 \quad [\%] \quad (2.78)$$

The above equation is used to measure the ratio between two resonators. Moreover, the equation is the power transmission efficiency between the resonators in Tx and Rx units as the effect of reflection from the input port is removed using the formula of the denominator.

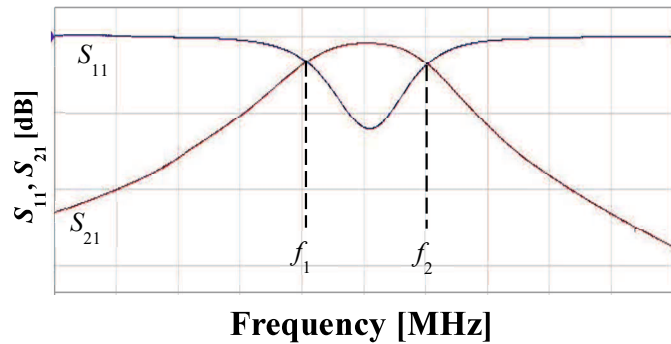


Figure 2.18 Frequency characteristic of S_{11} and S_{21} in VNA.

2.6.2 Results of Power Transmission Efficiency of RC-WPT

Systems

According to the design theory of the BPF circuit, to obtain the maximum power transmission efficiency of the RC-WPT system, the matching conditions for the RC-WPT system must be determined. The system matching conditions are the inverse of the external k : k_e as a function of distance a [cm], which is equal to the coupling coefficient k between the resonators as a function of d [cm]. Here, the sets of a and d can be obtained from the relation, $k = k_e$. For example, in the case of a system using Single-Spiral #2, as shown in Figure 2.19, when the distance a is 5.0 cm, the value of k_e is 0.017. Then, using the same value of k_e and the coupling coefficient k , which is 0.017, the distance between the spiral resonators d is determined as 50.0 cm, as shown in Figure 2.20.

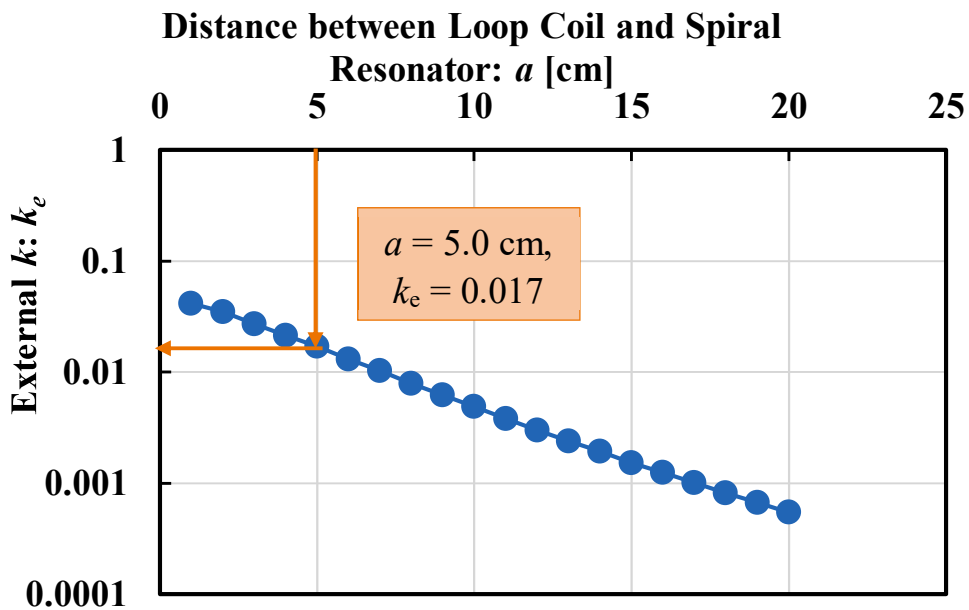


Figure 2.19 Matching Conditions for External k : k_e .

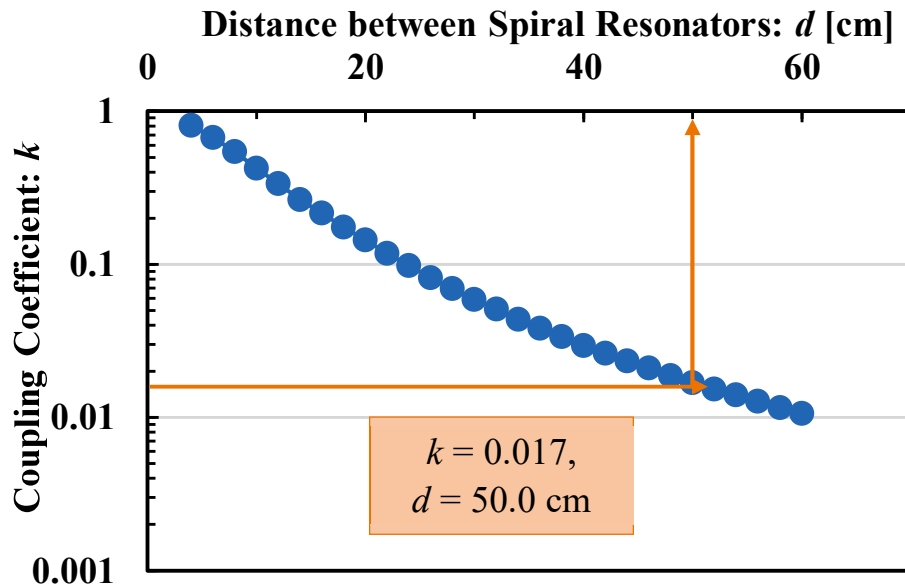


Figure 2.20 Matching Conditions for Coupling Coefficient k .

By choosing the set of a and d under matching conditions, after some fine adjustment of the distance d , the maximum power transmission efficiency was measured. This is shown in Figure 2.21.

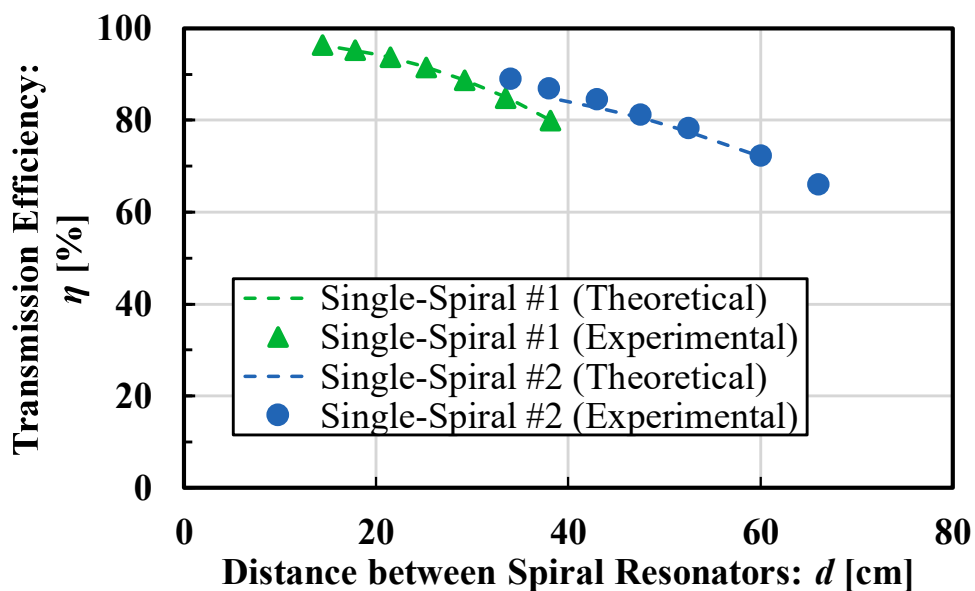


Figure 2.21 Results for Power Transmission Efficiency of RC-WPT System for Single-Spiral Resonators.

The results indicate that the theoretical and experimental values of the power transmission efficiency have good agreement between each other. In each spiral resonator, when the distance d increased, the power transmission efficiency of the RC-WPT system decreased. For Single-Spiral #1, the power transmission efficiency of the system is larger than that of Single-Spiral #2; however, the range of distance d where the power transmission efficiency is larger than 60% is smaller than that of Single-Spiral #2. This is because the structural parameters between those parameters differ. Since the coupling coefficient k of Single-Spiral #2 is larger than that of Single-Spiral #1, the range of distance d of the system's power transmission efficiency is larger for the system using Single-Spiral #2 than the one using Single-Spiral #1. However, since the diameter of Single-Spiral #2 is slightly greater than that of Single-Spiral #1, the wider spiral resonator generates an electromagnetic field. Here, the spread of the electric field formed by the resonator is larger, resulting in a larger loss. Therefore, the power transmission efficiency of the RC-WPT system for Single-Spiral #2 is lower than that of Single-Spiral #1 although the range of distance d where the power transmission efficiency is larger than 60% is wide.

2.7 Summary

The principle and the design procedure of the RC-WPT system using an equivalent circuit model of the system that is identical to the two-stage BPF circuit have been discussed in this chapter. Based on the BPF circuit design theory, the measurement methods and results of the properties of key elements of the RC-WPT system have been examined, including the Q -factors for the resonant system, the coupling coefficient between the spiral resonators, and the power transmission efficiency of the system using single-spiral resonators. These measured results showed it is important to consider many aspects of the optimum conditions to improve the RC-WPT system considerably.

Chapter 3: Effect of Lossy Mediums on the RC-WPT System

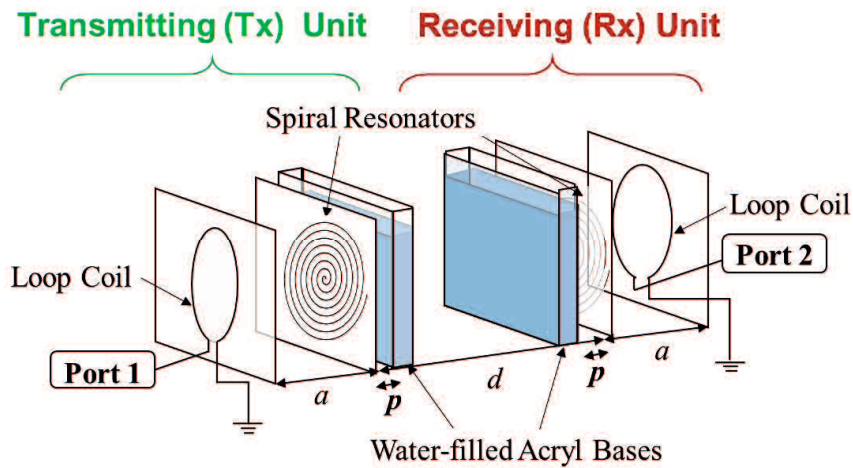
3.1 Foreword

The RC-WPT system has a longer power transmission distance than that of conventional WPT systems using the electromagnetic induction phenomena. So, the power transmission efficiency and operational reliability of the RC-WPT system are influenced by the environmental factors of the power transmission path, such as the presence of moisture-containing obstacles. In RC-WPT systems, the presence of obstacles with dielectric and/or conductive losses in the power transmission path, so-called lossy mediums, cause the transmitted power to decay; thus, the power transmission efficiency is decreased [22]-[25]. To make the RC-WPT systems truly practical, actions must be taken to prevent the effects of obstacles that exist in the power transmission path. In this chapter, the effect of lossy mediums on the RC-WPT system with the spiral resonator is experimentally investigated in detail and a proposed spiral resonator with a novel structure to prevent the effect of lossy mediums and the appropriate placement for constructive elements of the RC-WPT system are discussed.

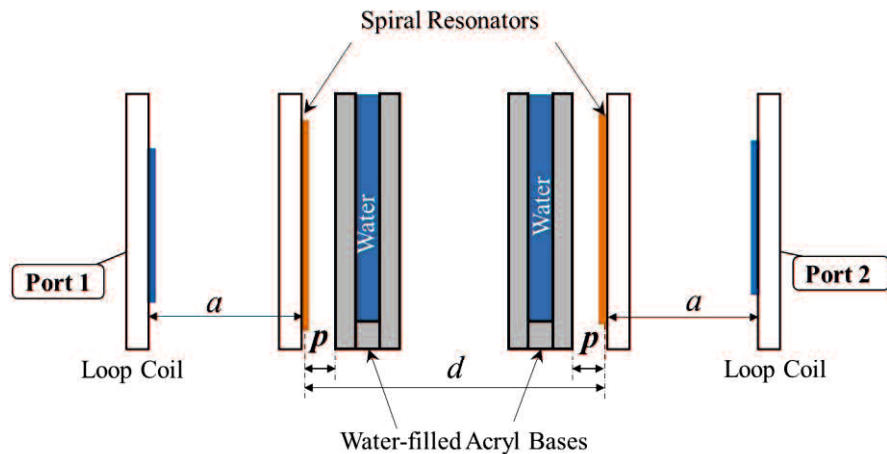
3.2 Measurement Setup for the RC-WPT System with Lossy Mediums

Figure 3.1 shows the configuration setup for the RC-WPT system, which involved the insertion of water-filled acryl bases or lossy mediums in the Tx and Rx units of the system.

The measurement setup is the same as that of the conventional RC-WPT system presented in Section 2.2, except for the insertion of the water-filled acryl bases.



(a) Schematic Setup



(b) Cross-sectional View of Measurement Setup

Figure 3.1 Configuration setup of RC-WPT System with Lossy Mediums.

Figure 3.2 shows the dimensions of the water-filled acryl bases, which are used as alternatives to water-containing obstacles in the RC-WPT system. In this figure, $w = 0.5$ cm is the width of the gap between two acryl plates, while $t = 0.5$ cm and $h = 50.0$ cm are the thickness and height of the acryl plates, respectively. Here, the distance p represents the distance between the spiral resonators and the lossy mediums; this is an important parameter of this measurement setup. When the distance p is short, this means the lossy mediums are close to the spiral resonators. The changes in distance p would affect the performance of the system when lossy mediums are inserted along the transmission path.

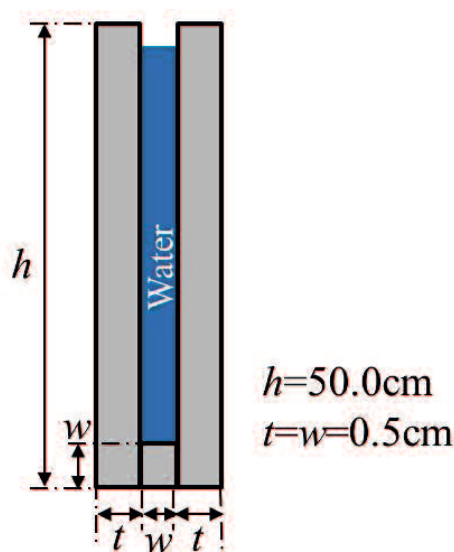


Figure 3.2 Dimension of Water-filled Acryl Bases.

For the lossy mediums, pure or tap water-filled acryl bases are used in this study. The acryl bases are kinds of lossy mediums with dielectric loss that also act as water containers. To ensure no errors occurred when observing the results, the acryl bases must

be clean when doing the experiments. Then, the acrylic bases are filled with pure or tap water. In this experiment, the conductivity of the tap water is approximately $223\mu\text{S}/\text{cm}$, whereas the conductivity of pure water is negligibly less than $0.1\mu\text{S}/\text{cm}$. In fact, water is a dielectric material with high permittivity. Tap water contains dissolved ionic salts, whereas pure water has been filtered and processed to remove impurities. As a result, when electric energy is transmitted through tap or pure water in the RC-WPT system, tap water dissipates the extremely substantial electric energy more than pure water.

As for the spiral resonators used in the system, Single-Spiral #1 and Single-Spiral #2, as mentioned in Chapter 2, are used. To characterize a single spiral resonator with adjacent lossy mediums, several parametric quantities need to be re-examined, such as the Q -factor and the coupling coefficient with the lossy mediums, since the performance of the system is affected by changes in these parameters. So, the following sections discuss the Q -factors, the coupling coefficient, and the power transmission efficiency of the system when lossy mediums exist in the power transmission path.

3.2.1 Q -factors with Lossy Mediums

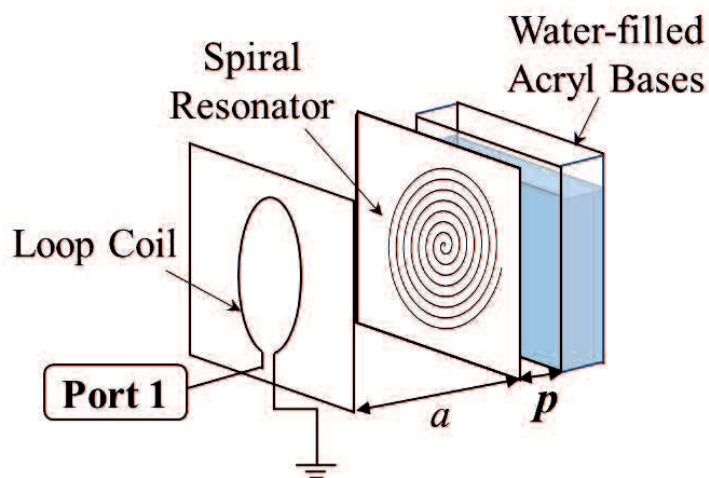


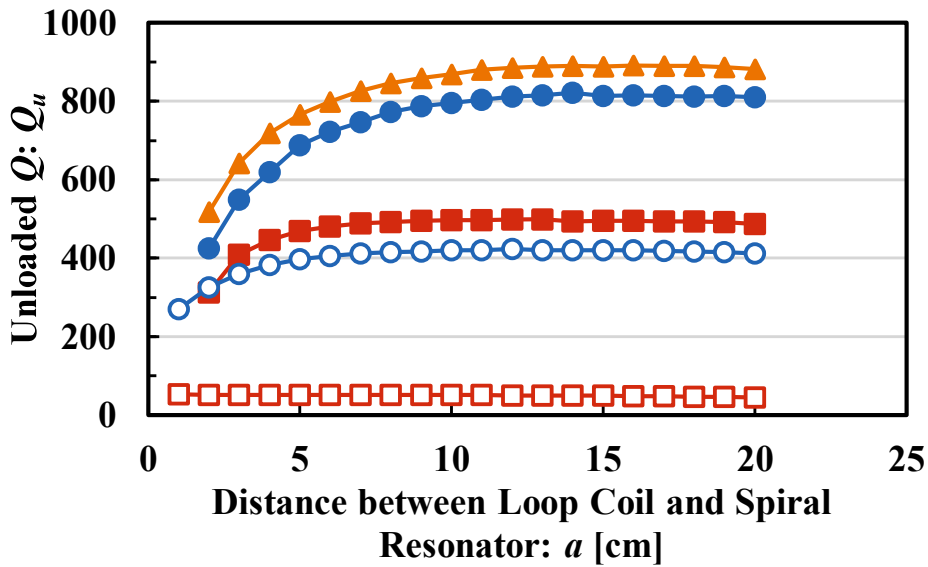
Figure 3.3 Measurement Setup of Q -factors with Lossy Mediums.

Figure 3.3 shows the measurement setup of the Q -factors with lossy mediums inside the RC-WPT system. This measurement setup is almost the same as the measurement setup outlined in Section 2.4.1, except for the installation of lossy mediums. By using this measurement setup, the unloaded Q : Q_u , the external Q : Q_e , and the external k : k_e with lossy mediums for the single-spiral resonators can be measured simultaneously. However, only the results for the unloaded Q : Q_u are presented in this section. The unloaded Q : Q_u with pure or tap water-filled acryl bases are measured by changing the distance between the single-spiral resonator and the acryl base from $p = 1.0$ cm to 7.0 cm.

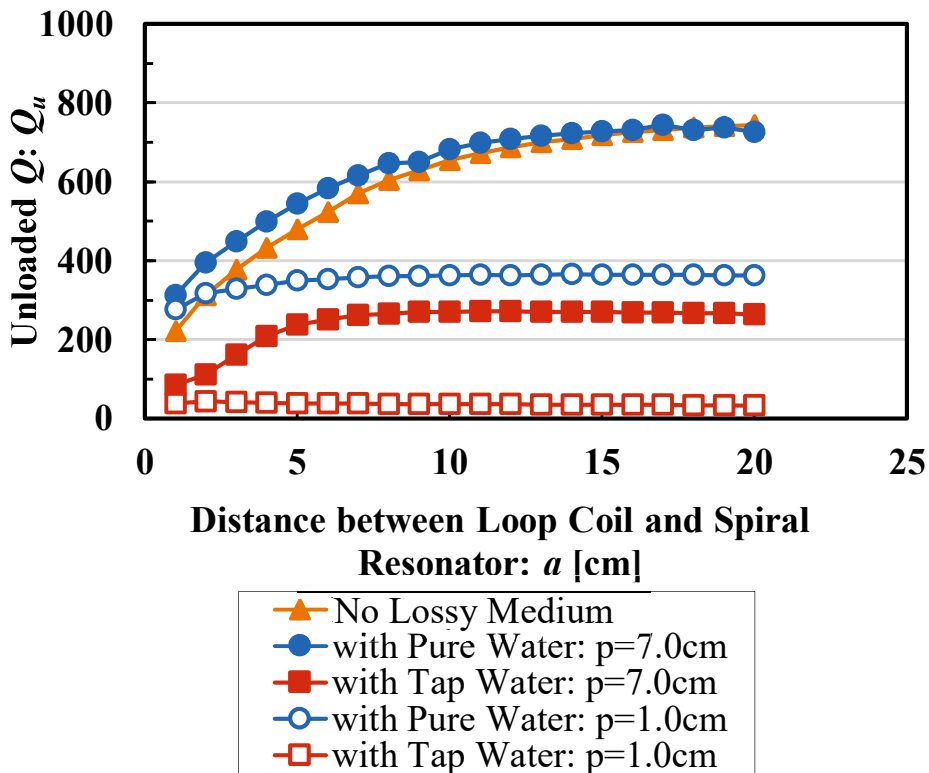
Figure 3.4 shows the results of the unloaded Q : Q_u with pure or tap water-filled acryl bases located at $p = 1.0$ cm and 7.0 cm. Single-Spiral #1 and Single-Spiral #2 were used for the cases in which the wire spacing of the spiral resonator $s_1 = 0.5$ cm and

$s_2 = 1.0$ cm, respectively. Here, the system with the pure water-filled acryl bases is defined as ■ and □, whereas the system with the tap water-filled acryl bases is defined as ● and ○. In the same figure, the results for the unloaded $Q: Q_u$ without lossy mediums for the single-spiral resonators (see Figure 2.12 in Chapter 2) are also included to show the comparison; these are represented by the triangle marks, ▲.

From the results shown in Figure 3.4, when the pure or tap water-filled acryl bases are inserted into the RC-WPT system, the unloaded $Q: Q_u$ for each spiral resonator drastically decreased compared to the equivalent without lossy mediums. This result indicates that the lossy mediums that existed on the power transmission path affected the deteriorating properties of the spiral resonators. On the contrary, as distance p increased, the unloaded $Q: Q_u$ obviously increased. Especially for Single-Spiral #2, it approached the equivalent without lossy mediums when $p = 7.0$ cm. Meanwhile, for Single-Spiral #1, the unloaded $Q: Q_u$ with lossy mediums when $p = 7.0$ cm was still further than that without lossy mediums. Here, the decreased rate for Single-Spiral #1 is larger than that of Single-Spiral #2. However, the unloaded $Q: Q_u$ with lossy mediums for Single-Spiral #1 is higher than that of Single-Spiral #2.



(a) Single-Spiral #1



(b) Single-Spiral #2

Figure 3.4 Results of Unloaded $Q: Q_u$ with Pure or Tap Water-filled Acryl Bases for Single-Spiral Resonators when $p = 1.0$ cm and 7.0 cm.

3.2.2 Coupling Coefficients with Lossy Mediums

Next, the coupling coefficient with lossy mediums for the single-spiral resonators is examined. Figure 3.5 shows the measurement setup of the coupling coefficient with lossy mediums. This measurement setup is almost the same as the measurement setup in Section 2.5.1, except for the installation of lossy mediums. Then, by changing the distance from $p = 1.0$ cm to 7.0 cm, the coupling coefficient with lossy mediums for Single-Spiral #1 and Single-Spiral #2 is examined.

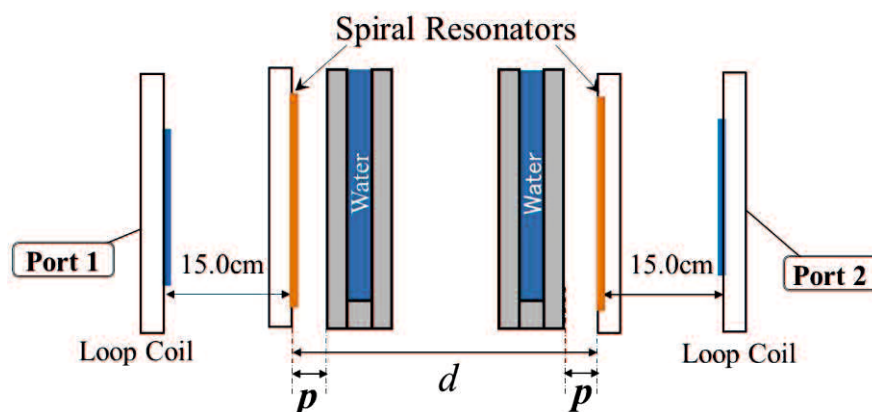
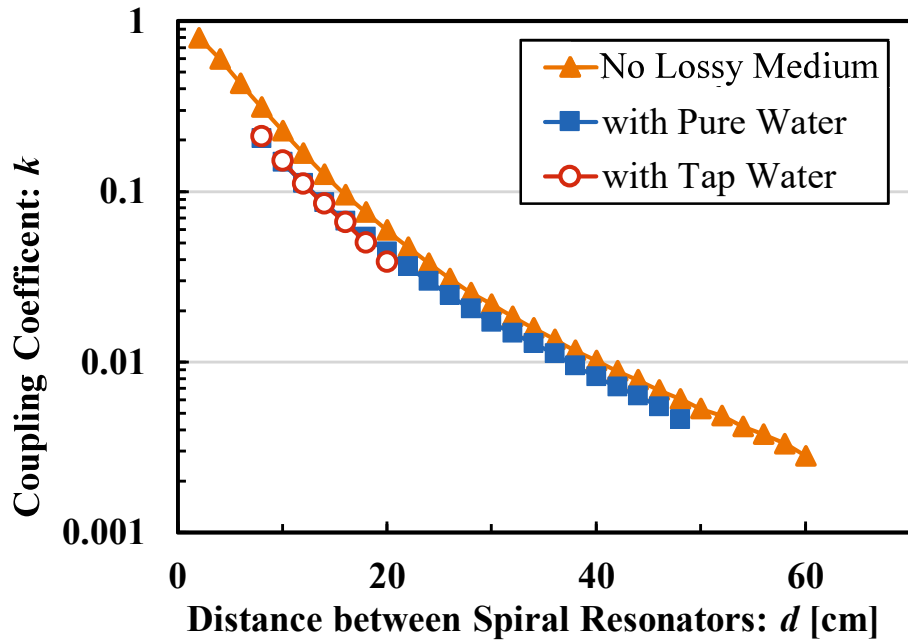


Figure 3.5 Measurement Setup of Coupling Coefficient with Lossy Mediums.

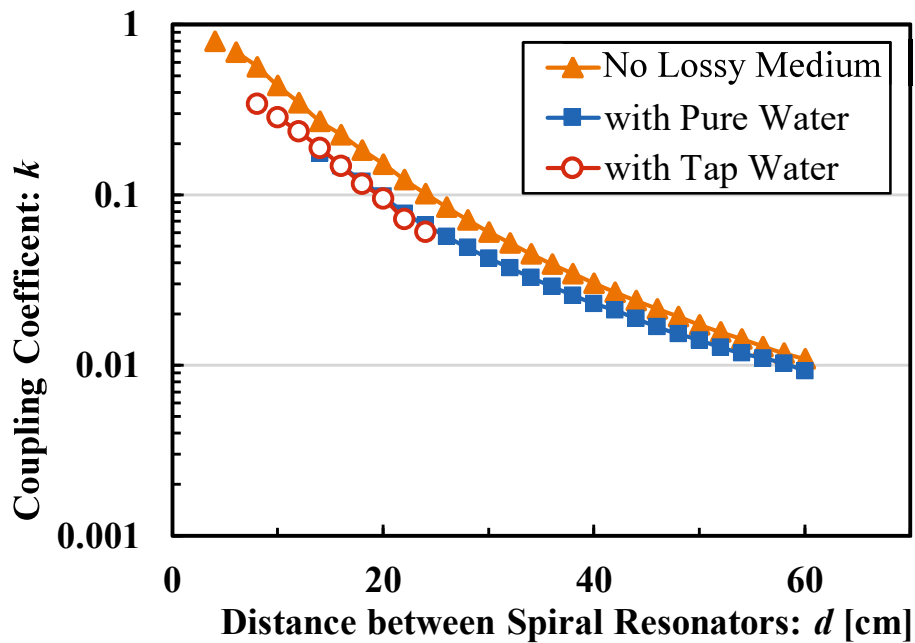
Figures 3.6 and 3.7 show the results for coupling coefficients using Single-Spiral #1 and Single-Spiral #2 when $p = 1.0$ cm and 7.0 cm, respectively. In the same figures, the system with pure water-filled acryl bases is represented as the symbol \circ , and the system with tap water-filled acryl bases is represented as the symbol \blacksquare . The coupling coefficient

k without lossy mediums (see Figure 2.16 in Section 2.5.2) for the single-spiral resonators

is also included to show the comparison; this is shown as the triangle marks, \blacktriangle .

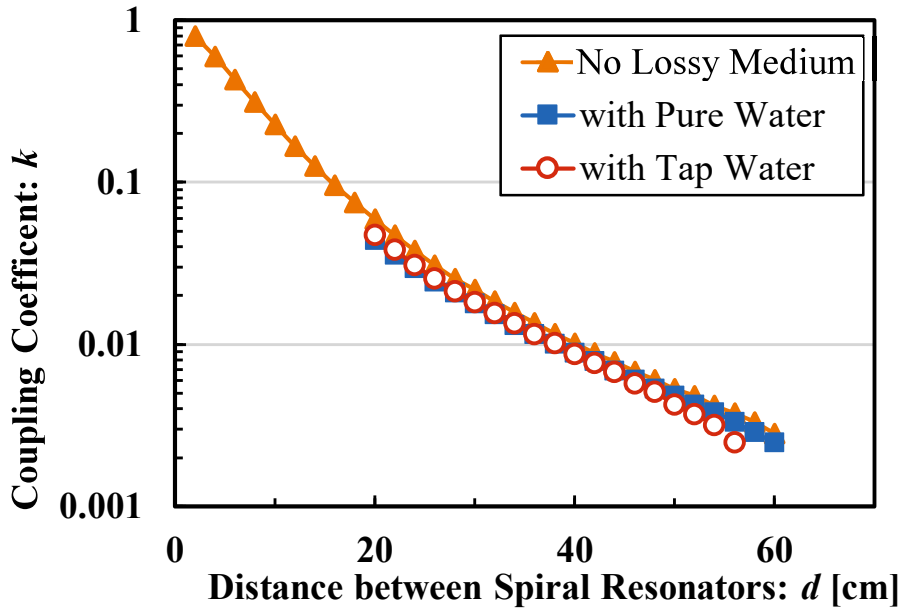


(a) Single-Spiral #1

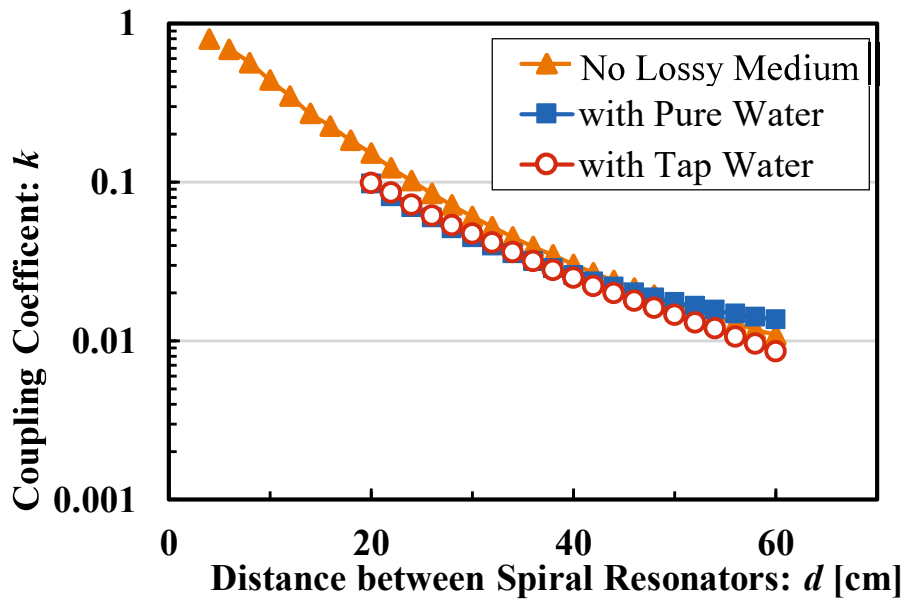


(b) Single-Spiral #2

Figure 3.6 Results of Coupling Coefficients with Lossy Mediums for Single-Spiral Resonators ($p = 1.0$ cm).



(a) Single-Spiral #1



(b) Single-Spiral #2

Figure 3.7 Results of Coupling Coefficients with Lossy Mediums for Single-Spiral Resonators ($p = 7.0$ cm).

From the results shown in Figures 3.6 and 3.7, when the pure or tap water-filled acrylic bases are close to the spiral resonators, the coupling coefficients for each resonator are lower than those without lossy mediums inside the system. In addition, the differences

between the coupling coefficients with and without lossy mediums were obviously smaller and had not changed as much as those of the unloaded $Q: Q_u$ (see Figure 3.4).

3.2.3 Power Transmission Efficiency with Lossy Mediums

As mentioned previously, the Q -factor and the coupling coefficient with lossy mediums in the RC-WPT system need to be examined because they affected the performance of the system. After examining the Q -factors and the coupling coefficients with lossy mediums, the power transmission efficiency of the RC-WPT system with lossy mediums for Single-Spiral #1 and Single-Spiral #2 can be evaluated. The measurement setup for the power transmission efficiency of the RC-WPT system with lossy mediums is exactly the same as the measurement setup shown in Figure 3.1. According to the design theory of the BPF circuit, the distances a and d must be set to satisfy the system matching conditions to obtain the maximum power transmission efficiency for each RC-WPT system. Since the measurements of the unloaded $Q: Q_u$ and the coupling coefficient k with lossy mediums have been reported in the previous section, the theoretical value of the power transmission efficiency of the RC-WPT system with lossy mediums can be examined using equation (2.77), as outlined in Section 2.6.1.

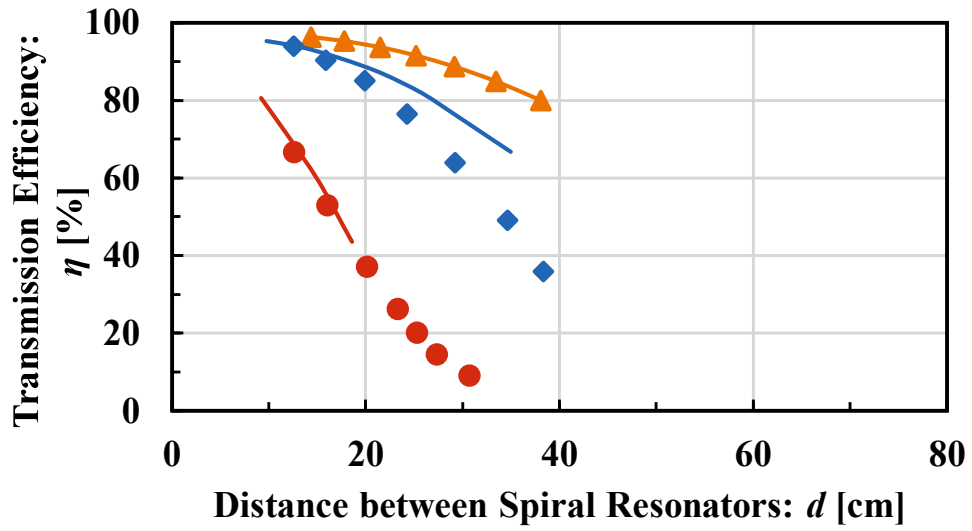
The results from the measurement of the theoretical and experimental values of power transmission efficiency of the system when pure or tap water-filled acryl bases

were used for Single-Spiral #1 and Single-Spiral #2, and where $p = 1.0$ and 7.0 cm, are shown in Figures 3.8 and 3.9, respectively. In these figures, the power transmission efficiency of the system without lossy mediums (see Figure 2.21) is also shown for comparison; this is represented by the symbol ▲. Meanwhile, the symbol ■ indicates the measured experimental results in the systems with a pure water-filled acryl base, while the symbol ● indicates the measured experimental results in the systems with a tap water-filled acryl base. Here, the dashed lines are the theoretical results estimated using equation (2.72).

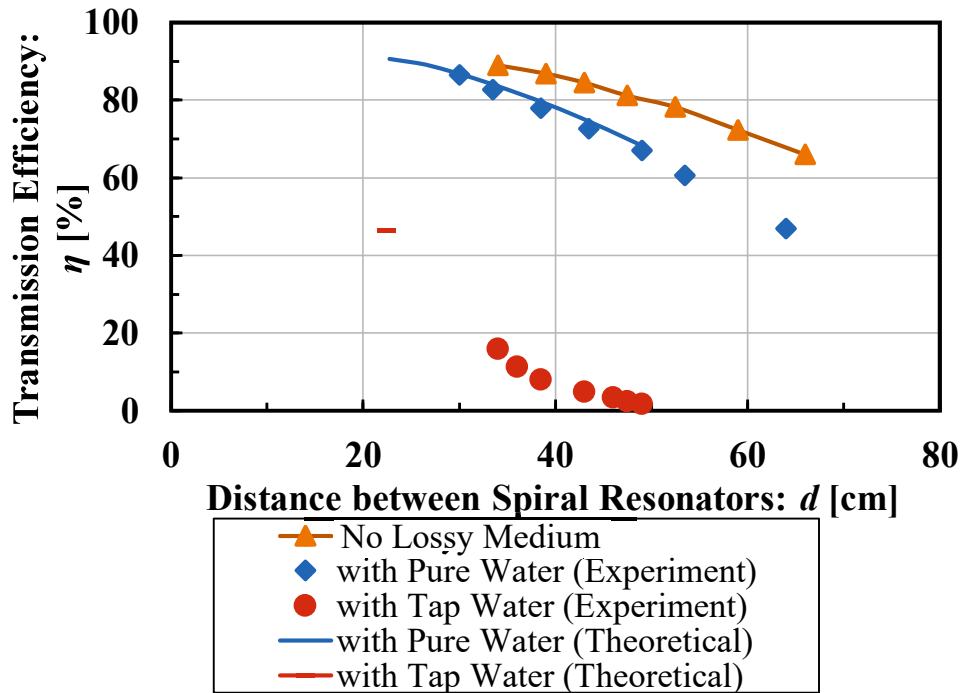
From the results shown in Figures 3.8 and 3.9, the theoretical and experimental values of the power transmission efficiency of the RC-WPT system for each spiral resonator show good agreement between each other except the power transmission efficiency of the system with tap water-filled acryl bases using Single-Spiral #2, as shown in Figure 3.8 (b). Here, when the distance p is short, this means the tap water-filled acryl bases are closer to the single-spiral resonators, the power transmission efficiency of the system decreases and only a few theoretical systems matching conditions are satisfied.

In the same figures, when the pure or tap water-filled acryl bases are inserted, the power transmission efficiency of the RC-WPT system for each resonator is far lower than that of the system with no lossy mediums. The reason is an acryl base is only a

dielectric material, whereas tap water and pure water are combinations of dielectric and conductive loss materials with high permittivity. If water-filled acrylic bases are inserted into the system, the effect of the dielectric and conductive loss will dissipate from the water, as will the dielectric loss from the acrylic bases. Thus, the electric fields leaked from the spiral resonators would be attenuated because of the dielectric and conductive loss [43], [44]. These decays cause reductions in electromagnetic energy and transmitted electric power. Furthermore, in each spiral resonator, the power transmission efficiency of the system with tap water-filled acrylic bases is lower than the system with pure water-filled acrylic bases. Due to the high conductivity of tap water, the power transmission efficiency of the system decreases. As described in Section 3.1, tap water has higher conductivity than pure water. As a result, the tap water-filled acrylic bases result in a lower transmission efficiency of the RC-WPT system than the bases with pure water.

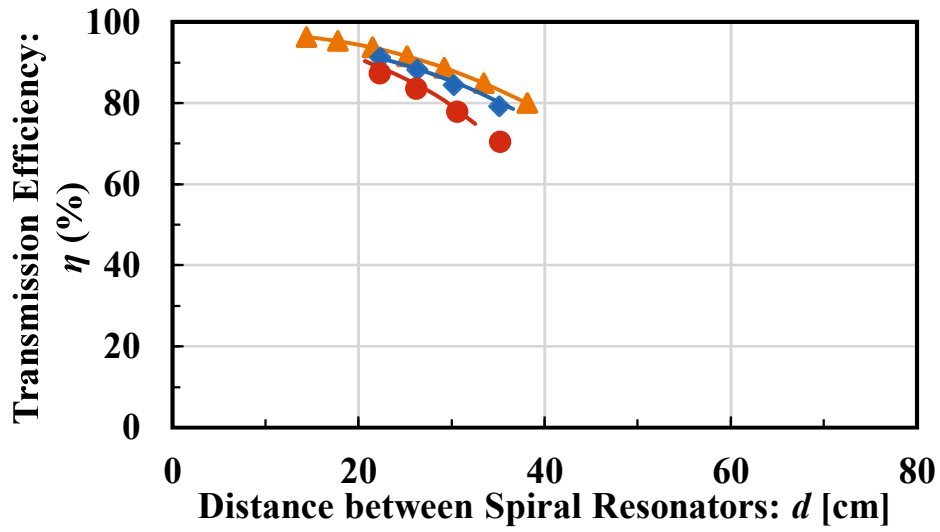


(a) Single-Spiral #1

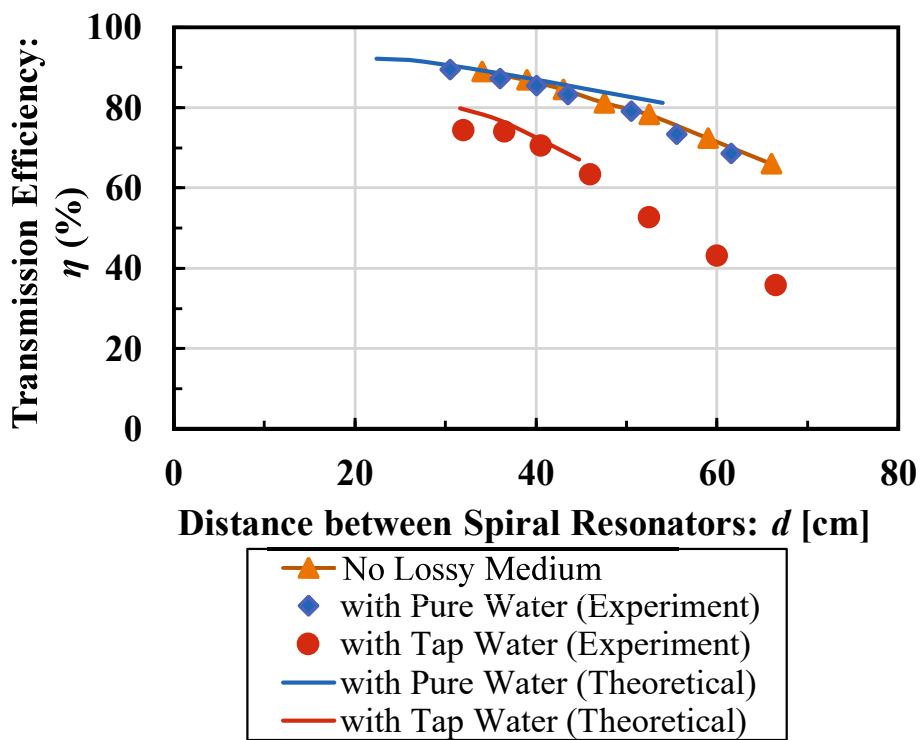


(b) Single-Spiral #2

Figure 3.8 Results of Power Transmission Efficiency of RC-WPT System with Lossy Mediums ($p = 1.0$ cm).



(a) Single-Spiral #1



(b) Single-Spiral #2

Figure 3.9 Results of Power Transmission Efficiency of RC-WPT System with Lossy Mediums ($p = 7.0$ cm).

As shown in Figures 3.8 and 3.9, when the distance p is the same, the decreased rate for Single-Spiral #1 is smaller and the power transmission efficiency of the system is higher than that of the system for Single-Spiral #2. However, the range of distance d where the transmission efficiency is larger than 40% is much narrower and only a few systems matching conditions were satisfied for Single-Spiral #1 (see Figure 3.9 (a)). On the other hand, the range of distance d where the transmission efficiency is larger than 40% for Single-Spiral #2 is wider and all the systems matching conditions were satisfied. Since Single-Spiral #2 performed better than Single-Spiral #1, in the next investigation, the single-spiral was limited to Single-Spiral #2 only.

It has been observed that when lossy mediums are inside the system, the power transmission efficiency of the RC-WPT system decreases. Observing the measurement results of the unloaded Q : Q_u and the coupling coefficient k (see Sections 3.2.1 and 3.2.2), when the pure or tap water-filled acrylic bases are inserted inside the RC-WPT system, the changes in the unloaded Q : Q_u are obvious. However, the coupling coefficient k is not changed as much. According to equation (2.76) (see Section 2.6.1), the transmission loss L of the RC-WPT system is proportional to the inverse of the product kQ_u . These findings mean that the insertion of lossy mediums would affect the resonator properties. In

particular, the unloaded $Q: Q_u$ would result in a lower power transmission efficiency of the entire RC-WPT system. Therefore, the shape of the resonator needed to be modified.

3.3 Modified Structure of Spiral Resonators

In this study, the power transmission efficiency in the RC-WPT system is closely related to the spread of the electromagnetic field formed by the resonator. When a lossy medium exists in the power transmission path, the power transmission efficiency of the RC-WPT system decreases. Therefore, lossy mediums, which consist of conductive and dielectric losses, form the main problem of this study. In a lossy medium, the expression of the total current is composed of the conduction current and the displacement current, so the dielectric loss and conductive loss must be considered.

Assuming the flux density vector is D , the electric field vector is E and the dielectric constant is ε , the relationship between the three is expressed as follows:

$$D = \varepsilon E \quad (3.1)$$

which also indicates the amount that mainly affects the electric field. Therefore, the relational expressions concerning the displacement current density J_D , the electric flux vector D , and the electric field vector E are represented by the following:

$$J_D = \frac{\partial D}{\partial t} = \varepsilon \frac{\partial E}{\partial t} \quad \left[\frac{A}{m^2} \right] \quad (3.2)$$

Next, the conductive loss occurs due to the conductivity of the substance. The relationship between the conductivity, σ and the conduction current density, J_s is as follows:

$$J_s = \sigma E \quad \left[\frac{A}{m^2} \right] \quad (3.3)$$

which also represents the loss generated by acting in the electric field [4]. Therefore, based on equations (3.2) and (3.3), the total current density J is given as follows:

$$J = J_s + J_D = \sigma E + \varepsilon \frac{\partial E}{\partial t} \quad \left[\frac{A}{m^2} \right] \quad (3.4)$$

From the equations above, it can be clarified that the dielectric loss and conductive loss are caused by the electric field, E . Here, by constructing resonators that tend to confine the electric field vectors, as shown in Figure 3.10, the electric field is not leaked toward the power transmission path and it is possible to reduce the influence of the lossy mediums [45]-[47]. In addition, the dual-spiral resonator has no lumped elements such as capacitors

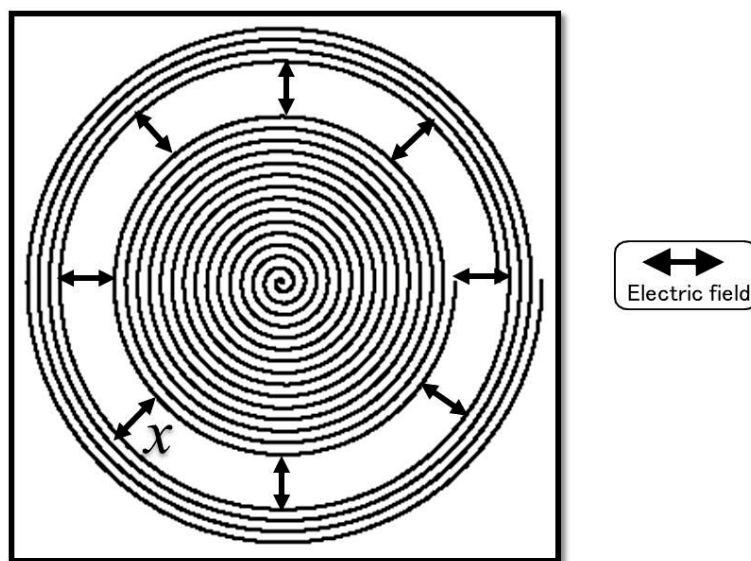


Figure 3.10 Image of Electric Field Lines in Dual-Spiral Resonators

[48], [49]; instead, the separation x between the resonators provides the capacitance component of the dual-spiral resonator. This is to increase the electric field vector of the resonator that lies in the spiral surface so that electric energy is confined in the resonator. Therefore, the dual-spiral resonator shown in Figure 3.11 is proposed in this study.

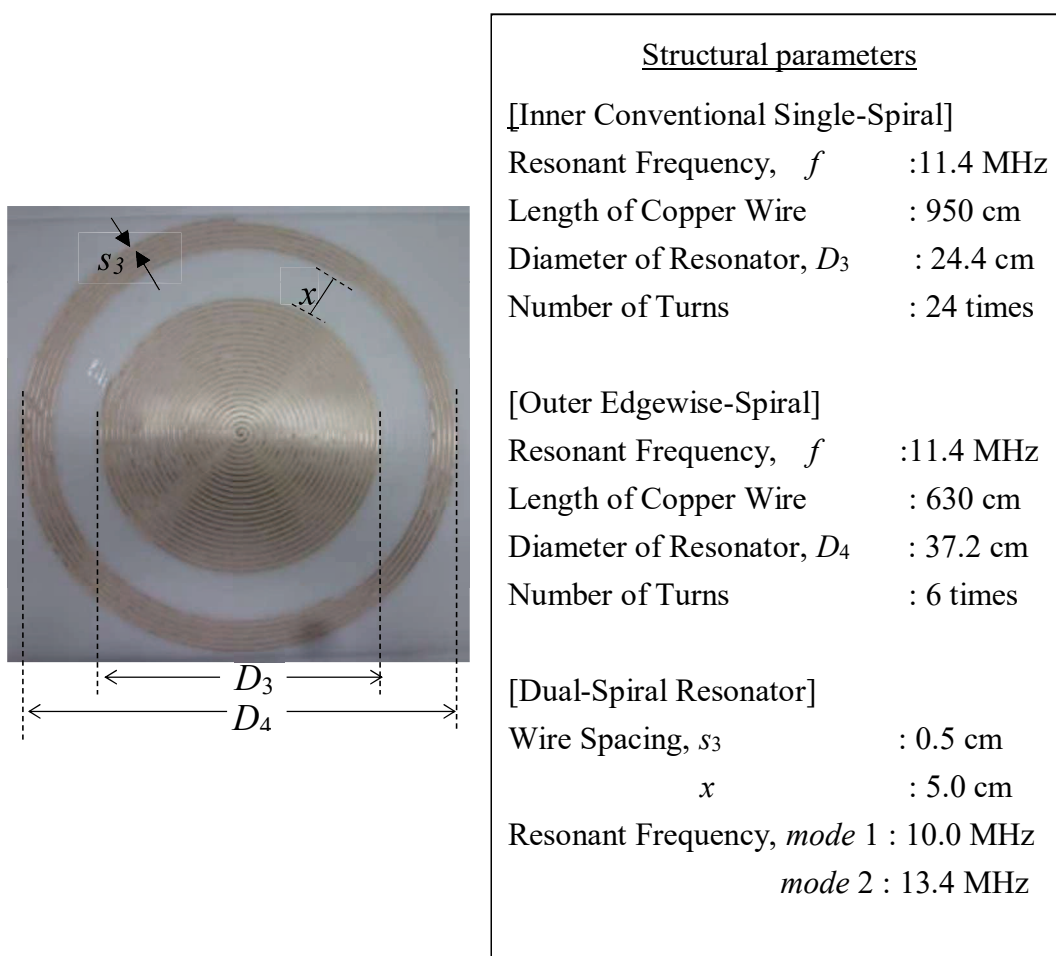


Figure 3.11 Fabricated Dual-spiral resonator and its Components.

The proposed dual-spiral resonator is expected to provide higher power transmission efficiency to the RC-WPT system with lossy mediums compared to the system with the single-spiral resonator. To make a fair performance comparison between the resonators, the resonant frequency, as well as the radial size of Single-Spiral #2 and the dual-spiral resonators, should be set as identical. Here, when the same input power is applied to port 1, the power density of the electromagnetic fields on the excited resonator surface is anti-proportional to that area size. Therefore, to unify the power density on each spiral resonator, the cross-sectional area sizes must be the same. For this reason, the diameters of Single-Spiral #2 and the dual-spiral resonators are adjusted in the same way, which automatically decided that D_4 is 37.2 cm. On the contrary, the wire spacing of Single-Spiral #2 and the dual-spiral resonators are different; that is, $s_2 = 1.0$ cm for Single-Spiral #2 and $s_3 = 0.5$ cm for the dual-spiral resonators. The wire spacings are different because, for the resonant frequency of the dual-spiral resonators to be $f = 10.0$ MHz, the wire spacing s_3 should be narrower than the wire spacing s_2 since the wire spacing s_3 needs to be narrower than that of the single spiral resonator s_2 [50], [51]. Since the groove spacing of the spiral guide uses a 0.5 mm interval and the wire spacing s_2 of the single spiral resonator is 1.0 cm, the wire spacing s_3 of the dual spiral resonators was set to 0.5 cm.

The dual-spiral resonator [52], [53] is a combination of the inner conventional single-spiral resonator and the outer edgewise-spiral resonator, which have the same resonant frequency on the same plane, as shown in Figure 3.11. In this study, since the dual-spiral resonator is made from different kinds of resonators, it has two resonant modes, [54] as shown in Figure 3.12. Here, the resonance mode at the lower resonance point, 10.0 MHz, is called *mode 1* and the other resonant point, 12.9 MHz, is called *mode 2*.

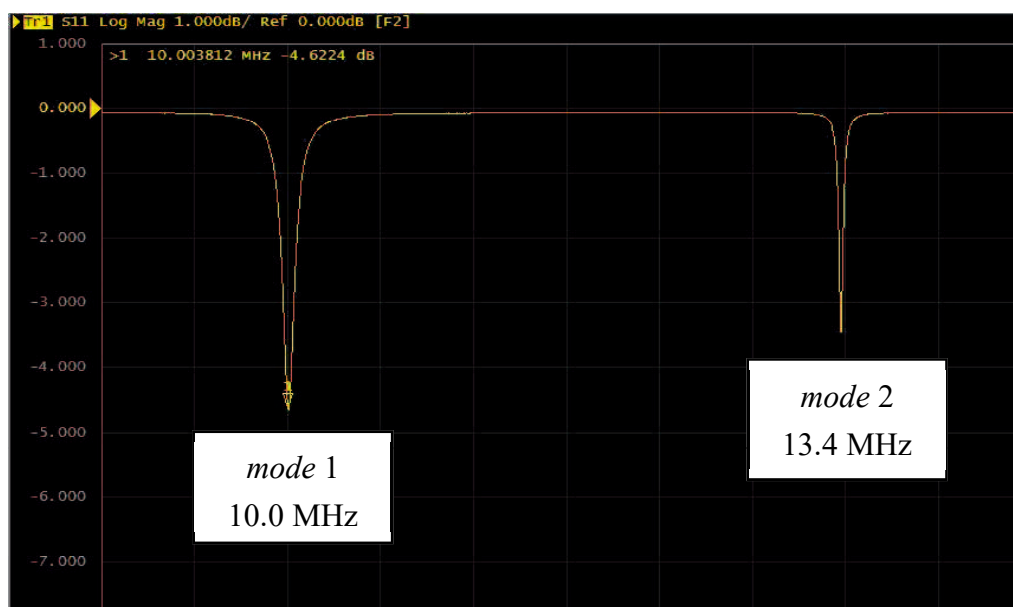


Figure 3.12 Emergence of Two Resonance Modes.

3.4 RC-WPT System using Modified Spiral Resonators with Lossy Mediums

3.4.1 Q -factors of Dual-Spiral Resonator

To determine the performance of the dual-spiral resonator, firstly, the unloaded Q : Q_u without lossy mediums is examined. The measurement setup is the same as the setup in

Figure 3.3. The measured results of the unloaded $Q: Q_u$ without lossy mediums, as a function of the distance between the loop coil and the spiral resonator, are shown in Figure 3.13. In the case of the dual-spiral resonator, the symbol \blacksquare represents the unloaded $Q: Q_u$ for *mode 1*, while the symbol \square represents the unloaded $Q: Q_u$ for *mode 2*. The unloaded $Q: Q_u$ for Single-Spiral #2 is also included for comparison purposes and is represented by the symbol \bullet .

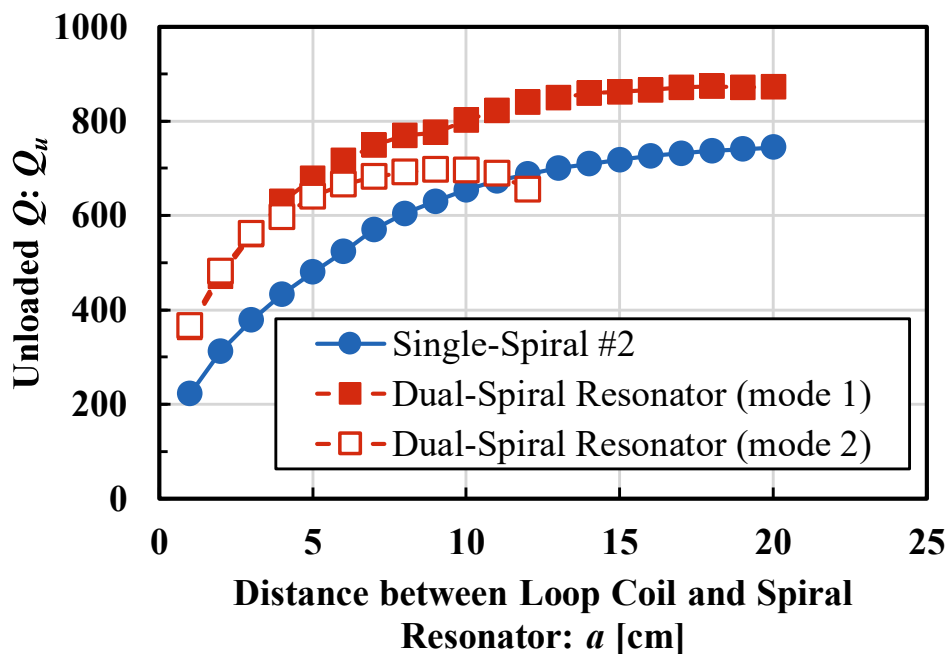


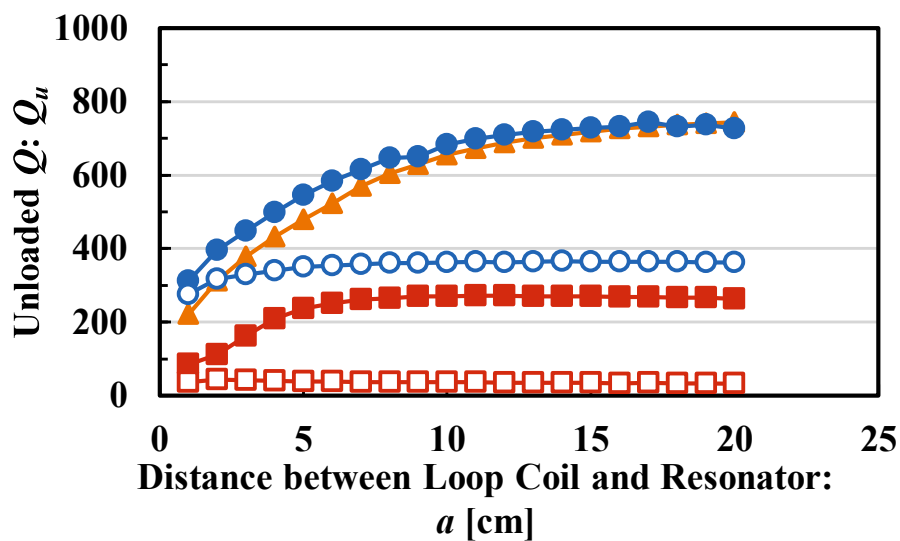
Figure 3.13 Results of Unloaded $Q: Q_u$ Without Lossy Mediums for Single-Spiral #1 and Dual-Spiral Resonators.

From the results shown in Figure 3.13, in the case of Single-Spiral #2, when the distance a is longer than 15.0 cm, it converged to a maximum value of 720. Meanwhile, *mode 1* shows the same characteristics as Single-Spiral #2; however, it converged to 860. Based on these findings, the unloaded $Q: Q_u$ for *mode 1* is higher than that of Single-Spiral #2.

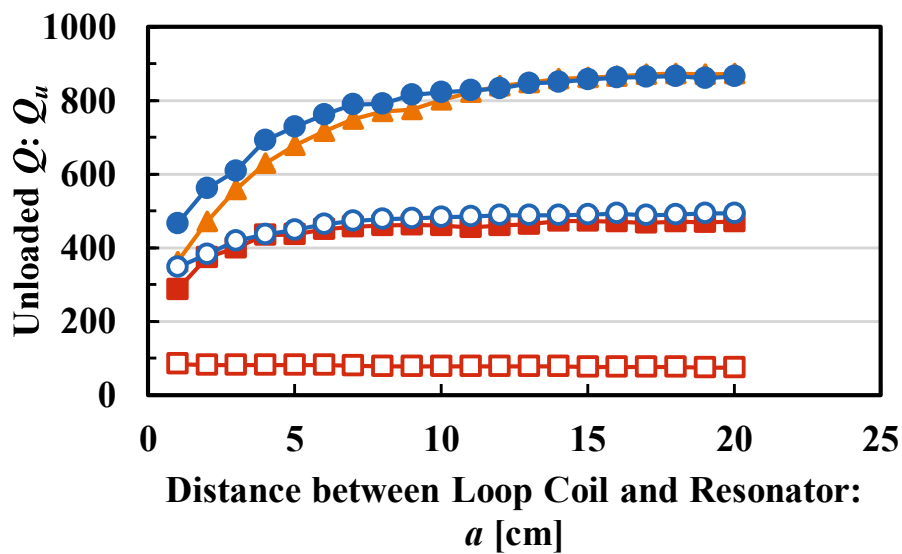
Meanwhile, the unloaded $Q: Q_u$ for *mode 2* shows the same characteristics when the distance a reaches up to 9.0 cm. Then, when the distance a is larger than 9.0 cm, the unloaded $Q: Q_u$ decreases. After the distance a exceeds 12.0 cm, the unloaded $Q: Q_u$ disappears and cannot be measured because it is unstable. Therefore, the following investigation of the dual-spiral resonator is limited to *mode 1* only because the operation mechanism of *mode 2* has yet to be determined.

3.4.2 Q -factors with Lossy Mediums

Next, the unloaded $Q: Q_u$ of the resonators with the lossy mediums was examined to check the properties of the spiral resonator when the lossy mediums are placed near the spiral resonators. Figures 3.14 (a) and (b) show the results of the unloaded $Q: Q_u$ for Single-Spiral #2 and the *mode 1* dual-spiral resonator when the lossy medium is close to the system. Here, the symbols \square and \circ represent when $p = 1.0$ cm, whereas the symbols \blacksquare and \bullet represent when $p = 7.0$ cm. In these figures, the unloaded $Q: Q_u$ without a lossy medium (see Figure 3.13) is also presented for comparison purposes and is represented by the symbol \blacktriangle .



(a) Single-Spiral #2



(b) Dual-Spiral Resonator (*mode 1*)

Figure 3.14 Results of the Unloaded $Q: Q_u$ with Lossy Mediums for Single-Spiral and Dual Spiral Resonators.

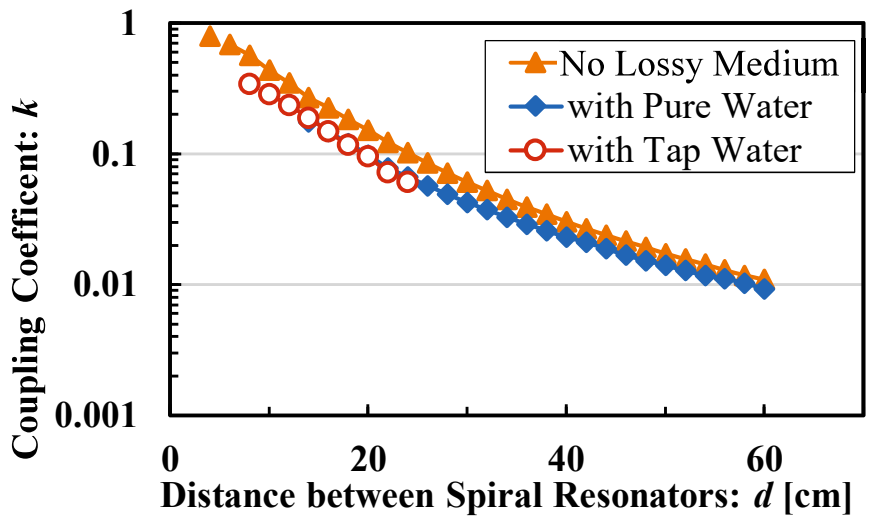
From the results shown in Figures 3.14 (a) and (b), when the lossy mediums are adjacent to the spiral resonators, the unloaded Q : Q_u decreased more substantially than was the case without the lossy mediums. It was discovered that the lossy mediums around the resonator impact the degrading properties of the spiral resonators. On the contrary, when the lossy mediums are slightly further from the resonators (that is, when $p = 7.0$ cm), the unloaded Q : Q_u obviously increased for both spiral resonators.

However, when the pure or tap water-filled acryl bases are inserted on the power transmission path, the unloaded Q : Q_u for *mode* 1 of the dual-spiral resonator is larger than that of Single-Spiral #2. It can be inferred that the electric field that leaked from the dual-spiral resonator is less than that which leaked from the single-spiral resonator. According to the findings of the unloaded Q : Q_u , when a lossy medium exists around the resonators, the dual-spiral resonator experiences a lower loss than the single-spiral resonator.

3.4.3 Coupling Coefficients with Lossy Mediums

Next, the coupling coefficient k with lossy mediums is examined, using the same measurement setup as shown in Figure 3.5. Also examined were the coupling coefficients for the RC-WPT system with lossy mediums for the single-spiral and dual-spiral resonators when $p = 1.0$ cm and 7.0 cm. The measured results for the coupling coefficient

between the spiral resonators with lossy mediums, as a function of distance d , are presented in Figures 3.15 and 3.16. In these figures, the system with pure water-filled acryl bases is represented by the symbol \circ , and the system with tap water-filled acryl bases is represented by the symbol \blacksquare . The coupling coefficient k without lossy mediums is also included for comparison and is represented by the symbol \blacktriangle .



(a) Single-Spiral #2

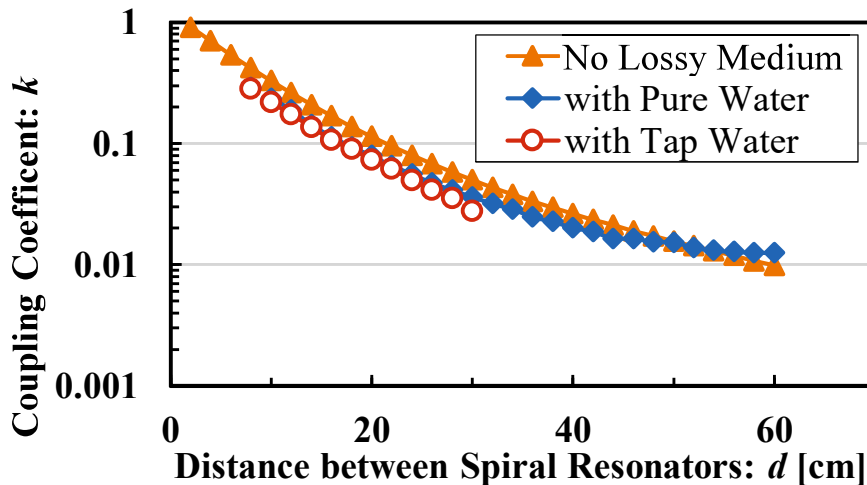
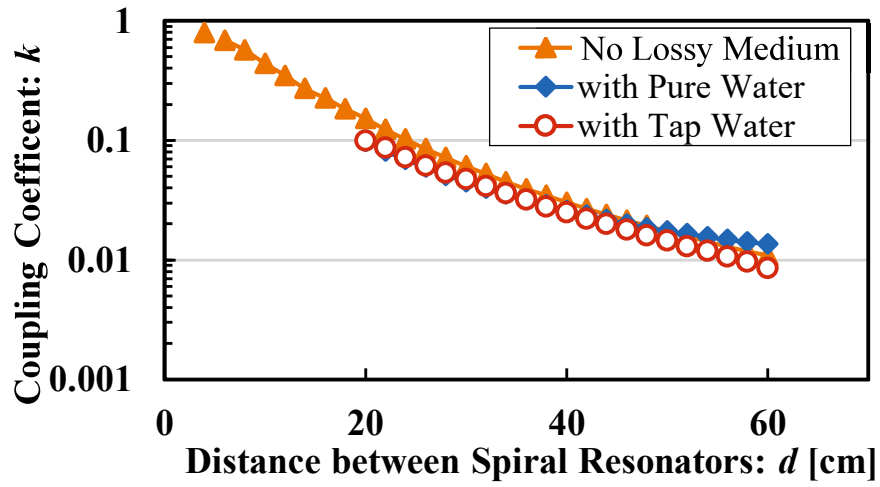
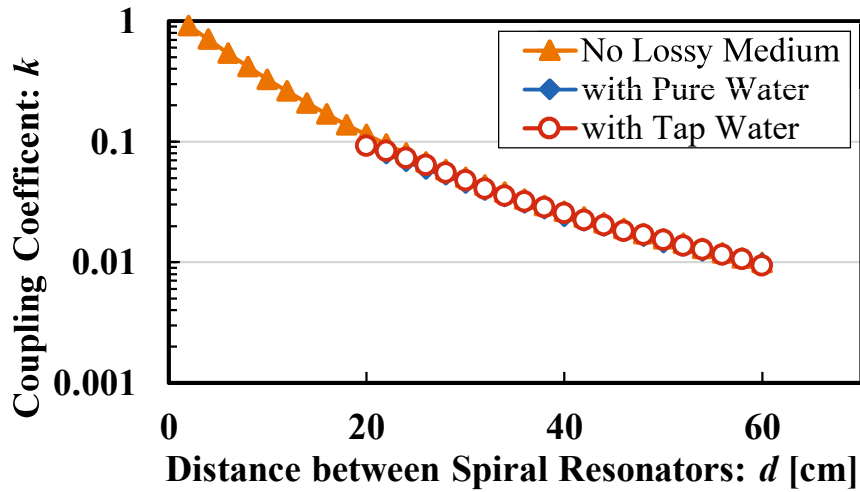
(b) Dual-Spiral Resonators (*mode 1*)

Figure 3.15 Results of Coupling Coefficients of RC-WPT system with Lossy Mediums for Single-Spiral and Dual-Spiral Resonators ($p = 1.0$ cm).



(a) Single-Spiral #2



(b) Dual-Spiral Resonators (*mode 1*)

Figure 3.16 Results for Coupling Coefficients of RC-WPT system with Lossy Medium for Single-Spiral and Dual-Spiral Resonators ($p = 7.0$ cm).

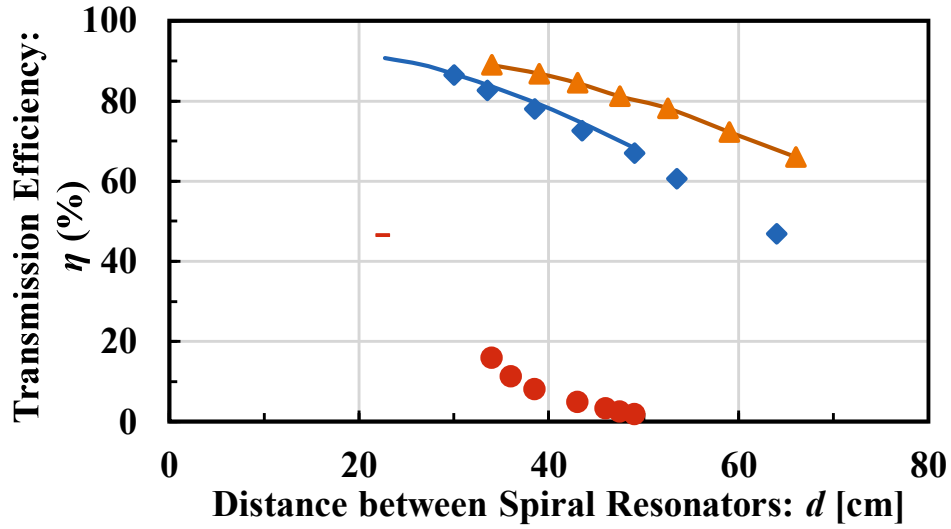
From the results in Figures 3.15 and 3.16, the coupling coefficients with tap water-filled acryl bases for each resonator were shown to be the lowest, while this was only over short distances d . Despite that, the coupling coefficients for the system without lossy mediums are slightly higher than those with tap and pure water-filled acryl bases. However, each

measured curve presented almost the same tendency. These differences were obviously smaller than those of the unloaded Q : Q_u (see Figure 3.14).

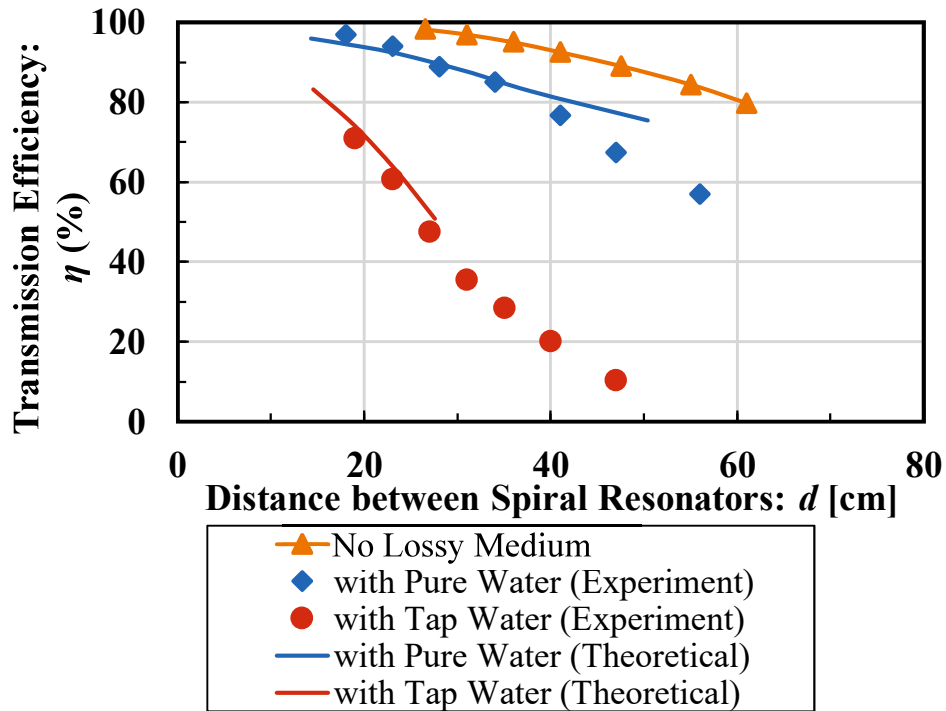
3.4.4 Power Transmission Efficiency with Lossy Mediums

Next, the power transmission efficiency of the RC-WPT system with lossy mediums for Single-Spiral #2 and *mode* 1 are examined. As the unloaded Q : Q_u and the coupling coefficient k with lossy mediums have been measured in the previous section, the theoretical value of the power transmission efficiency of the RC-WPT system with lossy mediums can be obtained using equation (2.77) (see Section 2.6.1). Based on the design theory of the BPF circuit, the distances a and d must be set to satisfy the system matching conditions to obtain the maximum power transmission efficiency for each RC-WPT system. Then, the power transmission efficiency of the RC-WPT system with the lossy medium is examined, whereby the separation between the spiral resonator and the acrylic base, p is fixed at 1.0 cm and 7.0 cm. These measured results are presented in Figures 3.17 and 3.18, respectively. The power transmission efficiency without a lossy medium for Single-Spiral #2 and *mode* 1 of the dual-spiral resonators are also included in the same figure for comparison; this is represented by the symbol ▲. Meanwhile, the symbol ◆ indicates the measured experimental results from the systems with pure water-filled acrylic bases, whereas the symbol ● indicates the measured experimental results from the

systems with tap water-filled acryl bases. The dashed lines are the theoretical results, which were estimated using equation (2.78).

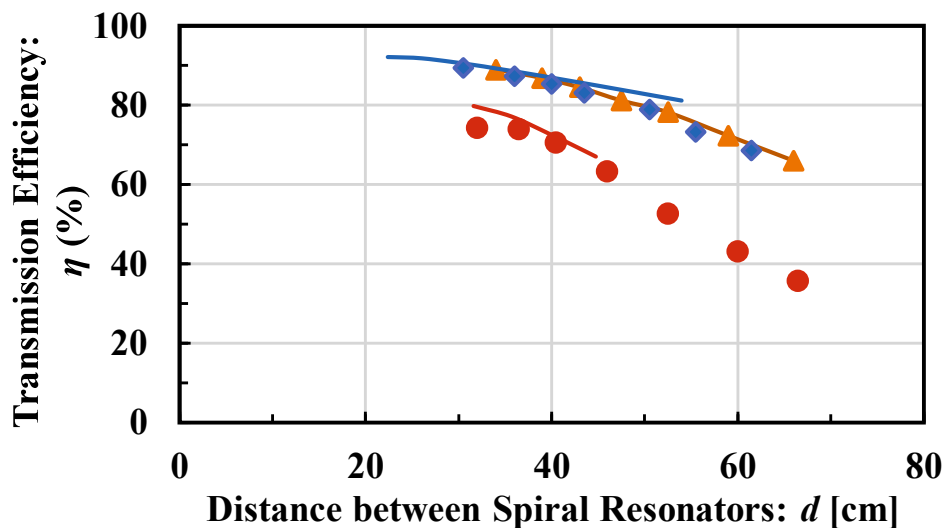


(a) Single-Spiral #2

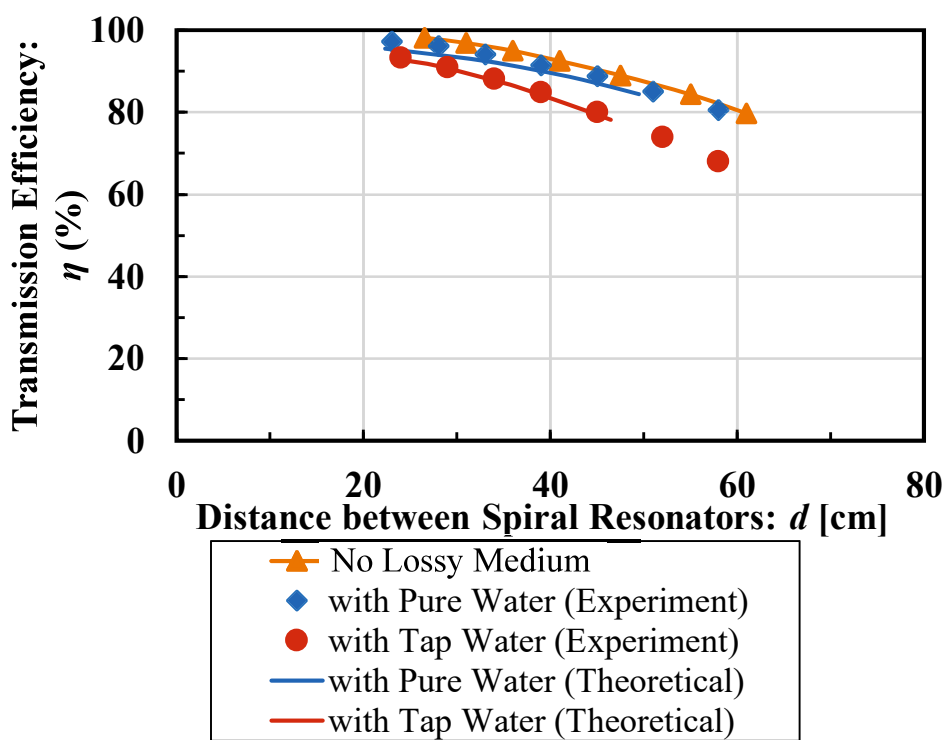


(b) Dual-Spiral Resonator (*mode 1*)

Figure 3.17 Results of Power Transmission Efficiency of RC-WPT System with Lossy Mediums for Single-Spiral and Dual-Spiral Resonators ($p = 1.0$ cm).



(a) Single-Spiral #2



(b) Dual-Spiral Resonator (*mode 1*)

Figure 3.18 Results of Power Transmission Efficiency of RC-WPT System with Lossy Mediums for Single-Spiral and Dual-Spiral Resonators ($p = 7.0$ cm).

From the results shown in Figures 3.17 and 3.18, when $p = 1.0$ cm and 7.0 cm, the power transmission efficiency for the single-spiral resonator with pure or tap water-filled acrylic bases is both further and less than that without lossy mediums inside the RC-WPT system. However, using the proposed dual-spiral resonator, the power transmission efficiency of the system with pure or tap water-filled acrylic bases improved, compared with the system using Single-Spiral #2. Furthermore, the power transmission efficiency for the system with the dual-spiral resonator approaches that of the system without the lossy medium. These results reveal that when a lossy medium is inserted into the system, the dual-spiral resonator displays a lower decrease in the rate of power transmission efficiency than that of the single-spiral resonator. In addition, when the distance p is the same, the dual-spiral resonator demonstrates a higher transmission efficiency of the system and a wide range of distance, d where the transmission efficiency is larger than 60%.

When the distance p increases to $p = 7.0$ cm, the power transmission efficiency of the RC-WPT system for Single-Spiral #2 and *mode 1* of the dual-spiral resonator improved, especially for the system using the dual-spiral resonators. Even with pure or tap water-filled acrylic bases, the power transmission efficiency of the system for the dual-spiral resonator is unaffected by distance p . These results indicate that the proposed dual-spiral resonator has more effectively confined the electric field compared to the single-

spiral resonators, since the dielectric and conductor losses are caused by the electric field acting on an electromagnetic field.

Therefore, the proposed dual-spiral resonator would be the most effective way to establish the RC-WPT system's strong resistance to lossy mediums. To confirm these statements, the modes of the spiral resonators using an electromagnetic simulator should be investigated in more detail.

One of the methods of realizing the arrangement described above is to package the loop coil and the resonator of the input or output unit in a highly sealed case, as shown in Figure 3.19. In this situation, an obstacle exists around the resonator, it is expected that a certain distance can be maintained between the resonator and the obstacle, so the influence of the obstacle can be continuously avoided.

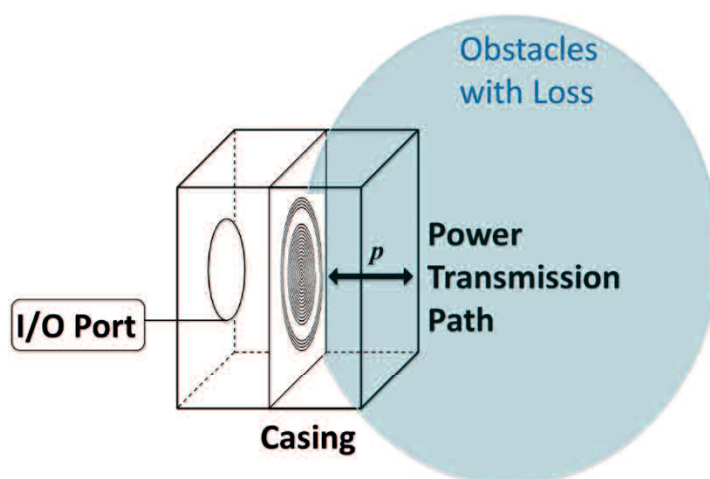


Figure 3.19 Expectation of Future Practical Application.

3.5 Summary

In this chapter, the effect of lossy mediums inside the RC-WPT system was investigated.

The measured results suggest that the influence of the lossy mediums drastically changes with the resonator properties. Especially when lossy mediums exist in the RC-WPT system, the unloaded Q : Q_u leads to a decrease in the power transmission efficiency of the system using single-spiral resonators. Therefore, the dual-spiral resonator is proposed, and this was fabricated in such a way that the electric field was confined inside the resonator to reduce the influence of the lossy mediums. The measurement results show that the system using the dual-spiral resonator is more superior against lossy mediums than the system using the single-spiral resonator. Even when the spiral resonator is further from the lossy mediums, the system with dual-spiral resonators can maintain a higher power transmission efficiency than the system with the single-spiral resonator.

Chapter 4: Effects of Some Misalignments between Tx/Rx Units of RC-WPT System

4.1 Foreword

The RC-WPT system can transmit electric power wirelessly over a middle-range distance.

As the transmission distance increases, the degree of freedom in the layout of the Tx and

Rx units increases, but the effects of angular and axial misalignment on the power

transmission efficiency of the WPT system need to be considered. Therefore, in this

chapter, the power transmission efficiency characteristics of RC-WPT systems with spiral

resonators that have an angular misalignment are investigated, based on experimental

values. The degradation of the power transmission efficiency due to angular

misalignments seems inevitable. Therefore, this section discusses in detail a method of

adding the appropriate axial displacement so that the decayed transmission power due to

angular misalignments can be improved.

4.2 Configuration Setup for RC-WPT System with Angular

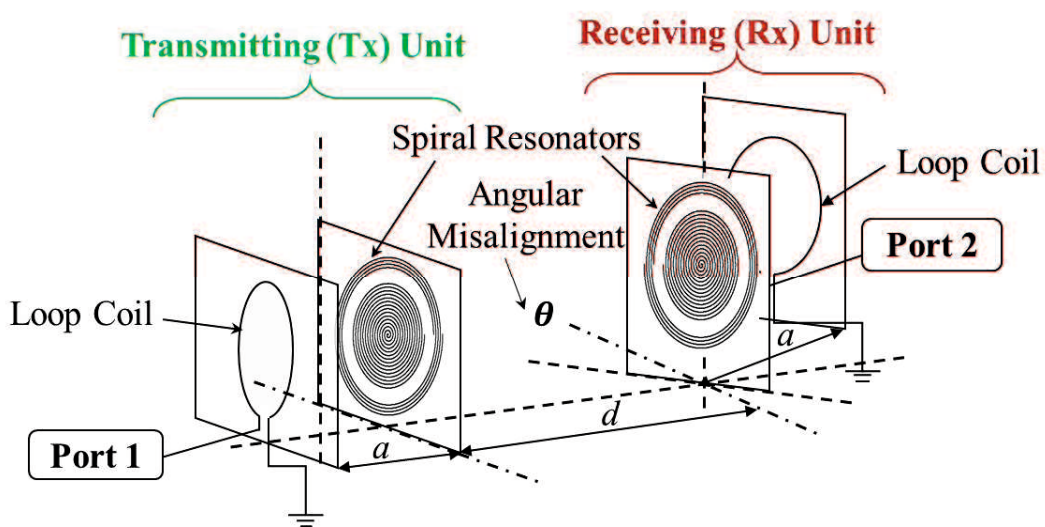
Misalignment

The configuration setup of the RC-WPT system with angular misalignments is presented

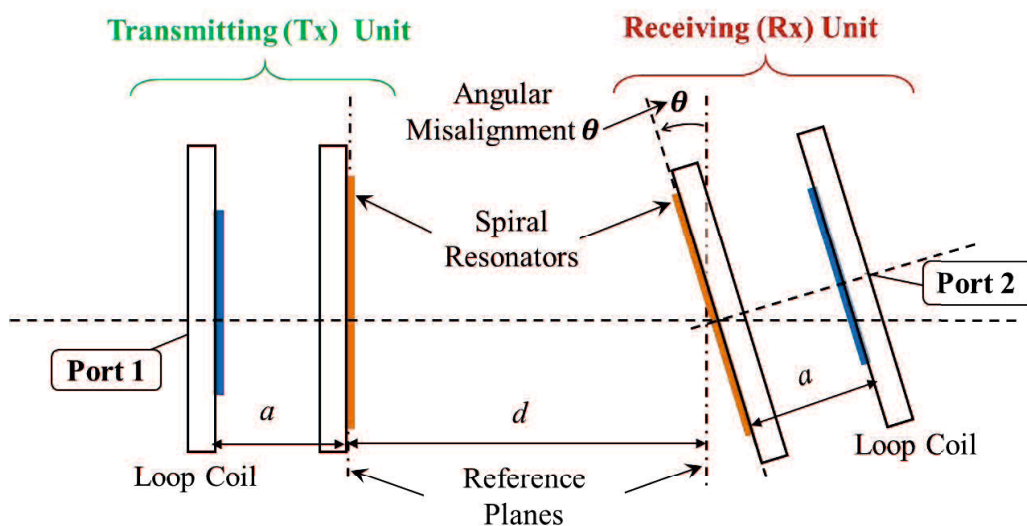
in Figure 4.1. The angular misalignments θ [°] have been defined by the angle between

the loop coil surface in the Tx unit and the spiral resonator surface in the Rx unit. When

the spiral resonators are observed from the Tx unit to the Rx unit, the winding direction of the spiral resonators in the Tx and Rx units are opposite to each other. For the spiral resonators, Single-Spiral #2 and *mode 1* of the dual-spiral resonators are used in this study. Henceforth, Single-Spiral #2 and *mode 1* of the dual-spiral resonators are referred to only as single-spiral and dual-spiral resonators, respectively.



(a) Schematic Outline



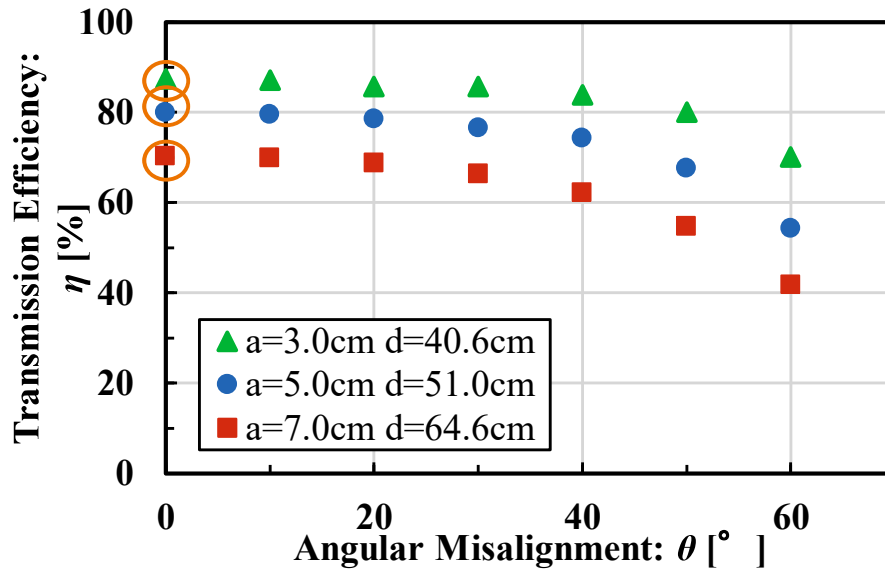
(b) Top View of the System.

Figure 4.1 Structure of RC-WPT System with Angular Misalignments.

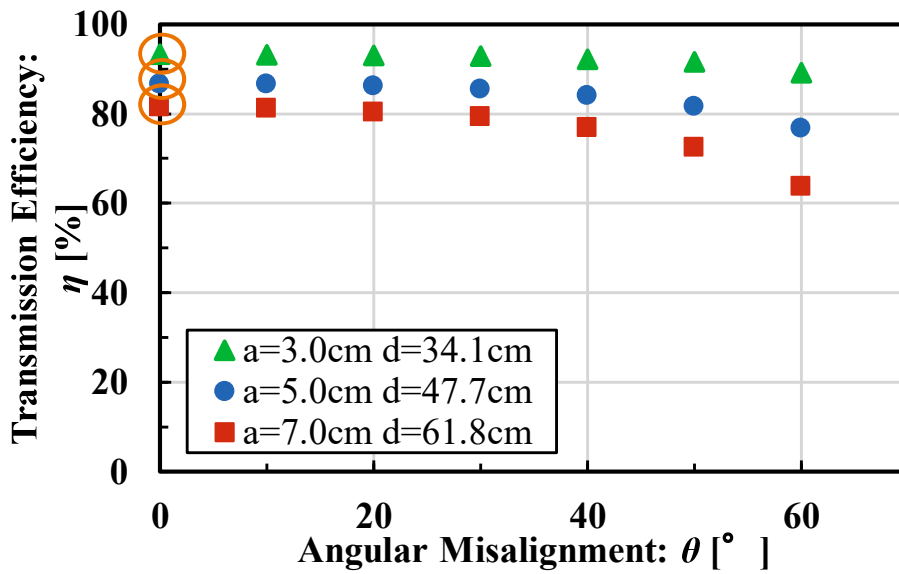
To measure the power transmission efficiency of the RC-WPT system with angular misalignment for those spiral resonators, the sets of distances a and d that satisfy the system matching conditions are determined, based on the system matching conditions described in Section 2.6.2. Then, the plane of the Rx units is tilted to form an angle θ through the center axis of the spiral resonator in Rx [55]-[57]. Here, the Rx unit is tilted by 10° in the range of $0^\circ \leq \theta \leq 60^\circ$. Then, the power transmission efficiency of the system with angular misalignment in the Rx unit is examined for those spiral resonators.

4.3 Measurement of Power Transmission Efficiency with Angular Misalignment

Figure 4.2 presents the measured results for the power transmission efficiency of the RC-WPT system as a function of angular misalignment in the range of $0^\circ \leq \theta \leq 60^\circ$ for Single-Spiral #2 and *mode* 1 of the dual-spiral resonators when $a = 3.0$ cm, 5.0 cm, and 7.0 cm. The measurement results for the other combinations of a and d had been examined, confirming that they have almost the same tendencies and/or characteristics. However, only $a = 3.0$ cm, 5.0 cm, and 7.0 cm are shown in this figure. In the same figure, the orange circles indicate the maximum values of the power transmission efficiency of the RC-WPT system when a [cm] and d [cm] are fixed states.



(a) Single-Spiral #2



(b) Dual-Spiral Resonator (*mode 1*)

Figure 4.2 Relationship between Power Transmission Efficiency and Angular Misalignments for Single-Spiral and Dual-Spiral Resonators when $a = 3.0\text{ cm}$, 5.0 cm , and 7.0 cm .

These results indicate that, in each case where $a = 3.0$ cm, 5.0 cm, and 7.0 cm, *mode 1* of the dual-spiral resonator has a higher power transmission efficiency of the RC-WPT system with angular misalignment compared to that of Single-Spiral #2. These results revealed that when the Rx unit is tilted, the dual-spiral resonator is more superior and less sensitive to angular misalignment than the single-spiral resonator.

However, for each spiral resonator, as the angular misalignments increase, the power transmission efficiency of the RC-WPT system decays in each case. It seems that the overlapping rate between the modal profiles of the resonators in the Tx and Rx units decreases due to the tilted Rx unit, resulting in the decayed power transmission efficiency of the RC-WPT system. Here, it is assumed that when there is no angular misalignment in the RC-WPT system, the spiral resonators are normal at their plane, so the magnetic flux is perpendicular to the spiral resonator. When the Rx unit of the system is tilted or has angular misalignment, less magnetic flux crosses the Rx unit [28] and causes the degree of coupling to decrease.

Based on these problems, the recovery method for addressing this performance degradation must be investigated. It is thought that the decayed transmission power due to angular misalignment could be recovered by adding appropriate axial displacement to the tilted Rx unit so that the rate of the overlapping area between the modal profiles of

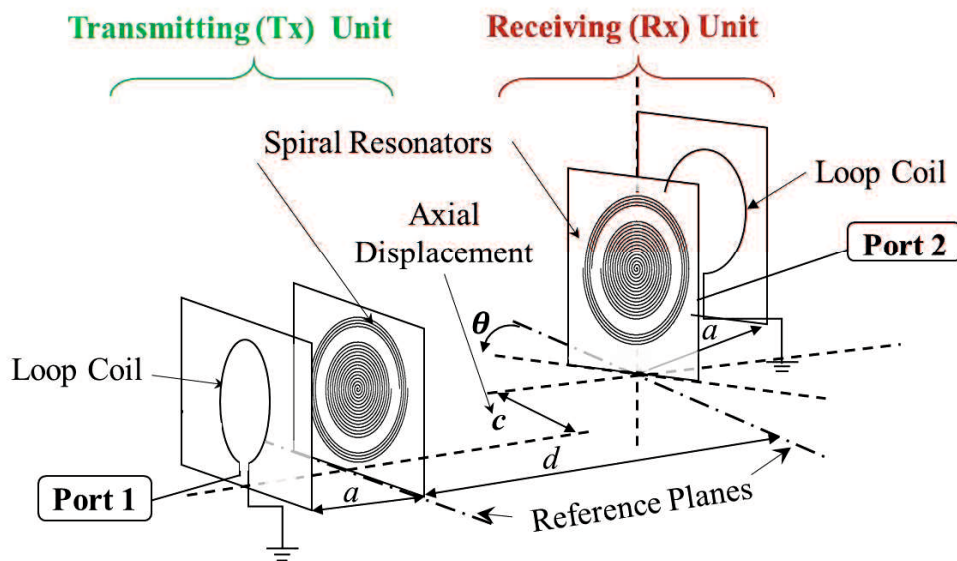
the Tx and Rx spiral resonators would grow. This recovery method for the RC-WPT system is examined and discussed in the next section.

4.4 Improvement of Power Transmission Efficiency with Some Misalignments

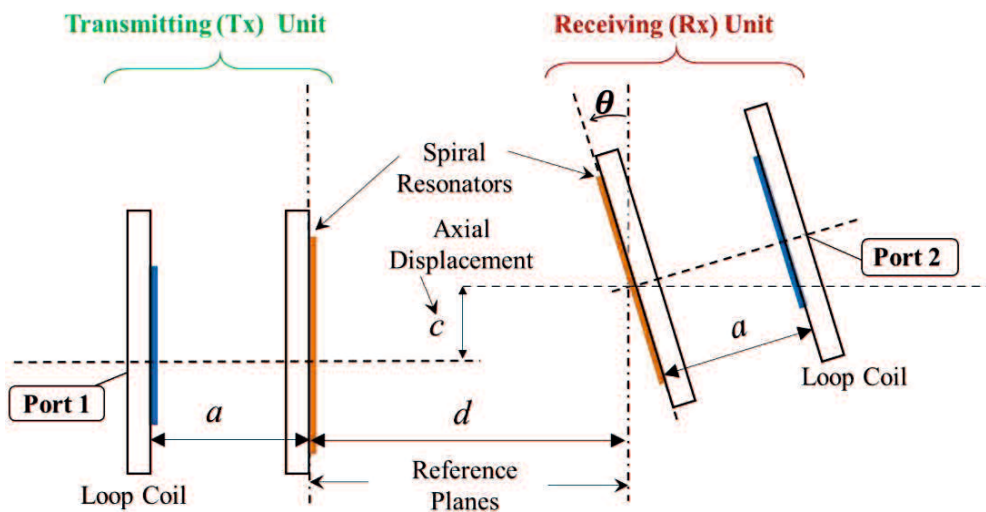
According to Refs. [29], [58]-[60], when axial misalignments exist between the Tx and Rx units of the system, the power transmission efficiency of the system declines due to these misalignments. However, this lower power transmission efficiency can be improved by adding some angular misalignments to the Rx unit of the system. Therefore, this section of the study investigates how the decreased power transmission efficiency of the RC-WPT system due to angular misalignments can be improved by adding the appropriate axial displacement to the tilted Rx unit of the system.

Figure 4.3 shows the measurement setup of the RC-WPT system with angular misalignment by adding axial displacements. Here, the distance c [cm] indicates axial displacement between the Tx and Rx units. These configuration system setups are almost the same as that of the RC-WPT system with angular misalignment outlined in Section 4.2, except for the existence of axial displacement. Therefore, the system without axial displacement (see Figure 4.1) is set as $c = 0$ cm. Using the same spiral resonators, which are Single-Spiral #2 and *mode 1* of the dual-spiral resonator, and keeping the same sets

of distance a and d as mentioned in Section 4.3, the improved power transmission efficiency of the RC-WPT system is inspected. To examine these circumstances, the angular misalignment is changed by $\theta = 10^\circ$ in the range of $0^\circ \leq \theta \leq 60^\circ$. The tilted Rx unit is then moved parallel toward the reference line by distance c .



(a) Schematic Outline of Angular Misalignment and Axial Displacement.

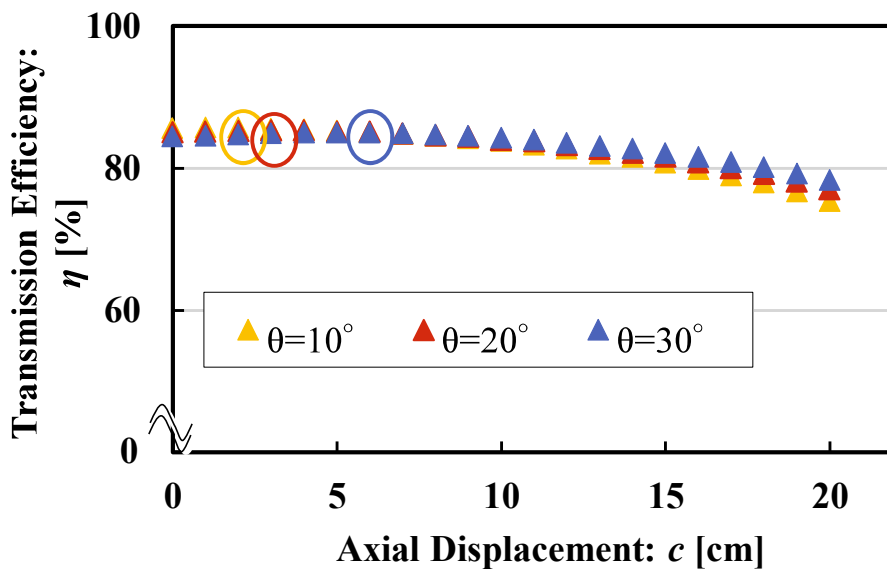


(b) Top View of the System with Angular Misalignment and Axial Displacement.

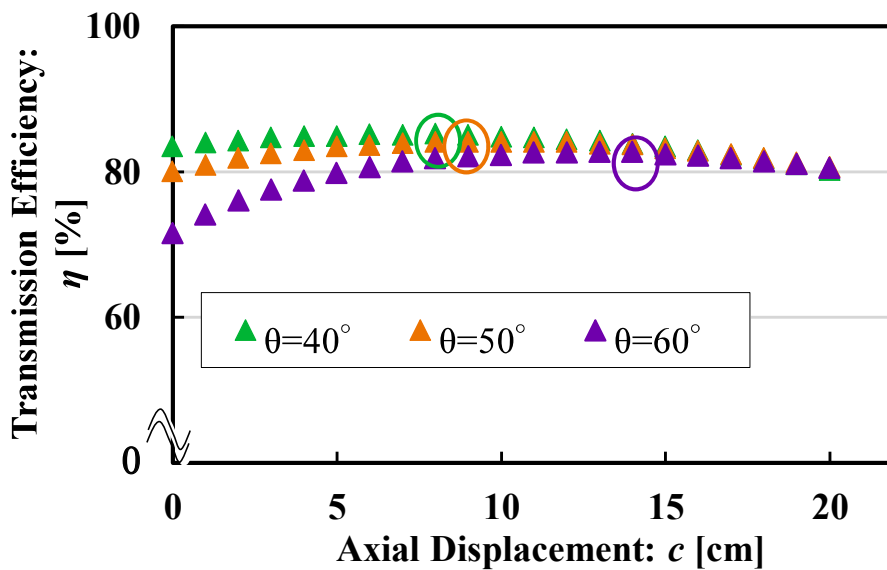
Figure 4.3 Measurement Setup of RC-WPT Systems with Some Misalignments

4.5 Measurement of Improvement of Power Transmission Efficiency with Some Misalignments

This section examines the power transmission efficiency of the RC-WPT system when the Rx units with angular misalignments are shifted in the range of $0^\circ \leq \theta \leq 60^\circ$ by different axial displacements, c , where $a = 3.0$ cm, 5.0 cm, and 7.0 cm. Figures 4.4, 4.6, and 4.8 show the measured results of the system using Single-Spiral #2, while Figures 4.5, 4.7, and 4.9 show the measured results of the system using *mode 1* of the dual-spiral resonator. In the same figures, the colored circle marks show the axial displacement where the maximum power transmission efficiency of the system is obtained, according to its angular misalignments. Here, for the angular misalignment $\theta = 10^\circ$ presented by \circ , 20° presented by \circ , 30° presented by \circ , 40° presented by \circ , 50° presented by \circ and 60° presented by \circ .

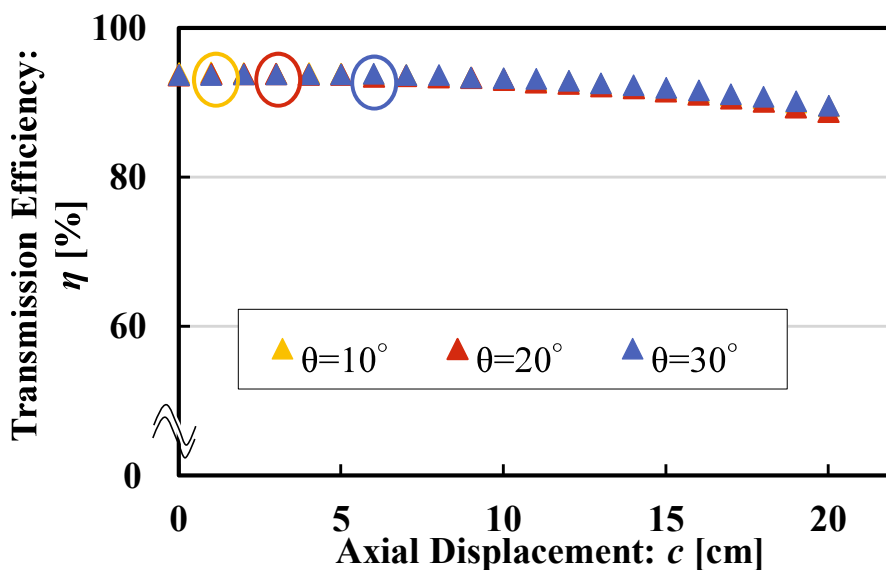


(a) $\theta = 10^\circ, 20^\circ,$ and 30°

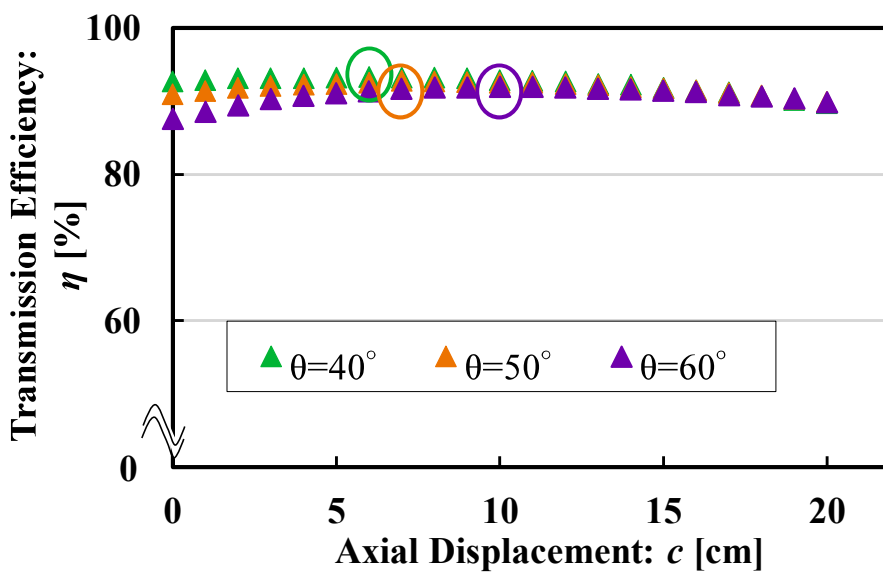


(b) $\theta = 40^\circ, 50^\circ,$ and 60°

Figure 4.4 Relationship between Power Transmission Efficiency and Axial Displacement for Single-Spiral #2 in the range of $0^\circ \leq \theta \leq 60^\circ$ when $a = 3.0$ cm and $d = 40.6$ cm.

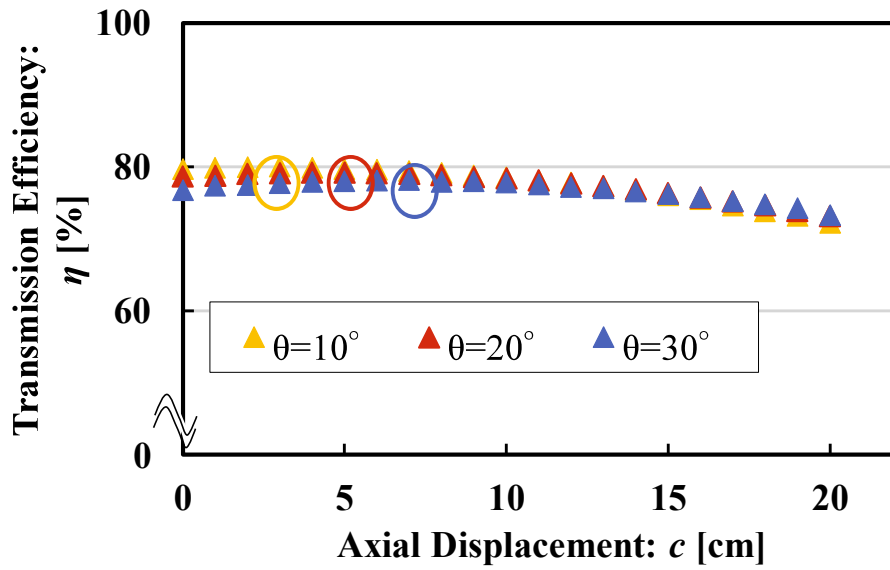


(a) $\theta = 10^\circ, 20^\circ$ and 30°

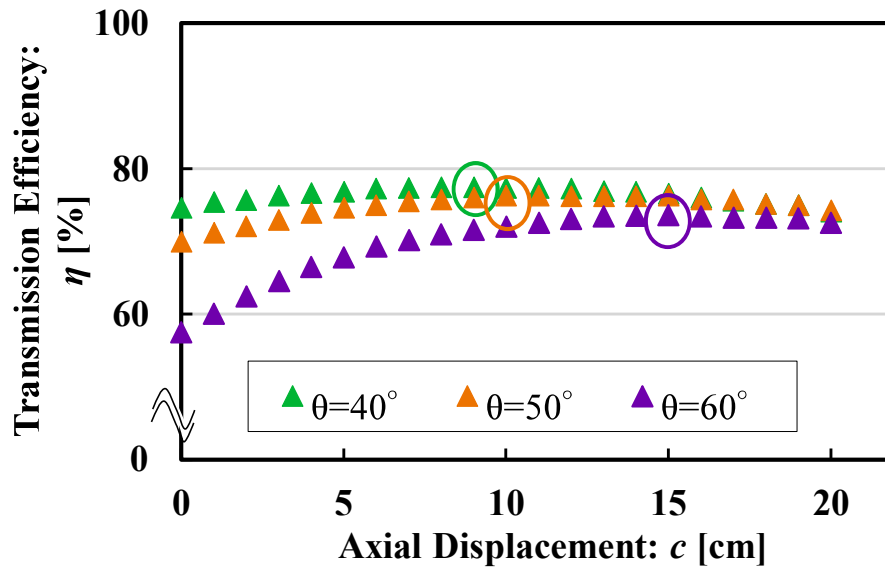


(b) $\theta = 40^\circ, 50^\circ$ and 60°

Figure 4.5 Relationship between Power Transmission Efficiency and Axial Displacement for Dual-Spiral Resonator (*mode 1*) in the range of $0^\circ \leq \theta \leq 60^\circ$ when $a = 3.0$ cm and $d = 34.1$ cm.



(a) $\theta = 10^\circ, 20^\circ,$ and 30°



(b) $\theta = 40^\circ, 50^\circ,$ and 60°

Figure 4.6 Relationship between Power Transmission Efficiency and Axial Displacement for Single-Spiral #2 in the range of $0^\circ \leq \theta \leq 60^\circ$ when $a = 5.0$ cm and $d = 51.0$ cm.

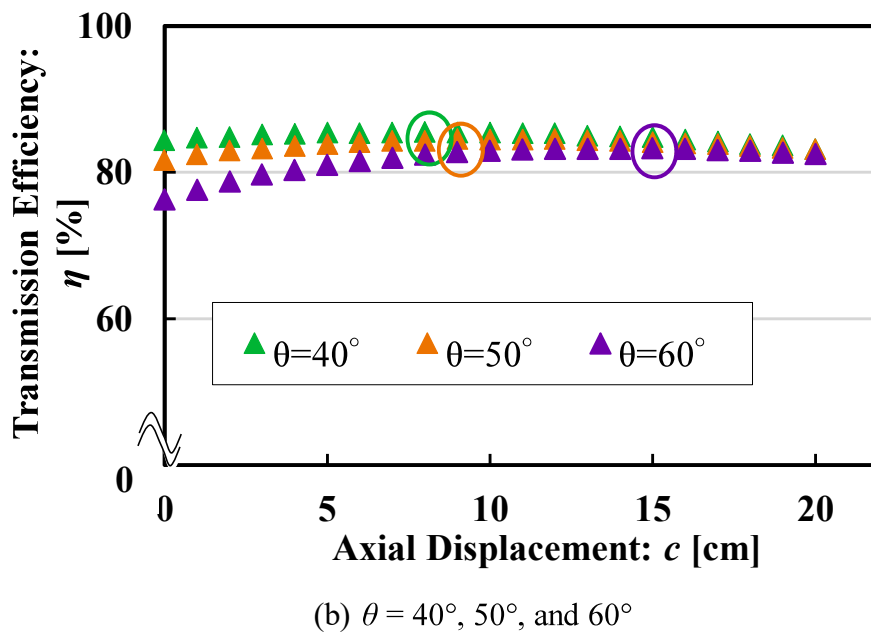
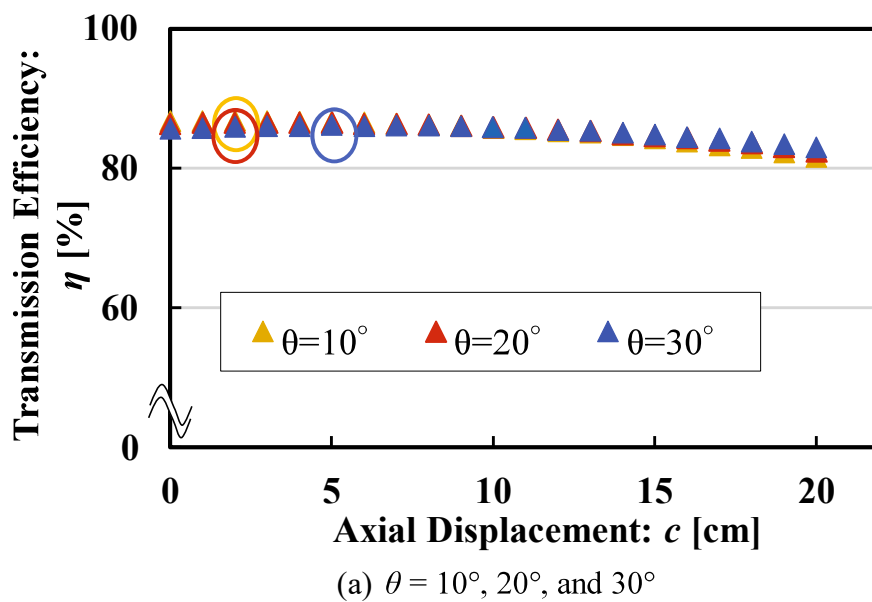
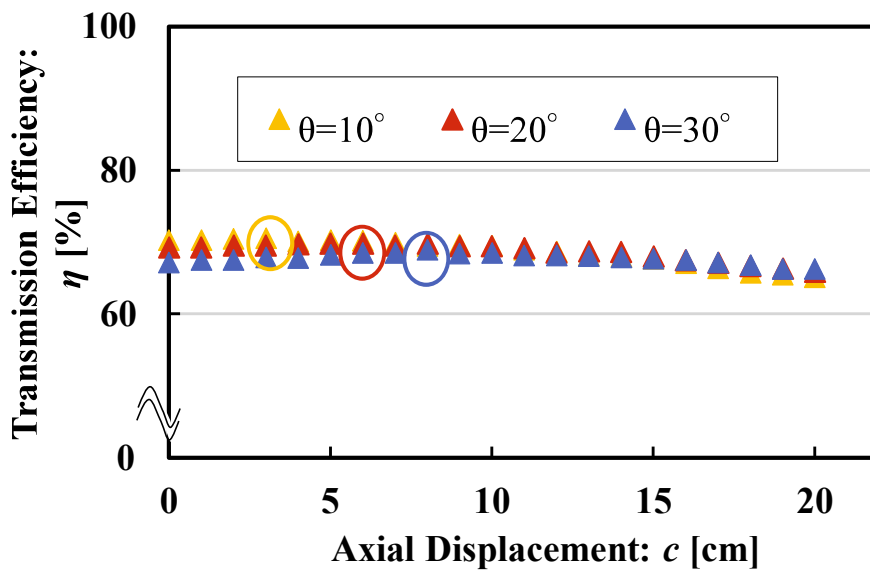
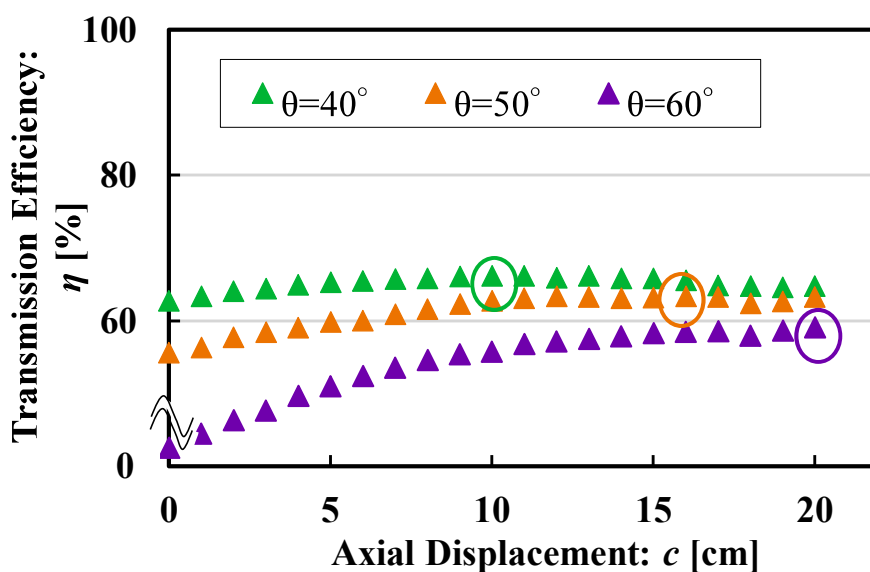


Figure 4.7 Relationship between Power Transmission Efficiency and Axial Displacement for Dual-Spiral Resonator (*mode 1*) in the range of $0^\circ \leq \theta \leq 60^\circ$ when $a = 5.0$ cm and $d = 47.7$ cm.

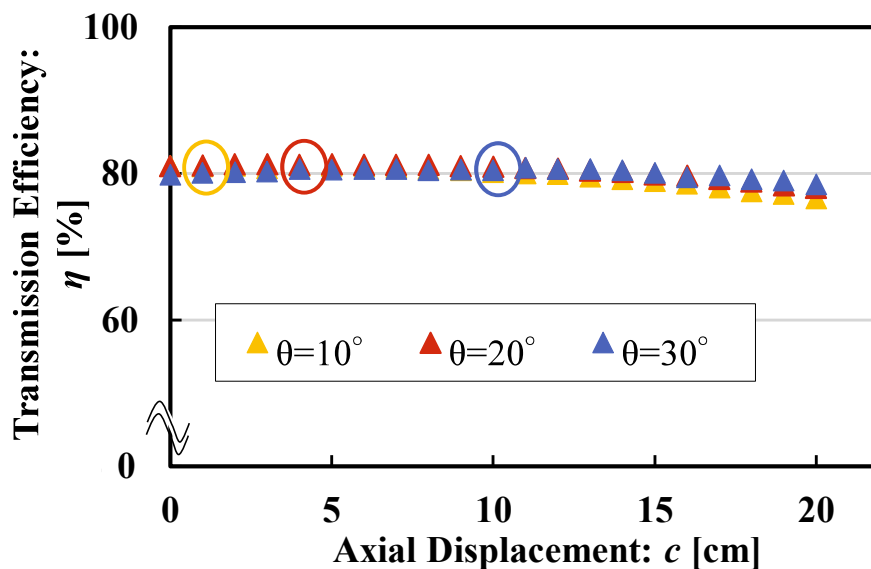


(a) $\theta = 10^\circ, 20^\circ, \text{ and } 30^\circ$

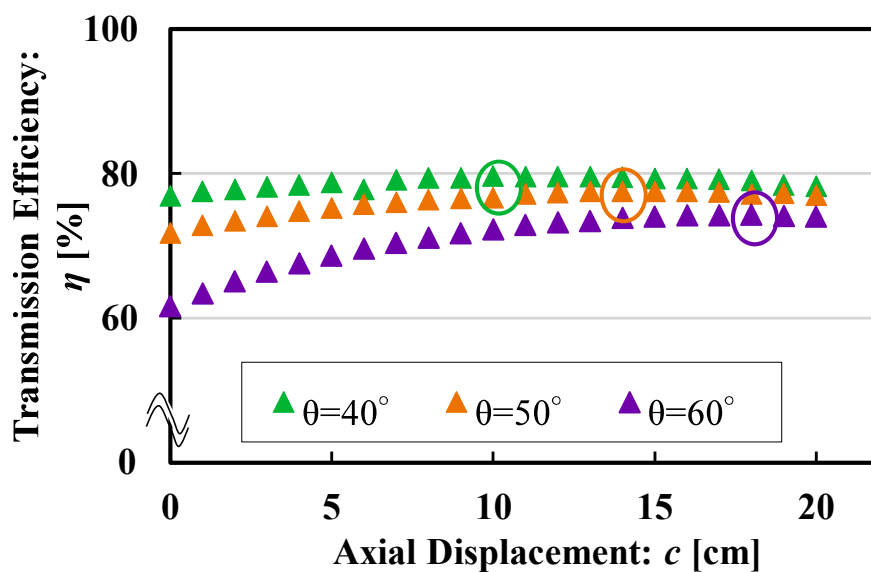


(b) $\theta = 40^\circ, 50^\circ, \text{ and } 60^\circ$

Figure 4.8 Relationship between Power Transmission Efficiency and Axial Displacement for Single-Spiral #2 in the range of $0^\circ \leq \theta \leq 60^\circ$ when $a = 7.0$ cm and $d = 64.6$ cm.



(a) $\theta = 10^\circ, 20^\circ,$ and 30°

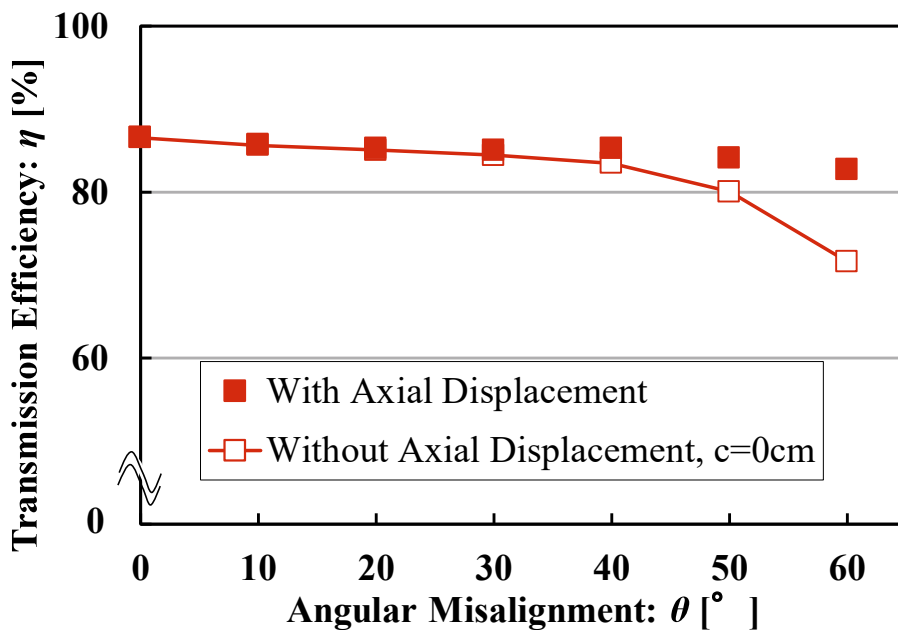


(b) $\theta = 40^\circ, 50^\circ,$ and 60°

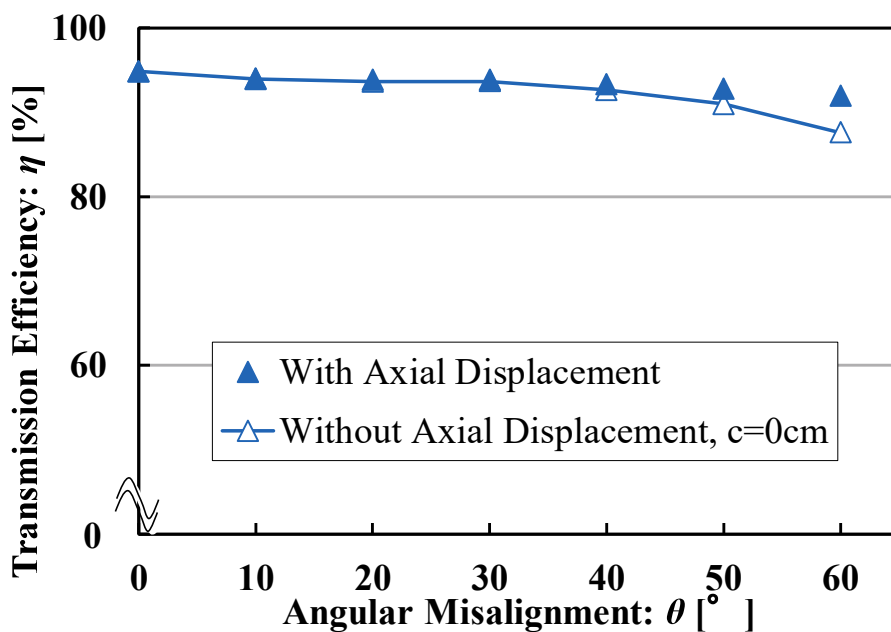
Figure 4.9 Relationship between Power Transmission Efficiency and Axial Displacement for Dual-Spiral Resonator (*mode 1*) in the range of $0^\circ \leq \theta \leq 60^\circ$ when $a = 7.0$ cm and $d = 61.8$ cm.

Based on Figures 4.4 to 4.9, these results confirm that there is an optimum value of the power transmission efficiency of the system, which can be significantly improved by adjusting the distance c for $a = 3.0$ cm, 5.0 cm, and 7.0 cm for Single-Spiral #2 and *mode* 1 of the dual-spiral resonator. Here, for the small angular misalignments $10^\circ \leq \theta \leq 30^\circ$, the improved rate of the power transmission efficiency is low. In contrast, for the large angular misalignments $40^\circ \leq \theta \leq 60^\circ$, the improved rate of the power transmission efficiency is large.

Then, to examine the recovered power transmission efficiency of the RC-WPT system for Single-Spiral #2 and *mode* 1 of the dual-spiral resonator, the optimum axial displacement against angular misalignments within the range $0^\circ \leq \theta \leq 60^\circ$ where $a = 3.0$ cm, 5.0 cm, and 7.0 cm is chosen and arranged, as shown in Figures 4.10, 4.11 and 4.12, respectively. The solid marks show the power transmission efficiency without axial displacement, which is $c = 0$ cm. The hollow marks show the improved power transmission efficiency by axial displacement. Comparisons of the optimum conditions for each angular misalignment and the recovered amount between those spiral resonators when $a = 3.0$ cm, 5.0 cm, and 7.0 cm are summarized in Tables 4.1, 4.2, and 4.3, respectively.

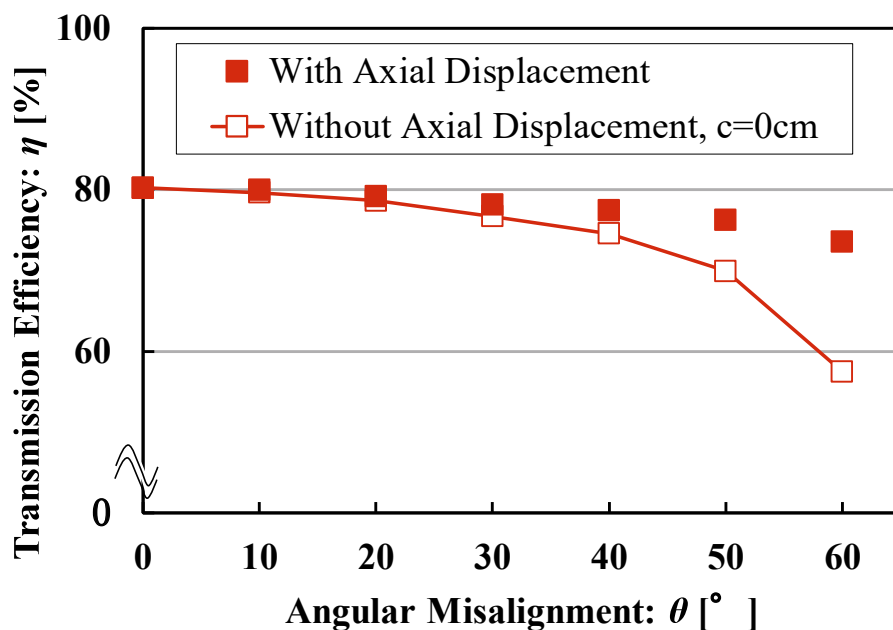


(a) Single-Spiral #2 where $a = 3.0$ cm, $d = 40.6$ cm.

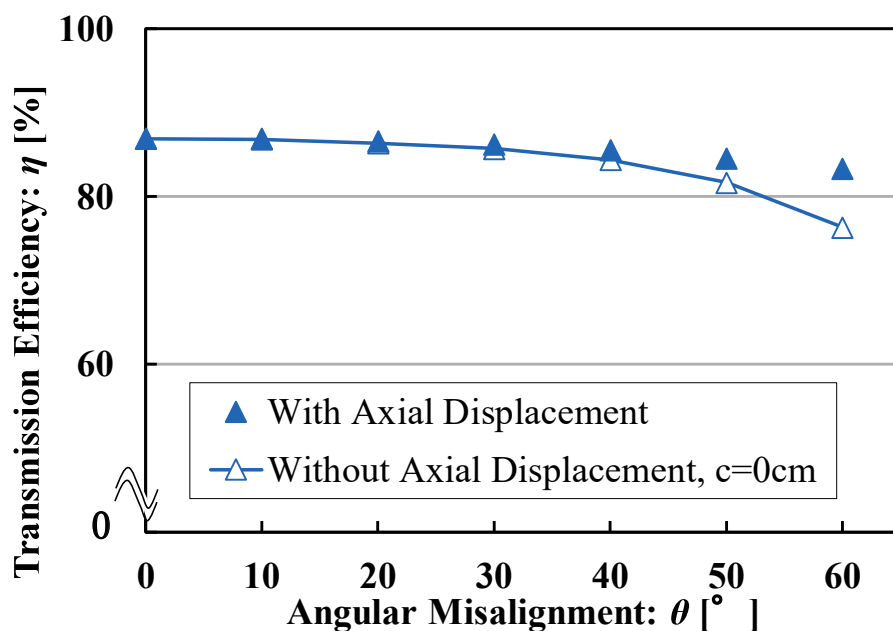


(b) Dual-Spiral Resonator (*mode 1*) where $a = 3.0$ cm, $d = 34.1$ cm.

Figure 4.10 Recovered Power Transmission Efficiency for the RC-WPT System with Angular Misalignment Obtained by Choosing the Optimum Axial Displacement where $a = 3.0$ cm.

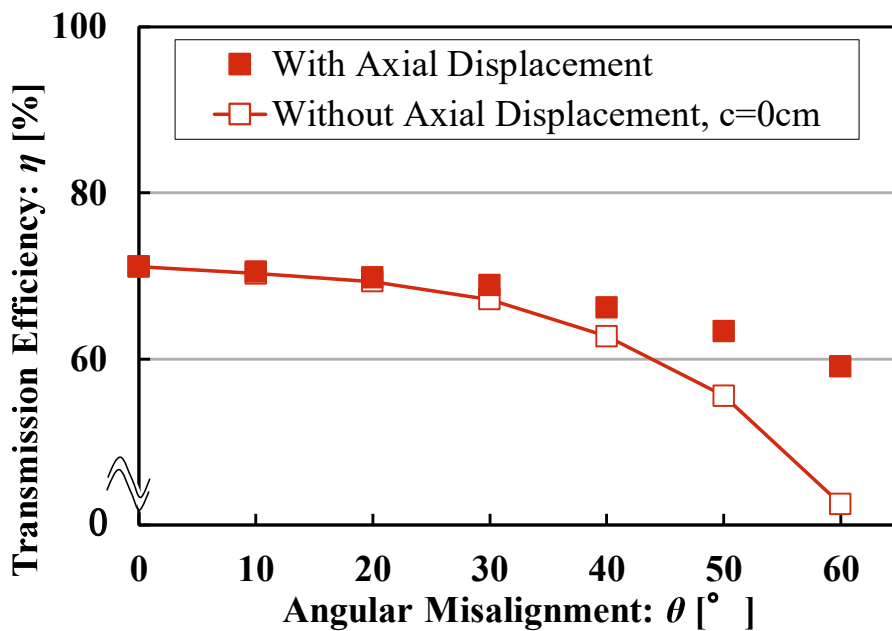


(a) Single-Spiral #2 where $a = 5.0$ cm, $d = 51.0$ cm.

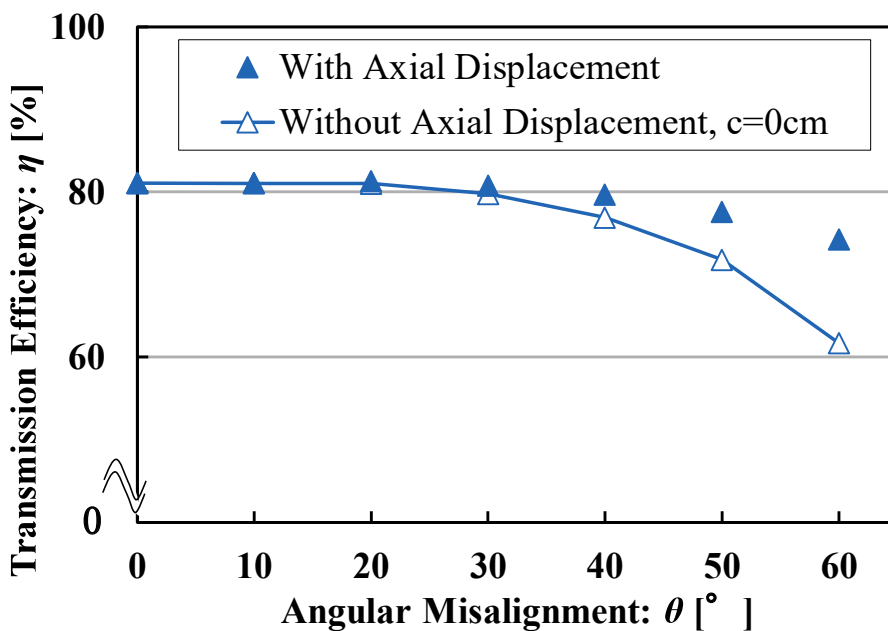


(b) Dual-Spiral Resonator (*mode 1*) where $a = 5.0$ cm, $d = 47.7$ cm.

Figure 4.11 Recovered Power Transmission Efficiency for the RC-WPT System with Angular Misalignment Obtained by Choosing the Optimum Axial Displacement where $a = 5.0$ cm.



(a) Single-Spiral #2 where $a = 7.0$ cm, $d = 64.4$ cm.



(b) Dual-Spiral Resonator (*mode 1*) where $a = 7.0$ cm, $d = 61.8$ cm.

Figure 4.12 Recovered Power Transmission Efficiency for the RC-WPT System with Angular Misalignment Obtained by Choosing the Optimum Axial Displacement where $a = 7.0$ cm.

Table 4.1 Comparison of Power Transmission Efficiency between No Axial Displacement and Recovered Value by Axial Displacement when $a = 3.0$ cm.

(a) Single-Spiral #2 where $a = 3.0$ cm and $d = 40.6$ cm.

Angular Misalignment: θ [°]	No Axial Displacement, $c = 0$ cm	Recovered Value by Choosing the Optimum Axial Displacement		
	Transmission Efficiency: η [%]	Axial Displacement: c [cm]	Transmission Efficiency: η [%]	Recovered Amount [%]
10	85.6	2.0	85.8	0.2
20	85.1	3.0	85.3	0.2
30	84.5	6.0	85.0	0.5
40	83.5	8.0	85.3	1.8
50	80.0	9.0	84.1	4.1
60	71.6	14.0	82.8	11.2

(b) Dual-Spiral Resonator (*mode 1*) where $a = 3.0$ cm and $d = 34.1$ cm.

Angular Misalignment: θ [°]	No Axial Displacement, $c = 0$ cm	Recovered Value by Choosing the Optimum Axial Displacement		
	Transmission Efficiency: η [%]	Axial Displacement: c [cm]	Transmission Efficiency: η [%]	Recovered Amount [%]
10	93.9	1.0	94.0	0.1
20	93.6	3.0	93.8	0.2
30	93.6	6.0	93.8	0.2
40	92.7	6.0	93.3	0.6
50	91.0	7.0	92.8	1.8
60	87.6	10.0	92.0	4.4

Table 4.2 Comparison of Power Transmission Efficiency between No Axial Displacement and Recovered Value by Axial Displacement when $a = 5.0$ cm.

(a) Single-Spiral #2 where $a = 5.0$ cm and $d = 51.0$ cm.

Angular Misalignment: θ [°]	No Axial Displacement, $c = 0$ cm	Recovered Value by Choosing the Optimum Axial Displacement		
	Transmission Efficiency: η [%]	Axial Displacement: c [cm]	Transmission Efficiency: η [%]	Recovered Amount [%]
10	79.7	3.0	80.0	0.3
20	78.6	5.0	79.2	0.6
30	76.7	7.0	78.2	1.5
40	74.6	9.0	77.4	2.8
50	70.0	10.0	76.3	6.3
60	57.5	15.0	73.5	16.0

(b) Dual-Spiral Resonator (*mode 1*) where $a = 5.0$ cm and $d = 47.7$ cm.

Angular Misalignment: θ [°]	No Axial Displacement, $c = 0$ cm	Recovered Value by Choosing the Optimum Axial Displacement		
	Transmission Efficiency: η [%]	Axial Displacement: c [cm]	Transmission Efficiency: η [%]	Recovered Amount [%]
10	86.8	2.0	86.9	0.1
20	86.4	2.0	86.6	0.2
30	85.7	5.0	86.2	0.5
40	84.4	8.0	85.5	1.1
50	81.7	9.0	84.6	2.9
60	76.3	15.0	83.3	7.0

Table 4.3 Comparison of Power Transmission Efficiency between No Axial Displacement and Recovered Value by Axial Displacement when $a = 7.0$ cm.

(a) Single-Spiral #2 where $a = 7.0$ cm and $d = 64.4$ cm.

Angular Misalignment: θ [°]	No Axial Displacement, $c = 0$ cm	Recovered Value by Choosing the Optimum Axial Displacement		
	Transmission Efficiency: η [%]	Axial Displacement: c [cm]	Transmission Efficiency: η [%]	Recovered Amount [%]
10	70.3	3.0	70.5	0.2
20	69.3	6.0	69.8	0.5
30	67.1	8.0	68.9	1.8
40	62.7	10.0	66.2	3.5
50	55.5	16.0	63.4	7.9
60	42.5	20.0	59.1	16.6

(b) Dual-Spiral Resonator (*mode 1*) where $a = 7.0$ cm and $d = 61.8$ cm

Angular Misalignment: θ [°]	No Axial Displacement, $c = 0$ cm	Recovered Value by Choosing the Optimum Axial Displacement		
	Transmission Efficiency: η [%]	Axial Displacement: c [cm]	Transmission Efficiency: η [%]	Recovered Amount [%]
10	81.1	2.0	81.1	0.0
20	81.0	5.0	81.3	0.3
30	79.8	11.0	80.8	1.0
40	77.0	10.0	80.0	3.0
50	72.0	14	77.6	5.6
60	62.0	18	74.3	12.3

From the measured results, when $a=3.0$ cm, 5.0 cm, and 7.0 cm, the recovered amount for the single-spiral resonator is larger than that of the dual-spiral resonator. However, the power transmission efficiency for the RC-WPT system with angular misalignment is higher for the dual-spiral resonator than it is for the single-spiral resonator. Besides, the dual-spiral resonator performed better than the single-spiral resonator against the misalignment between the Tx and Rx units of the RC-WPT system. It can be inferred that dual-spiral resonators are more superior in overcoming the sensitivity of positioning/misalignment of the RC-WPT system.

On the other hand, judging from the measured results of the method of improving the RC-WPT system using single-spiral and dual-spiral resonators, it is obvious that the proposed improvement method for the performance of the RC-WPT system would be effective for the WPT system. According to Refs. [61] and [62], the power transmission efficiency of the butt-joint between the optical waveguides through an air gap and between the single-mode and multi-mode waveguides has relied on the overlapping rate of their modal profile. Therefore, through the proposed improvement method of adding axial displacement to the tilted Rx unit of the RC-WPT system, it is assumed that the decayed power transmission efficiency of the RC-WPT system can be recovered because the rate of overlapping area between the modal profiles of the Tx and Rx spiral resonators

would grow. As a result, the degree of coupling between the resonators would improve, resulting in higher power transmission efficiency. To confirm these assumptions, the modal shape of the spiral resonators should be investigated more in detail using an electromagnetic simulator.

One way to achieve this is shown in Figure 4.13. This proposed method might allow a comprehensive degree of freedom when placing devices, without the positioning of the devices being a matter of concern.

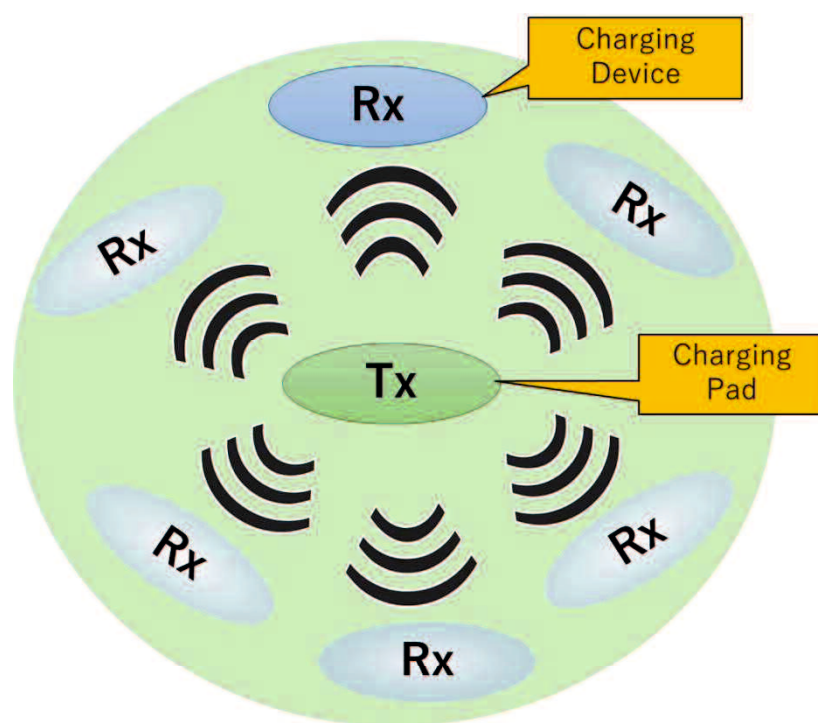


Figure 4.13 Expectation of Future Practical Application.

4.6 Summary

In this chapter, the power transmission efficiency of the RC-WPT system with angular misalignments, which are when the Rx unit is tilted, has been investigated. The results show that when the power transmission distance is increased, the power transmission efficiency generally decreases due to angular misalignment. Furthermore, the method of adjusting the RC-WPT system to improve the power transmission efficiency in the case of angular misalignment has been studied, while the power transmission characteristics when the Rx with angular misalignment was shifted on its axis has been investigated as a method. The findings indicate that the decayed power transmission efficiency of the RC-WPT system due to angular misalignment was improved for both the single-spiral and dual-spiral resonators by adding axial displacement to the tilted Rx unit.

Chapter 5: Conclusions

This paper presents a comprehensive and detailed study of how to reduce the effect of lossy mediums in the power transmission path and how to avoid a loss in power transmission efficiency due to the misalignment between the Tx/Rx units of the system, in order to make RC-WPT systems an effective and practical power source for mobile equipment, sensors embedded in IoT devices, and other items. Consequently, several effective approaches and improved methods have been proposed to further enhance the performance of the RC-WPT system. As concluding remarks, the major improvements and their methods are summarized below.

a) The effects of lossy mediums around the power transmission path of the system

By adopting the RC-WPT system, the power transmission distance can be increased. However, as the power transmission distance grows, the space between the Tx and Rx units of the system becomes larger, and the possibility of obstacles entering this space also increases. Therefore, to avoid the influence of obstacles in the power transmission line, a resonator structure has been proposed that can confine the electric field of its eigenmode as much as possible inside the resonator; this is the "dual-spiral resonator". In this study, for the practical application of the RC-WPT system using dual-spiral resonators, the method of efficiently transmitting power in various environments,

such as humid outdoor environments, was investigated in detail by comparing the system with that of conventional single-spiral resonators.

In the WPT system using conventional single-spiral resonators, it has been experimentally presented that when a lossy medium, such as acrylic bases filled with pure water or tap water, is placed into the power transmission path, the characteristics of the resonators are significantly degraded and the power transmission efficiency of the entire WPT system is decreased drastically. Therefore, by optimizing the structure of the spiral resonator to the proposed dual-spiral resonator, it was possible to significantly suppress the effect of the lossy medium. The design concept of the dual-spiral resonator enables the electric field, which causes the loss, to be confined within the resonator as much as possible. The experimental results show that when a lossy medium is placed in the power transmission path of the WPT system with dual-spiral resonators, the attenuation of the power transmission efficiency is improved and the performance degradation is far less than that of the system with single-spiral resonators. It was also shown that even if the lossy medium is more than several centimeters away from the resonators, the power transmission efficiency of the system with dual-spiral resonators can be significantly improved. The results demonstrate that the system using dual-spiral resonators can avoid the decreased power transmission efficiency caused by lossy mediums, while the dual-

spiral resonator is also more robust in overcoming lossy mediums than the single-spiral resonator.

b) Performance Improvement for some misalignments between the Tx/Rx units of the system

Next, the effect of some misalignments between the Tx and Rx units of the RC-WPT system was discussed. As the angular misalignment between the Tx and Rx units of the RC-WPT system increased, the power transmission efficiency of the RC-WPT system with single-spiral and dual-spiral resonators decreased. This decrease in power transmission efficiency due to the angular misalignment became more significant for longer power transmission distances. As a countermeasure, the power transmission efficiency was improved by shifting the tilted Rx unit to a direction parallel to the spiral plane of the Tx unit, considering the shape of the magnetic field formed by the resonator. As a result, it was confirmed that the power transmission efficiency degraded by the angular misalignment could be recovered in both the single-spiral resonator system and the WPT system with dual-spiral resonators.

This improvement method is expected to be applicable in cases where the Tx and Rx units have large axial displacement and/or angular misalignment when supplying

power to sensors for IoT devices and mobile communication devices such as smartphones, which are currently in widespread use.

From the above explanations, it can be concluded that the WPT system is practical, effective, and can perform even better. In the future, it will be necessary to develop a more practical and efficient WPT system and to consider the effects of the electromagnetic field formed by the WPT system on the human body.

Finally, it will be a considerable pleasure for the author if the results obtained in this study can contribute to improvements in people's QoL (Quality of Life) in the future.

Acknowledgements

First, I would like to express my deepest gratitude to Associate Professor Masashi Hotta, Graduation School of Sciences and Technology for Innovations, Yamaguchi University, who supervised my research and study from 2015 to 2022. I learned a lot from his guidance, including his technical knowledge and attitude toward research. He is also a very supportive and kind professor who never refuses to help me when I have problems with experiments or papers, even though he is busy. He also patiently guided and advised me even when I made many mistakes.

I would like to express my gratitude to Professor Setsuo Yamamoto, Professor Yuji Wakasa, Professor Nobuyoshi Tamura and Associate Professor Hiroaki Yamada for their useful advice. In addition, I would like to thank Dr. Hiroshi Kubo, Professor Emeritus of Yamaguchi University and Dr. Tsunayuki Yamamoto, Associate Professor of Tsuyama National College of Technology, who helped me in my master's program. This research cannot be completed without their support.

Furthermore, I would like to show my gratitude to all fellow members of the laboratory for their great help. Although our native languages are different, they still tried their best to assist me in laboratory work.

Next, I would like to thank my husband, Muhammad Amirulhakim, my son, Areeq Aisuke, my parents and my Malaysian friends for their spiritual support and continuous encouragement during my doctoral program.

Last but not least, I would like to thank Yayasan Pelajaran Mara (YPM) and Yoneyama Rotary Memorial Foundation for providing financial support during my studies in Japan.

References

- [1] H. Matsuki and T. Takahashi, "A Book to Understand Wireless Power Transfer Technology", *Ohmsha*, pp.72-74, 2011. (in Japanese)
- [2] J. Voitkans and A. Voitkans, "Tesla Coil Theoretical Model and its Experimental Verification" *Electrical, Control and Communication Engineering*, vol.7, pp.11-19, July 2014. DOI: 10.1515/ecce-2014-0018.
- [3] G. A. Covic and J. T. Boys, "Inductive Power Transfer," *Proc. of the IEEE*, vol.101, no.6, pp.1276–1289, June 2013.
- [4] N. Shinohara, "Theory and Technologies of Wireless Power Transmission on Various Transmission Distance," *IEICE Trans. on Fundamentals of Electronics, Communications and Computer Sciences Journal B*, vol.J96-B, no.9, pp.881-893, Sept. 2013.
- [5] M. Kesler, "Highly Resonant Wireless Power Transfer: Safe, Efficient, and over Distance" *Witricity Corporation*, pp.1–32, 2013.
- [6] A. Kurs, A. Karalis, R. Moffatt, J. D. Joannopoulos, P. Fisher and M. Soljčić, "Wireless Power Transfer via Strongly Coupled Magnetic Resonances," *Science*, vol.317, no.5834, pp.83-86, Jul. 2007. DOI: 10.1126/science.1143254
- [7] A. Karalis, J. D. Joannopoulos and M. Soljčić, "Efficient wireless *non-radiative mid-range* energy transfer," *Annals of Physics*, vol.323, no.1, pp.34-48, Jan. 2008.
- [8] T. Ishizaki, T. Komori, T. Ishida, and I. Awai, "Comparative study of coil resonators for wireless power transfer system in terms of transfer loss," *IEICE Electronics Express*, vol.7, no.11, pp.785-790, June 2010. DOI: 10.1587/elex.7.785
- [9] C. R. Valenta and G. D. Durgin, "Harvesting Wireless Power: Survey of Energy-Harvester Conversion Efficiency in Far-Field, Wireless Power Transfer Systems," *IEEE Microwave Magazine*, vol.15, no.4, pp.108-120, June 2014. DOI: 10.1109/MMM.2014.2309499.
- [10] K. Makinde, F. O Enemuoh, O. K. Lawal, I. Umar, B. Abubakar and M. K. Mahmood, "A Review of Wireless Power Transmission Via Solar Power Satellite," *IOSR Journal of Engineering*, vol.4, no.6, pp.9-12, June 2014.
- [11] S. Dunbar, F. Wenzl, C. Hack, R. Hafeza, H. Esfeer, F. Defay, S. Prothin, D. Bajon and Z. Popovic, "Wireless Far-Field Charging of a Micro-UAV," *Proc. of the 2015 IEEE Wireless Power Transfer Conference (WPTC)*, pp.1-4, 2015. DOI:10.1109/WPT.2015.7140154.
- [12] J. Garnica, R. A. Chinga and J. Lin, "Wireless Power Transmission: From Far Field to Near Field," *Proc. of the IEEE*, vol.101, no.6, pp.1321-1331, June 2013. DOI: 10.1109/JPROC.2013.2251411.

- [13] H. Matsuki and T. Takahashi, "A Book to Understand Wireless Power Transfer Technology", *Ohmsha*, pp.44-45, 2011. (in Japanese)
- [14] W. Ahn, S. Jung, W. Lee, S. Kim, J. Park, J. Shin, H. Kim and K. Koo, "Design of coupled resonators for wireless power transfer to mobile devices using magnetic field shaping," *Proc. 2012 IEEE Int. Sympo. on Electromagnetic Compatibility (EMC)*, Pennsylvania, USA, pp.772-776, Aug. 2012. DOI: 10.1109/ISEMCMC.2012.6351667
- [15] W. X. Zhong, X. Liu and S. Y. R. Hui, "A Novel Single-Layer Winding Array and Receiver Coil Structure for Contactless Battery Charging Systems with Free-Positioning and Localized Charging Features," *IEEE Trans. on Industrial Electronics*, vol.58, no.9, pp 4136–4144, 2011.
- [16] Y. S. Seo, M. Q. Nguyen, Z. Hughes, S. Rao and J. -C. Chiao, "Wireless Power Transfer by Inductive Coupling for Implantable Batteryless Stimulators," *Proc. of the IEEE MTT-S Int. Microwave Syms. (IMS) Digest*, pp.1–3, June 2012.
- [17] E. Waffenschmidt and T. Staring, "Limitation of inductive power transfer for consumer applications," *Proc. of the 13th European Conference on Power Electronics and Applications (EPE) 2009*, Barcelona, Spain, pp.1–10, 2009.
- [18] W. C. Cheah, S. A. Watson and B. Lennox, "Limitations of wireless power transfer technologies for mobile robots," *Wireless Power Transfer*, vol.6, no.2, pp.175-189, 2019. DOI:10.1017/wpt.2019.8
- [19] D. V. Wageningen and T. Staring, "The Qi Wireless Power Standard," *Proc. 14th Int. Power Electronics and Motion Control Conf. (EPE-PEMC)*, pp.S15-25-S15-32, Sept. 2010. DOI: 10.1109/EPEPEMC.2010.5606673
- [20] S. Y. Hui, "Planar Wireless Charging Technology for Portable Electronic Products and Qi," *Proc. of the IEEE*, vol.101, no.6, pp.1290-1301, June 2013. DOI: 10.1109/JPROC.2013.2246531.
- [21] R. Alrawashdeh, "A Review on Wireless Power Transfer in Free Space and Conducting Lossy Media", *Jordanian Journal of Computers and Information Technology (JJCIT)*, vol.3, no.2, pp.71-88, Aug. 2017. DOI:10.5455/jjcit.71-1483030287
- [22] I. Awai, Y. Sawahara, K. Yamaguchi, M. Hotta and T. Ishizaki, "Miscellaneous Electromagnetic Phenomena in Wireless Power Transfer under Water," *Trans. of the IEICE B, Communications* (in Japanese), vol.J96-B, no.11, pp.1284-1293, Nov. 2013. ISSN: 1344-4697
- [23] I. Awai, "Energy-exploiting Electronics: Dawn of Wireless Power Transfer," *Journal of the IEICE*, vol.100, no.9, pp.943-948, Sept. 2017.
- [24] T. Haruyama, T. Yuki, M. Hotta, M. Hano and I. Awai, "Effect of Water for Resonant Type Wireless Power Transfer System," *Proc. 14th IEEE Hiroshima Section Student Sympo. (HISS)*, Okayama, Japan, no.B-17, pp.326-329, Nov. 2012. ISSN: 2188-0824

- [25] M. Hotta, A. Nobu, T. Haruyama, T. Yuki and M. Hano, "Effect of Water and/or Dielectric Materials for Resonant Type Wireless Power Transfer System," *The Japanese Journal of the Institute of Industrial Applications Engineers*, vol.2, no.2, pp.23-31, Sept. 2014.
- [26] M. M. Rana, W. Xiang, E. Wang and B. J. Choi, "The Internet of Things Infrastructure for Wireless Power Transfer Systems," *IEEE Access*, vol.6, pp.19295-19303, Jan. 2018. DOI: 10.1109/ACCESS.2018.2795803
- [27] S. D. Barman, A. W. Reza, N. Kumar, M. E. Karim and A. B. Munir, "Wireless powering by magnetic resonant coupling: Recent trends in wireless power transfer system and its applications," *Renewable and Sustainable Energy Reviews*, vol.51, pp.1525–1552, July 2015.
- [28] A. P. Sample, D. T. Meyer and J. R. Smith, "Analysis, Experimental Results, and Range Adaptation of Magnetically Coupled Resonators for Wireless Power Transfer," *IEEE Trans. on Industrial Electronics*, vol.58, no.2, pp.544-554, 2011.
- [29] T. Yuki, M. Hotta, M. Hano and I. Awai, "Setup Tolerance for Resonant-type Wireless Power Transfer," *Proc. of the 13th IEEE Hiroshima Sec. Student Sympo. (HISS)*, no. B-3, pp. 220-223, March 2011.
- [30] W. X. Zhong, C. Zhang, X. Liu and S. Y Hui "A methodology for making a three-coil wireless power transfer system more energy efficient than a two-coil counterpart for extended transfer distance." *IEEE Transactions on Power Electronics*, vol.30, no2, pp.933-942.
- [31] S. Y. R Hui, W. Zhong and C. K. Lee, "A critical review of recent progress in mid range wireless power transfer." *IEEE Transactions on Power Electronics*, vol.29, no.9, pp.4500-4511.
- [32] A. Mahmood, A. Ismail, Z. Zaman, H. Fakhar, Z. Najam, M. S. Hasan and S. H. Ahmed, "A Comparative Study of Wireless Power Transmission Techniques," *Journal of Basic and Applied Scientific Research*, vol.4, no.1, pp.321-326, 2014. ISSN 2090- 4304
- [33] M. M. E. Rayes, G. Nagib and W. G. A. Abdelaal, "A Review on Wireless Power Transfer," *Int. Journal of Engineering Trends and Technology (IJETT)*, vol.40, no.5, pp.272-280, Oct. 2016. ISSN: 2231-5381
- [34] I. Awai and T. Ishida, "Design of Resonator-Coupled Wireless Power Transfer System by Use of BPF Theory," *Journal of the Korean Institute of Electromagnetic Engineering and Science*, vol.10, no.4, pp.237-243, Dec. 2010. DOI: 10.5515/JKIEES.2010.10.4.237.
- [35] I. Awai and T. Komori, "A Simple Design of Resonator-coupled Wireless Power Transfer System," *IEEJ Trans. Electronics, Information & Systems* (in Japanese), vol.130, no.12, pp.2198-2203, Dec. 2010. DOI: 10.1541/ieejieiss.130.2198
- [36] I. Awai, "Design Theory of Wireless Power Transfer System Based on Magnetically Coupled Resonators," *Proc. of 2010 IEEE International Conference on Wireless*

- Information Technology and Systems (ICWITS)*, pp.1-4, 2010. DOI: 10.1109/ICWITS.2010.5611902
- [37] Y. Kobayashi, "Measurement Techniques of Microwave Resonator", *MWE Microwave Workshop Digest*, pp.431-442, Nov. 2000. (in Japanese)
- [38] Y. Kobayashi, S. Yasuo and K. Yoshinori, "Microwave Dielectric Filters", *IEICE*, pp.207-211, 2007. (in Japanese) ISBN: 978-4885522208
- [39] T. Ishida, I. Awai and I. Sugiyama, "Measurement of resonator parameters for wireless power transmission system", *Proc. of IEEE MTT-S International Microwave Workshop Series on Innovative Wireless Power Transmission: Technologies, Systems, and Applications (IMWS-IWPT) 2011*, pp.211-214, 2011. DOI: 10.1109/IMWS.2011.5877132
- [40] I. Awai, T. Komori, T. Ishida and T. Ishizaki, "Comparative Study of Resonators for Resonant-type Wireless Power Transfer System," *Technical Report of IEICE*, no.WPT2010-01, pp. 1-7, April 2010. (in Japanese)
- [41] I. Awai, Y. Zhang, T. Komori and T. Ishizaki, "Coupling coefficient of spiral resonators used for wireless power transfer," *Proc. of 2010 Asia-Pacific Microwave Conf. (APMC)*, Yokohama, Japan, pp.1328-1331, Nov. 2012.
- [42] I. Awai and T. Ishizaki, "Design of "Magnetic Resonance Type" WPT Systems Based on Filter Theory," *IEEJ Trans. on Electronics, Information and Systems*, vol.132-C, no.3, 2012. DOI:10.1109/IMWS.2012.6215800
- [43] N. A. M. Halim, M. Hotta and M. Hano, "Influence of Dielectrics and/or Water for Power Transmission Efficiency of Resonator-Coupled Type Wireless Power Transfer System," *Proc. 17th IEEE Hiroshima Sec. Student Sympo. (HISS)*, Okayama, Japan, no.A-22, pp.71-74, Nov. 2015. ISSN: 2188-0824
- [44] N. N. M Zakaria, N. A. M. Halim, M. Hotta and M. Hano, "Influence of Lossy Materials for Resonant Coupling Type Wireless Power Transfer System," *Proc. 18th IEEE Hiroshima Sec. Student Sympo. (HISS)*, Ube, Japan, no.B2-20, pp.294-297, Nov. 2016. ISSN: 2188-0824
- [45] M. Hotta, Nur Syafiera Azreen Norodin, N. N. M. Zakaria, H. Onari and T. Takegami, "Influence of Lossy Objects for Resonator-Coupled Type Wireless Power Transfer System with Coplanar Dual-Spiral Resonators", *Proc. of 2018 Asia-Pacific Microwave Conference*, Kyoto, Japan, WE1-C2-1, pp. 40-42, Nov. 2018.
- [46] I. Awai, Y. Sawahara and T. Ishizaki, "Fabrication of a new high-performance WPT system by electric energy confinement," *2013 IEEE Wireless Power Transfer (WPT)*, pp.214-217, DOI: 10.1109/WPT.2013.6556921.
- [47] I. Awai, Y. Sawahara and T. Ishizaki, "EM Field Made by a Dual Spiral Resonator and Its Application to the WPT System," *Technical Report of the IEICE*, WPT2012-20, Aug. 2012.

- [48]I. Awai, Y. Sawahara and T. Ishizaki, "Choice of Resonators for a WPT System in Lossy Materials," *Proc. of 2014 IEEE Wireless Power Transfer Conf.*, Jeju, South Korea, pp.106-109, May 2014. DOI: 10.1109/WPT.2014.6839605
- [49]M. Najjarzadegan, I. Ghotbi, S. J. Ashtiani, O. Shoaie and M. Shahabadi, "Improved Wireless Power Transfer Efficiency Using Reactively Terminated Resonators," *IEEE Antennas and Wireless Propagation Letters*, vol.17, no.5, pp.803-807, May 2018. DOI:10.1109/LAWP.2018.2816787.
- [50]N. S. A. Norodin, M. Hotta and K. Nakamura, "Existence of Lossy Objects through Power Transmission Path of Resonator-Coupled Type Wireless Power Transfer System," *Proc. 2020 Asia-Pacific Microwave Conf. (APMC)*, Hong Kong, China, no.RS07-03, pp.190-192, Dec. 2020. DOI: 10.1109/APMC47863.2020.9331646
- [51]N. S. A. Norodin, K. Nakamura and M. Hotta, "Effects of Lossy Mediums for Resonator-Coupled Type Wireless Power Transfer System using Conventional Single- and Dual-Spiral Resonators", *IEICE Trans. on Electron.*, vol.E105-C, no.3, March 2022.
- [52]X. Duan, K. Harada, H. Onari and M. Hotta, "Fundamental Characteristics of Resonator-Coupled Type Wireless Power Transfer System By Using Planar Type Dual-Spiral Resonators," *Proc. 19th IEEE Hiroshima Sec. Student Sympo. (HISS)*, Matsue, Japan, no.A1-7, pp.17-20, Dec. 2017. ISSN: 2188-0824
- [53]X. Duan, N. S. A. Norodin, A. Sakata and M. Hotta, "Fundamental Characteristics of Some Modified Shape Spiral Resonators Used for Resonator Coupled Type Wireless Power Transfer System," *Proc. 21th IEEE Hiroshima Sec. Student Sympo. (HISS)*, Soja, Japan, no.B1-10, pp.294-297, Nov. 2019. ISSN: 2188-0824
- [54]R. Itoh, Y. Sawahara, T. Ishizaki and I. Awai, "Wireless power transfer to moving ornamental robot fish in aquarium," *Proc. 2014 IEEE 3rd Global Conf. on Consumer Electron. (GCCE)*, Tokyo, Japan, pp.459-460, Oct. 2014. DOI: 10.1109/GCCE.2014.7031277
- [55]N. S. A. Norodin, D. Sugita and M. Hotta, "Study on Performance of 10MHz Resonator-Coupling type Wireless Power Transfer System with Some Misalignments", *Proc. of the 19th IEEE Hiroshima Sec. Student Sympo. (HISS)*, Matsue, Japan, A1-6, pp. 13-16, Dec. 2017.
- [56]D. Sugita, M. Hotta and M. Hano, "Transmission Characteristics for Resonator-Coupled Type Wireless Power Transfer System with Angular Misalignment," *Proc. of the 18th IEEE Hiroshima Sect. Student Sympo. (HISS)*, Ube, Japan, no.B2-19, pp. 290-293, Nov. 2016. (in Japanese)
- [57]N. S. A. Norodin and M. Hotta, "Performance Improvement of Resonator-Coupled Wireless Power Transfer System using Dual-Spiral Resonator with Angular Misalignments," *URSI Radio Science Bulletin*, vol.372, pp.22-28, March 2020. DOI : 10.23919/URSIRSB.2020.9240098

- [58] Japanese Patent, “WIRELESS POWER TRANSMISSION METHOD UTILIZING MAGNETIC FIELD RESONANCE,” *HITACHI MAXELL ENERGY LTD*, JP 2012-191699 A, Oct. 2012. (in Japanese)
- [59] M. Hotta, T. Yuki, T. Haruyama and M. Hano, “Improvement of Power Transfer Rate for Resonant-Type Wireless Power Transfer System with Axially Misalignment,” *Journal of Communication Science (C)*, vol.J97-C, no.12, Dec. 2014.
- [60] Y. Imamura, M. Hotta and M. Hano, “Improvement of Power Transmission Efficiency on Coupled-Resonator Type Wireless Power Transfer System with Axial Misalignment,” *Proc. of the 18th IEEE Hiroshima Sect. Student Sympo. (HISS)*, Ube, Japan, no.A2-20, pp.66-68, Nov. 2016. (in Japanese) ISSN : 2188-0824
- [61] M. Hotta, M. Geshiro, K. Kanoh and H. Kanetake, “Effects of Air Gaps on Butt-Joints between Isotropic and Anisotropic Planar Waveguides,” *IEICE Trans. on Electronics*, vol.E76-C, no.8, pp. 1345-1349, Aug. 1993.
- [62] M. Hotta, M. Geshiro and S. Sawa, “Application of Beam Propagation Method to Discontinuities of Weakly Guiding Structure,” *IEICE Trans. on Electronics*, vol.E76-C, no.8, pp.1333-1338, Aug. 1993.